

3D MODELING OF ACCRETIONARY BODIES ON A LATE CRETACEOUS
POINT BAR IN DINOSAUR PROVINCIAL PARK, ALBERTA, CANADA
USING ARCHITECTURAL-ELEMENT ANALYSIS

by

Alexander Torres

Bachelor of Science, 2014
Purdue University
West Lafayette, Indiana

Submitted to the Graduate Faculty of
The College of Science and Engineering
Texas Christian University
In partial fulfillment of the requirements for the degree of

Master of Science

May 2016

Copyright by
Alexander Torres
2016

ACKNOWLEDGEMENTS

First, I would like to thank my advisor Dr. John Holbrook, whose mentoring made this work possible. I would also like to thank my thesis committee, Dr. Xiangyang Xie and Dr. Mike Slattery, for also mentoring me throughout this process. I'd like to give a special thanks to Matthew Palmer for assisting me throughout this project and always having a positive attitude.

I'd like to thank Lionel and Sally White, Carlos Aiken, Tara Urbanski, and Becky Aguilar from the University of Texas at Dallas for shooting and making the 3D LiDAR model. Also, I would like to thank Paul Durkin and Stephen Hubbard from the University of Calgary for providing great insights regarding point bar deposition at Dinosaur Provincial Park. Thank you Chris Seibel and colleagues at Nexen for providing great insights and support for the project. A big thank you to Tamie Morgan for always taking the time to assist me with technological issues along the way.

Lastly and most importantly, I'd like to thank my Mom and Dad, Marlene and Luis Torres, for mentoring and supporting me every step of the way. You both are my biggest role models and are the reason I am where I am today.

TABLE OF CONTENTS

ACKNOWLEDGEMENTS	ii
TABLE OF CONTENTS.....	iii
LIST OF FIGURES	vi
LIST OF TABLES	ix
CHAPTER 1 INTRODUCTION	1
1.1 Fundamentals of Point Bar Growth and Migration.....	2
1.2 Point Bar Facies & Architecture	6
1.3 Other Point Bar Processes.....	8
1.3.1 Counter Point Bar	9
1.3.2 Muddy Normal Point Bar	10
1.3.2 Pseudo Point Bars.....	11
1.4 Dinosaur Park Formation	12
1.5 Powder River.....	15
CHAPTER 2	17
2.1 Location of Ancient Point Bar Field Site.....	17
2.2 Stratigraphic Sections.....	18
2.3 Terrestrial Laser Scanning	20
2.4 Architectural-Element Analysis	22
2.5 Strike and Dip Measurements on a 3D Model	23
2.6 Location of Modern Point Bar Field Site.....	27
2.7 Trenching a Point Bar, Correlating Yearly Surveys, and Analysis.....	27
CHAPTER 3 RESULTS	33
3.1 Stratigraphic Sections Dinosaur Provincial Park	33
3.1.1 Stratigraphic Sections of Point Bar Story.....	33
3.1.2 Drape Types.....	34
3.1.3 Stratigraphic Section of Accretionary Bodies	37
3.2 Architectural-Element Analysis	40
3.2.1 Zero Order Surface	40
3.2.2 First Order Surface	41
3.2.3 Second Order Surface.....	44

3.2.4 Third Order Surface	44
3.2.5 Fourth Order Surface	51
3.2.6 Fifth Order Surface	51
3.2.7 Sixth Order Surface (Master Surface)	51
3.3 Characteristics of 3 rd and 2 nd Order Surfaces	55
3.4 Strike & Dip Measurements	58
3.4.1 Location A	58
3.4.2 Location B	58
3.4.3 Location C	59
3.4.4 Location D	59
3.4.5 Location E	59
3.4.6 Location F	59
3.5 Powder River Stratigraphic Section	68
3.5.1 PR141A Stratigraphic Sections	68
3.5.2 PR163 Stratigraphic Section	69
3.6 Architectural-Element Analysis Powder River	72
3.7 Comparison of Powder River Surveys	78
3.7.1 PR141A Survey Lines	78
3.7.2 PR163 Survey Lines	79
CHAPTER 4 DISCUSSION	85
4.1 Interpretation of Fragmentary Bar Architecture	85
4.1.1 Zero Order Surface	85
4.1.2 First Order Surface Set	85
4.1.3 Second and Third Order Surface Sets	86
4.1.4 Fourth Order Surface Sets	89
4.1.5 Fifth Order Surface Set	89
4.1.6 Sixth Order Surface Set	90
4.2 How is a Fragmentary Point Bar Fragmented?	90
CHAPTER 5 CONCLUSIONS	105
REFERENCES	107
APPENDIX	114

VITA
ABSTRACT

LIST OF FIGURES

1. Point bar accretion and helical flow.....	3
2. Point bar growth and migration	5
3. Lower and upper point bar units	8
4. Classic “Normal” point bar accretion model	9
5. Counter point bar model	10
6. Pseudo point bar model.....	12
7. Stratigraphy of Belly River Group.....	13
8. Geologic map of Steveville Area.....	15
9. Powder River extent from stream gage at Moorehead and Broadus, MN.....	16
10. Location of Steveville area of Dinosaur Provincial Park	17
11. Location of 3D model relative to geologic map	18
12. Location of Amphitheater A stratigraphic sections	19
13. Location of Amphitheater B stratigraphic sections	20
14. Terrestrial laser scanning device.....	22
15. Location of strike and dip measurements	25
16. GHVM GeoAnalysis Tools strike and dip tool.....	26
17. Location of PR141A and PR163 point bars.....	27
18. Location of PR141A trench	29
19. Location of PR163 trench	30
20. PR141A survey line cross section.....	31
21. PR163 survey line cross section	31
22. Stratigraphy of point bar story	35
23. Drape types	36
24. Amphitheater A stratigraphic sections A through G	38
25. Amphitheater B stratigraphic sections A through F	39
26. Full model interpreted.....	40
27. Zero and first order surfaces	42
28. Pebble lag deposits along point bar platform.....	43

29. Geometry of 2 nd and 3 rd order surfaces in 3D model	45
30. Geometry of 2 nd and 3 rd order surfaces at Amphitheater A in 3D model	46
31. Photo of 2 nd and 3 rd order surfaces Amphitheater A.....	47
32. Amphitheater A stratigraphic section correlation	48
33. Photo of 2 nd and 3 rd order surfaces Amphitheater B	49
34. Amphitheater B stratigraphic section correlation	50
35. Fourth order surface	52
36. Fifth order surface	53
37. Sixth order surface	54
38. Composite constructional surface in ancient	56
39. Composite constructional and continuous surface in modern	57
40. Location A through F strike and dip data	62
41. PR141A stratigraphic sections at stations 20m, 25m, 30m, and 35m	70
42. PR163 stratigraphic section at station 25m.....	71
43. Interpreted PR141A trench	74
44. Third and 2 nd order surfaces PR141A	75
45. Interpreted PR163 trench	76
46. Geometry of unit bars at PR163 trench.....	77
47. PR141A trench survey lines.....	81
48. Deviation of survey lines from 3 rd order surfaces.....	82
49. PR141A deposition below October 2, 1995 survey line.....	83
50. Ridges and swales PR141A	84
51. Successive accretionary surface scenarios.....	92
52. Crossplots.....	94
53. Small accretionary surface separation example	99
54. Truncation of surface with high pole variation.....	100
55. Segmented point bar.....	102
56. Stacking and erosional patterns of 2 nd order surfaces	104
57. Detailed Amphitheater A stratigraphic sections A through G	114

58. Detailed Amphitheater B stratigraphic sections A through F.....	118
59. Detailed PR141A stratigraphic sections at stations 20m, 25m, 30m, and 35m.....	121

LIST OF TABLES

1. Summary of strike and dip data.....	61
--	----

CHAPTER 1

INTRODUCTION

Point bar deposits are intrinsic architectural elements of meandering rivers. Point bars are depositional bodies that form along the inner cut bank of meandering rivers (Allen, 1965; Bridge, 2003). The standard model for point bar growth presumes that accretionary bodies plaster against the convex inner channel bend during discrete, repetitive, and periodic flow events with sheet-form sand layers that cover much of the wetted bend surface. Repetition of this process produces sandy bodies partitioned with regularly spaced, gently dipping, bar-extensive surfaces. This “normal” point bar model is confirmed from field studies. Recent field examination of the Dinosaur Park Formation of the Belly River Group and active point bars along the Powder River in southeastern Montana, however, show an alternative method of point bar accretion here called the fragmentary point bar model.

This study will use architectural-element analysis techniques in both the ancient and modern to address the following questions:

1. What is a fragmentary point bar?
2. What architectural elements make up a fragmentary point bar and what are their geometries?
3. What causes a fragmentary point bar to be fragmentary?
4. How does a fragmentary point bar in the ancient compare with that in the modern? Are there any similarities/differences?

Point bar accretion directly influences the way fluids flow in a reservoir and are of importance to those interested in connectivity and permeability of these deposits. If bar accretion is fragmented rather than continuous, then fluids will follow tortuous migration pathways

through and around less predictable discontinuous accretionary bodies. Fragmentation would lead to increased uncertainty in modeling of point-bar reservoirs. Addressing the driving mechanisms of point bar accretion and the resultant architecture will aid in reservoir analysis and provide insights into the fundamental process of point-bar accretion.

1.1 Fundamentals of Point Bar Growth & Migration

Studies on flow dynamics and lithofacies document the geometry and depositional process of point bars (Allen, 1963; Allen, 1970; Donselaar and Overeem, 2008). Point bars form along the inner convex bank of a meander bend and are documented in meandering and braided systems and similar alternate bars are intrinsic to straight (Miall, 1996; Bridge, 2003; Moody & Meade, 2014). As water flows into a curved channel, centrifugal forces lead to an excess of water along the outer concave bank. This causes a slight superelevation of water toward the outer bank and a void of water along the convex bank (Einstein and Barbarossa, 1952; Allen, 1965; Bridge, 2003). The superelevation generates a slight increase in depth of the water column along the concave bank increasing the shear stress and strengthening the flow's erosional potential. Water must change to a helical flow to accommodate for the superelevation and void of water along the inner bank (Figure 1) (Einstein and Barbarossa, 1952; Allen, 1965; Leeder, 1999; Bridge, 2003). The combination of superelevation and helical flow in the meander bend generates a downstream velocity component as well as a lower magnitude cross-channel, lateral, component (Allen, 1965; Leeder, 1999; Bridge, 2003). The lateral velocity component is approximately 10-20% the downstream velocity component (Allen, 1965). The lateral component moves toward the concave bank near the water surface and toward the convex bank near the river bed (Allen, 1965; Leeder, 1999; Bridge, 2003). Flow velocities reach a maximum near the concave bank and wane toward the inner bank and up the point bar slope (Allen, 1965;

Donselaar and Overeem, 2008). Furthermore, the flow loses velocity as it moves downstream along the point bar (Smith et al., 2009; Smith et al, 2011). Material that is eroded on the concave bank will typically deposit on subsequent point bars downstream (Allen,1965; Pyrcce and Ashmore, 2005).

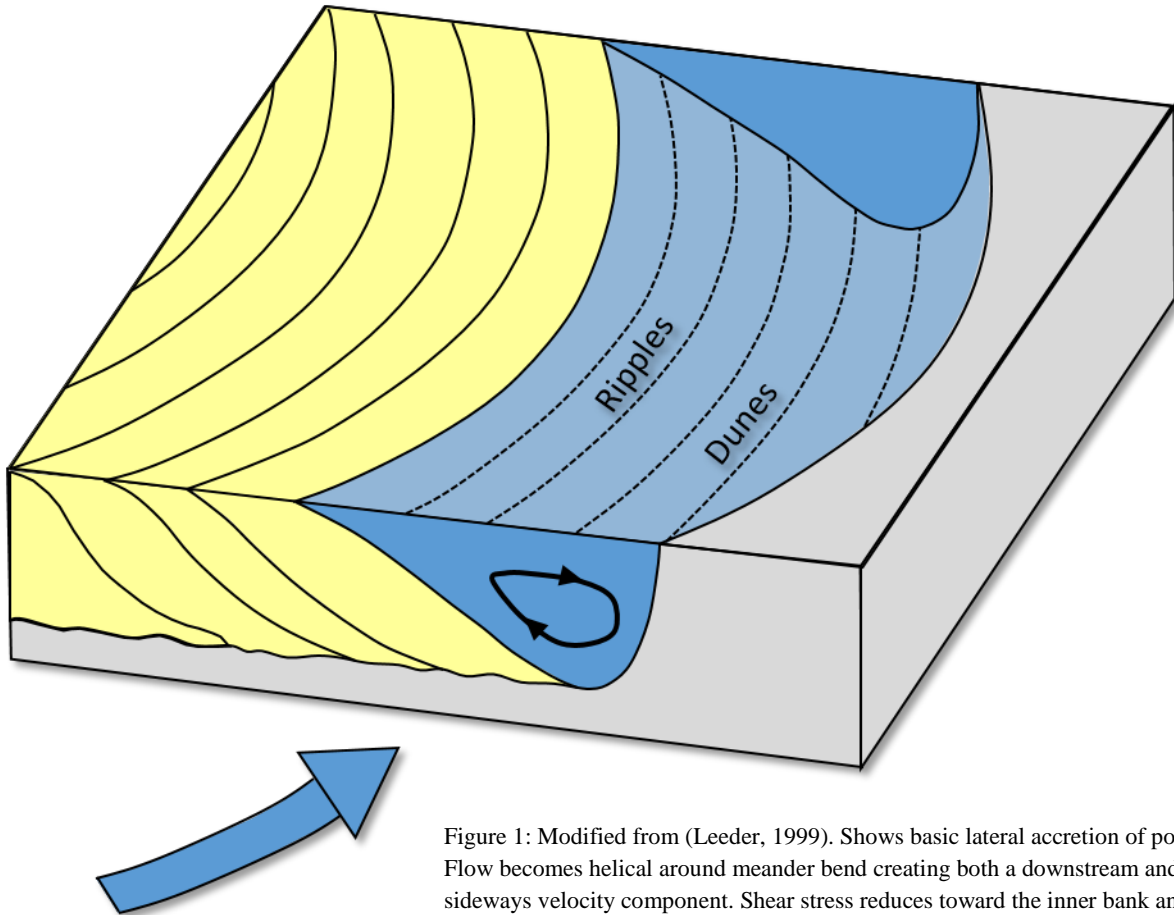


Figure 1: Modified from (Leeder, 1999). Shows basic lateral accretion of point bar. Flow becomes helical around meander bend creating both a downstream and sideways velocity component. Shear stress reduces toward the inner bank and up the point bar slope.

Ridge and swale topography seen on aerial photos record the migration trends of point bars. Lower topography swales separate ridges known as scroll bars (Jackson 1976; Nanson, 1980). Preservation of scroll bars occurs along the inner bend of meanders parallel to the curved channel (Jackson 1976; Nanson, 1980). Flume experiments by Van de Lageweg et al. (2014) test whether point bar migration is a result of “bank pull” (outer bank widening) or “bank push” (inner bank deposition) forces. His results show that as a channel widens, the shear stress

decreases owing to a decrease in both the downstream and lateral velocity component (van de Lageweg et al., 2014). Progressive widening of the outer bank eventually reduces shear stress to a critical point where some grains cannot entrain, but instead deposit along the inner bank. Van de Lageweg et al. (2014) concludes that point bar deposition is a result of channel widening from “bank pull” rather than “bank push” forces.

Erosion along the cutbank and deposition along the inner bank leads to unidirectional point bar migration over time. Point bars migrate laterally toward the cutbank as material continues to deposit along the inner bank. Point bar migration will increase the sinuosity of the channel belt, which reduces effective slope and consequently reduces the bed shear stress along the channel bend (Gay et al., 1998; Constantine and Dunne, 2008). Point bar migration will continue to occur until the bed shear stress reaches a point where it cannot entrain grains along the channel bed. At this point, the channel will abandon the primary course by cutting through a portion of the point bar to form a chute cutoff (Gay et al., 1998). Alternatively, if the meander neck continues to narrow, then the channel at both ends of the meander will eventually meet resulting in a neck cutoff and the development of an oxbow lake (Fisk, 1944; Gay et al., 1998; Constantine and Dunne, 2008). In either case, deposition along the original point bar will cease and a new point bar will develop.

Daniel (1971) identified models of point bar growth and channel migration by expansion, translation, and rotation (Figure 2). Expansional point bars are point bars that grow normal to the channel bank. Expansional point bars form large broad loops that increase in meander-bend sinuosity over time (Willis and Tang, 2010). They typically form when dense vegetation or clay plugs restrict movement of the banks along the end points of the meander axis (Daniel, 1971). Translational bars migrate downstream rather than normal to the valley axis. The cause of

translational migration is unknown, but some speculate that low sinuosity and resistant bodies of sediment along or near the valley sides inhibit expansion of the bar (Bristow and Best, 1993; Smith et al., 2009). Lastly, rotational migration occurs when a bar grows obliquely owing to variable rates of erosion along the channel loop (Daniel, 1971). Point bars may show some variation of the three migration patterns.

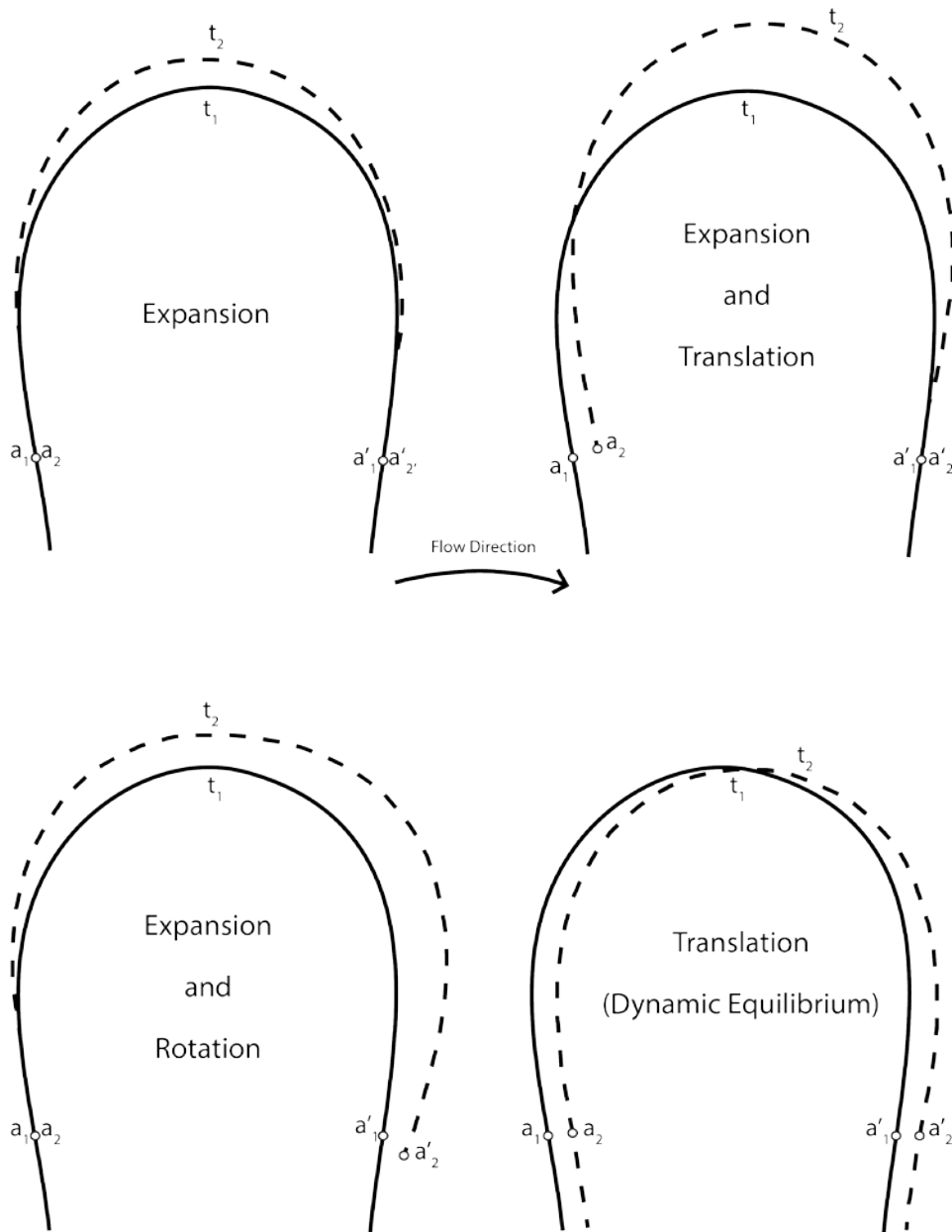


Figure 2: Modified from (Daniel, 1971). Shows point bar growth by expansion, translation, and rotation. Solid lines represent initial time (t_1). Dashed lines represent final time after migration (t_2).

1.2 Point Bar Facies & Architecture

Point bar deposits are macroforms that consist of inclined strata and are broken up into a lower and upper point bar deposit (Allen 1965; Bridge and Tye, 2000). Over the basal scour surface lies a medium-to-coarse grained sandstone with rip-up clasts and/or extraclasts larger than sand. (Cant, 1982; Labrecque, Jensen, and Hubbard, 2011). This deposit records the thalweg channel lag as the new channel migrates and scours into the landscape below. Thick cross-stratified sandstones mark the facies above, which are hydrocarbon reservoirs in many plays including the McMurray Formation (Figure 3) (Labrecque, Jensen, and Hubbard, 2011; Nardin, Feldman, and Carter, 2013). Smaller unit bar deposits, which grow in height by accretion of bedform deposits such as dunes, sheets, or ripples make up the lower bar deposit (Bridge and Tye, 2000; Bridge, 2003). The bedforms within unit bars scale to channel depth while the unit bar itself scales to channel width (Allen 1965; Bridge, 2003). The cross-stratified laminae within unit bars indicate paleocurrent direction. Point-bar deposits commonly fine upward owing to decreasing shear stress up the point bar slope (Allen, 1965; Cant, 1982; Bridge and Tye, 2000; Bridge, 2003; Labrecque, Jensen, and Hubbard, 2011; Nardin, Feldman, and Carter, 2013). Furthermore, individual cross-stratified sets thin upward into small-scale cross-strata or climbing ripples overlain by thin silty-to-muddy drapes representative of waning flow conditions (Jordan and Pryor, 1992; Bridge, 2003). The thick cross-stratified sands deposited during high flow stages and lead to the formation of unit bars with smaller-scale versions of this fining-upward trend (Bridge, 2003; Labrecque, Jensen, and Hubbard, 2011).

Upper point bar deposits are commonly more heterolithic than the lower bar deposits beneath. The deposits above the lower thick cross-stratified sandstone ranges from fine-grained sandstone to siltstone. Upper point bar deposits record an overall decrease in flow regime of the

river (Labrecque, Jensen, and Hubbard, 2011; Nardin, Feldman, and Carter, 2013). The base of the upper point bar deposits increase in concentration of siltstone beds with sandstone and mudstone interbeds (Labrecque, Jensen, and Hubbard, 2011; Nardin, Feldman, and Carter, 2013). Mudstones with siltstones and thin organic rich beds dominate the upper portion of the upper-bar deposit (Bridge and Tye, 2000; Labrecque, Jensen, and Hubbard, 2011; Nardin, Feldman, and Carter, 2013).

Bioturbated siltstone/mudstone caps the upper-bar and is characteristic of the channel levee facies. Lastly, highly bioturbated composite soils of a mudflat environment caps the levee and point bar deposits.

In some special cases, the concentration of mud drapes throughout the point bar is particularly thick. Inclined Heterolithic Strata (IHS) describes point bars with intense heterogeneity (Thomas et al., 1987). More specifically, Thomas et al. (1987) defines IHS deposits as slightly dipping beds that locally alternate between coarser and finer-grained deposits (Thomas et al., 1987). Thomas et al. (1987) infers that small scale IHS develops from sporadic growth of point bars whereas larger scale IHS deposits form from lateral migration of channels undergoing abandonment.

In addition to changes in facies up a vertical stratigraphic column of a point bar, point bars also transition in facies downstream. The upstream portion of the point bar is generally sandier compared to the downstream portion (Smith et al., 2009; Smith et al, 2011). Smith et al. (2009; 2011) theorizes that point bars fine downstream because the flow velocity decreases as it moves along the meander bend downstream further leading to a reduction in stream power.

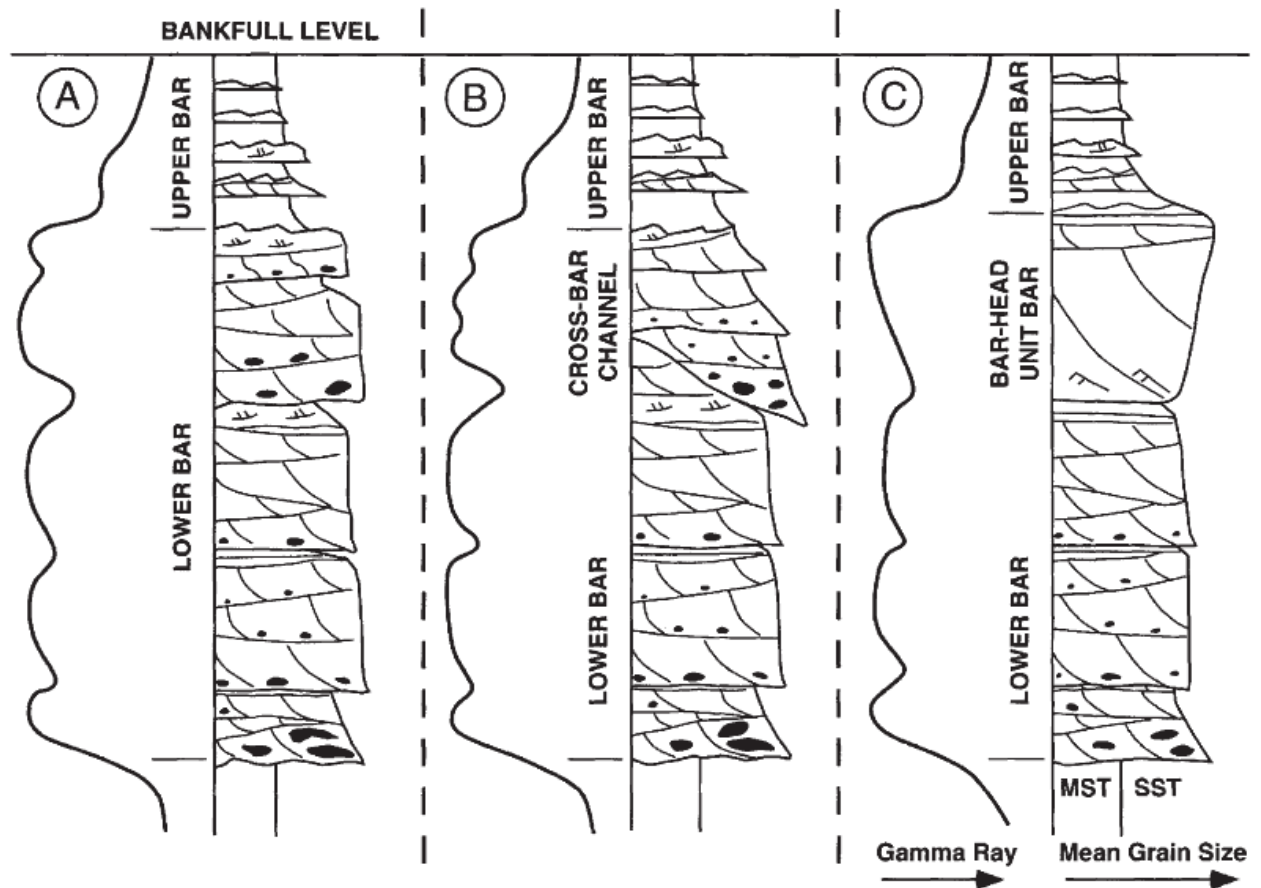


Figure 3: From (Bridge and Tye, 2000). Basic vertical stratigraphic point bar sequence showing both the lower and upper part of the bar. Gamma ray log included to show what a point bar sequence typically looks like on a log.

1.3 Other Point Bar Processes

The most common type of point bar addressed in literature is the “normal” point bar (Figure 4). The normal point bar is sandy with regular and parallel accretion surfaces convex to the channel. Besides the fragmentary point bar defined in this study, there are three additional point bar processes that each have their own unique internal structure. These include the counter, muddy-normal, and pseudo point bars.

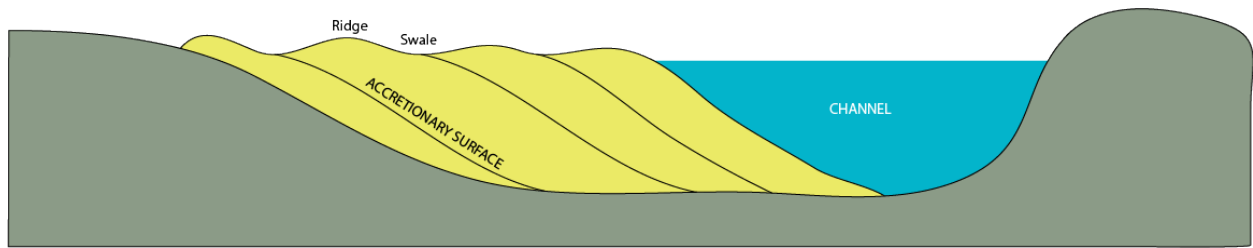


Figure 4: Modified from (Donselaar and Overeem, 2008). “Normal” point bar model showing accretionary surfaces that extend along the full bar surface and match the location of ridges.

1.3.1 Counter Point Bar

Counter point bars form along the most distal parts of point bars and have a concave scroll pattern as opposed to the convex scroll pattern associated with traditional point bars (Figure 5) (Smith et al. 2009). Studies along the Peace River show counter point bar deposits associated with the distal tail end of translating point bars allowing a hydraulic separation zone to develop and reverse eddy currents to move upstream (Smith et al., 2009). Counter point bars have a wedge-shaped geometry that thickens away from the meander inflection. Furthermore, finer grained sediments dominate counter point bar deposits as compared to normal point bar deposits (Smith et al., 2009).

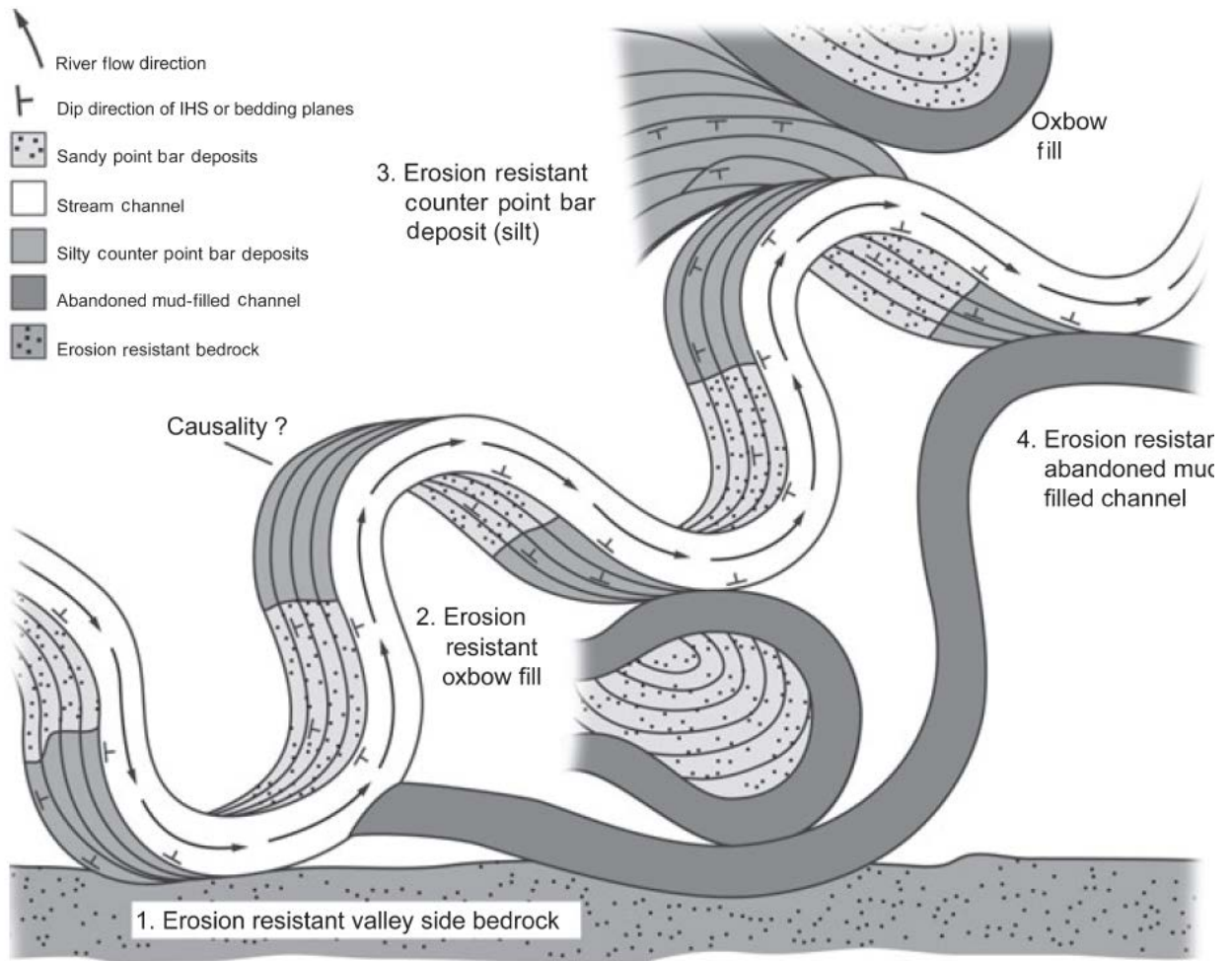


Figure 5: From (Smith et al., 2009). Counter point bar deposits show more of a concave depositional pattern as opposed to the convex depositional pattern of point bar deposits. Notice that these deposits are located on the downstream end of point bar deposits.

1.3.2 Muddy Normal Point Bar

Like the normal point bar, the muddy normal point bar has long continuous accretion surfaces that extend down much of the wetted bend surface. However, these deposits are much muddier than their sandier counterpart. Muddy point bar deposits are commonly associated with tidal influence, are not necessarily tidal in origin in all cases (Thomas et al., 1987). Furthermore, a recent study by Blum (2015) shows that the paleogeographic location of some muddy point bar

deposits within the McMurray Formation are well to far out up dip to be tidally influenced. The cause and characteristics of non-tidal muddy normal point bars is unknown. They are however heterolithic. What is assumable about these bars is that they record times of high shear stress that lead to sandier deposits along with times of prolonged low shear stress leading to muddier deposits.

1.3.3 Pseudo Point Bars

Unlike the previous point bar processes mentioned earlier, pseudo point bars are deposits formed along braided rivers rather than meandering river systems. These point bars form when a braided river system preferentially accretes mid-channel bars toward one side (Allen, 2014). Over time growth of mid-channel bars leads to their amalgamation on one side forming what seems to be a traditional point bar within a braided river system (Figure 6). Mid-channel accretion point bars have the general shape of “normal” point bars, but their architecture is noticeably different. Deposits of mid-channel accretion bars consist of lobate sandy bodies that show bi-directional accretionary orientations.

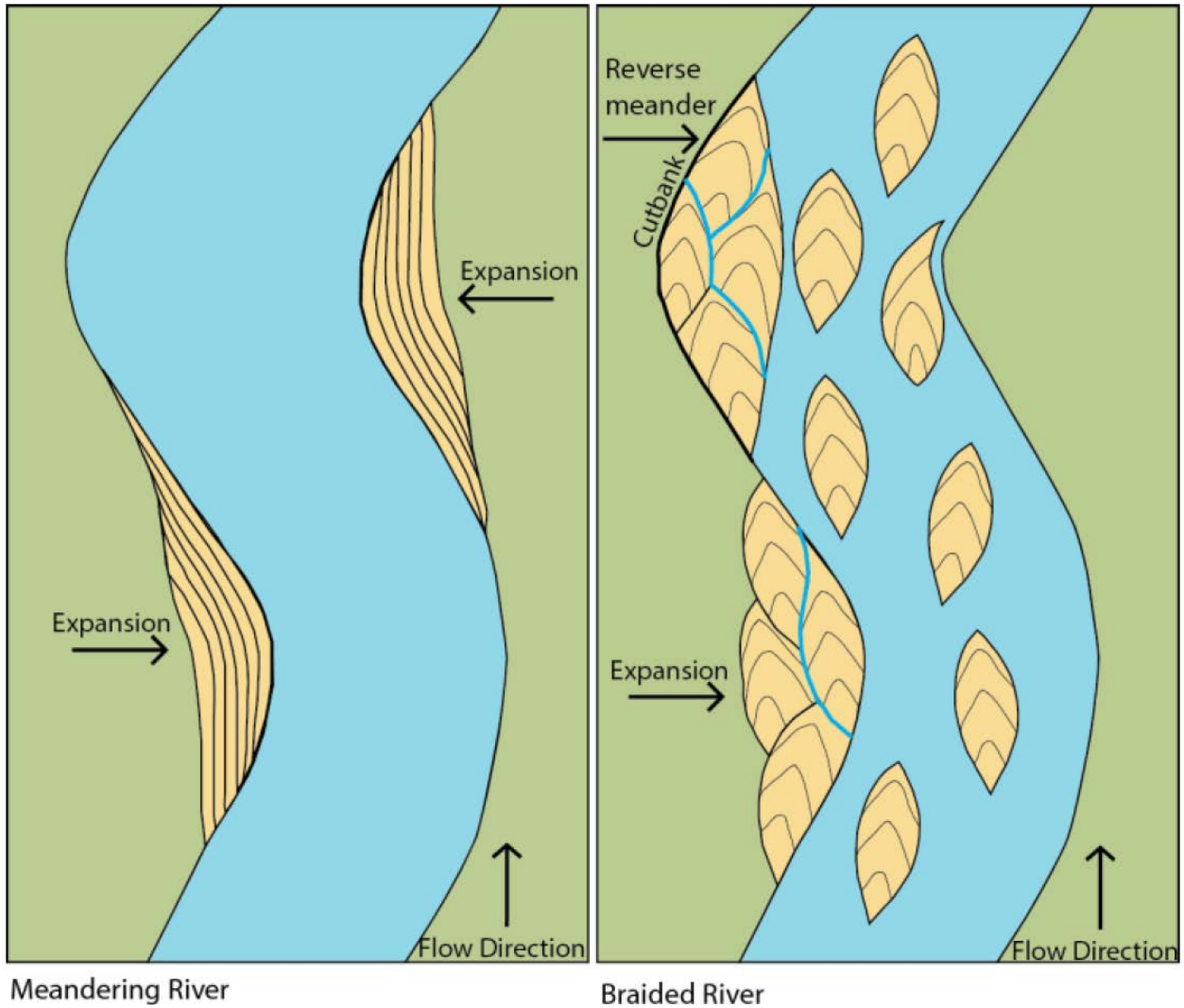


Figure 6: From (Allen, 2014). Pseudo Bar model showing how mid-channel bars over time amalgamate and form a pseudo point bar along a braided river system.

1.4 Dinosaur Park Formation

This study will target point bars in the Dinosaur Park Formation within southeastern Alberta, Canada. The Dinosaur Park Formation is part of the Belly River Group, also known as the Judith River Formation. The Belly River Group consists of the Foremost Formation at the base, Oldman Formation in the middle, and Dinosaur Park Formation at the top. The Belly River Group overlies the Pakowki Shale and the marine Bearpaw Shale overlies the Belly River Group (Figure 7). The Belly River Group spans from 80-75Ma (middle to late Campanian of the

Cretaceous) (Hamblin and Abrahamson, 1996). Within Dinosaur Provincial Park the Belly River Group is approximately 275m thick with the Dinosaur Park Formation accounting for 80m (Eberth and Hamblin, 1993; Wood, 1989). The foredeep of the Western Canada Sedimentary Basin acted as a sink for sediment of the Belly River Group (Hamblin and Abrahamson, 1996). During the middle part of the Campanian the location of present day Dinosaur Provincial Park was between the Western Interior Seaway to the east and the active Cordilleran Belt to the west. Hamblin and Abrahamson (1996) and Wood (1989) argue that the depositional environment of the Belly River Group was a distal fluviodeltaic coastal plain. Hamblin and Abrahamson (1996) and Wood (1989) infer a warm and humid temperate-to-subtropical paleoclimate with annual rainfalls around 120cm (Hamblin and Abrahamson, 1996; Wood, 1989).

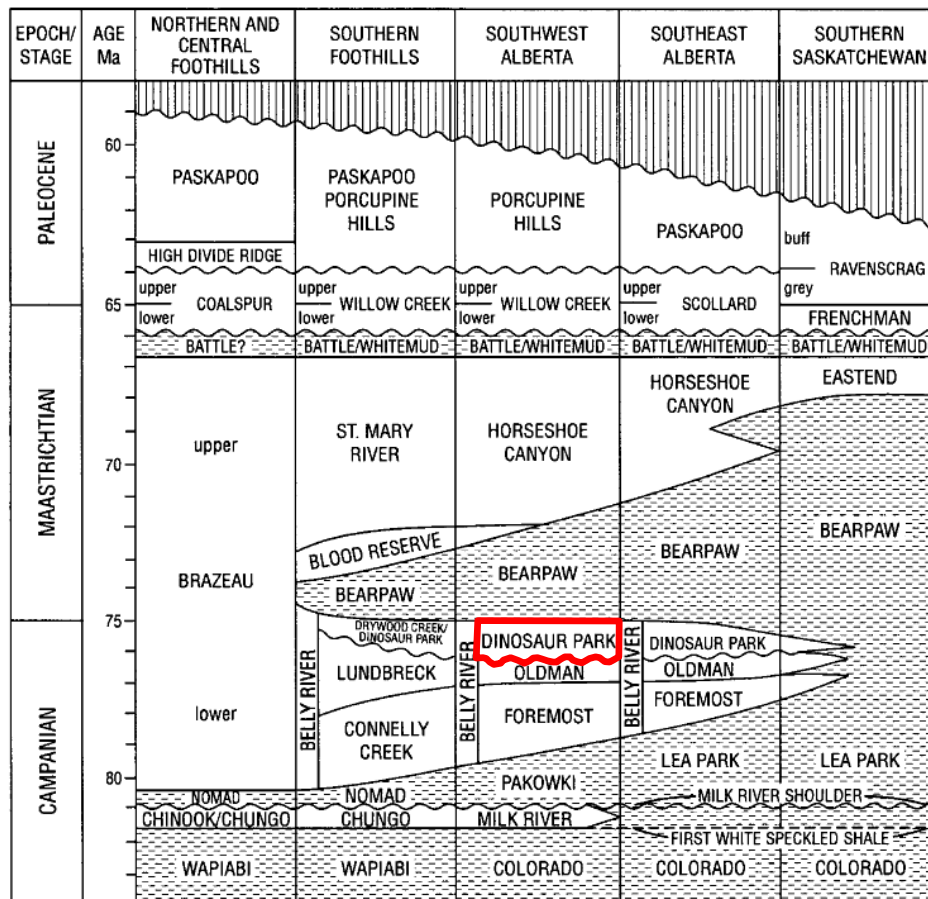


Figure 7: Modified from (Hamblin, 1997b). Distribution of the Belly River Group throughout the Western Canada Sedimentary Basin. Dinosaur Park Formation near Dinosaur Provincial Park outlined in red.

The Dinosaur Park Formation of the Belly River Group is composed of a lower and upper member. Cores and outcrop from Hamblin (1997a) show a lower Dinosaur Park Formation (approximately 40-50m thick) consisting of thick fine-to-coarse sandstones with thinner beds of grey sandy siltstones to very fine sandstones. The sands near the base are cross-stratified and fine upwards to more heterolithic strata with ripple cross-laminations near the top. The upper unit of the Dinosaur Park Formation is approximately 30-40m thick and consists of thin interbedded mudstones and very fine to medium-grained sandstone lenses (Hamblin, 1997a). The Dinosaur Park Formation unconformably overlies the Oldman Formation and the Bearpaw Formation conformably overlies the Dinosaur Park Formation. Base level fell rapidly following deposition of the Oldman Formation resulting in the development of a subaerial unconformity. Increase of accommodation owing to base level rise provide the circumstances for fluvial dominated deposition of the Dinosaur Park Formation (Hamblin, 1997a). Rapid marine transgression led to subsequent deposition of the overlying Bearpaw Formation. (Hamblin, 1997a).

Durkin (2015) defined the distribution of channels and point bars within one channel belt system in the Dinosaur Park Formation located near the Steeveville area of Dinosaur Provincial Park (Figure 8). This study will focus on a single point bar story mapped by Durkin et al. (2015). Matthew Palmer and I measured strikes and dips at various locations along the point bar to confirm its existence and extent (Palmer, 2015).

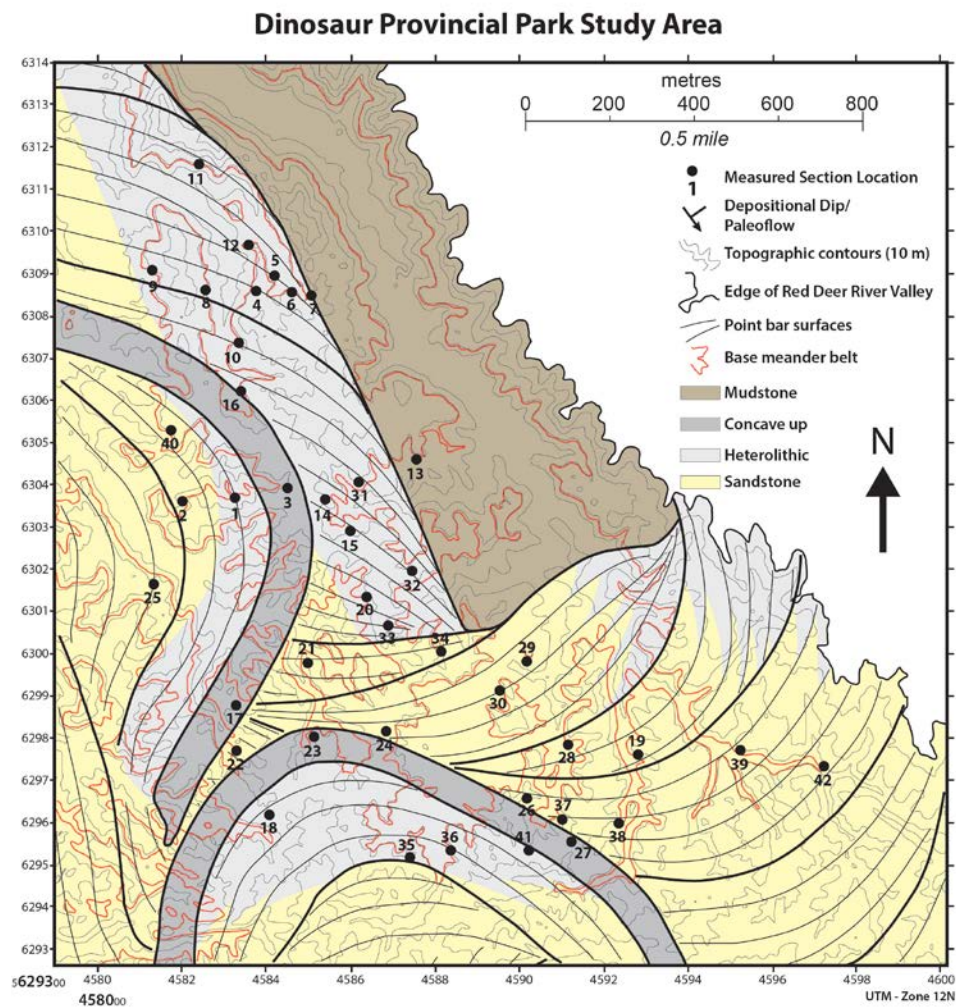


Figure 8: From (Durkin et al, 2015). Geologic map showing the distribution of bars and channels within a single channel belt in the Dinosaur Park Formation.

1.5 Powder River

The Powder River is a modern river with little human influence making it ideal for observing point bar architecture (Moody and Meade, 2014). The Powder River is located in northeastern Wyoming and southeastern Montana (Figure 9). The Big Horn Mountains in Wyoming feed sediment into the Powder River (Hembree et al., 1952). Sediment from the Big Horn Mountains includes pre-Cambrian granites, schists, and Paleozoic limestone and sandstone

(Hembree et al., 1952). The Powder River erodes sandstone, siltstone, and shale from the Mesozoic and Cenozoic erathems that outcrop on the eastern edge of the Big Horn Mountains as well as the plains in the lower slopes. The Powder River transports a high concentration of suspended load at 2-3 million metric tons per year (Hembree et al., 1952; Moody and Meade, 2008; Moody and Meade, 2014).

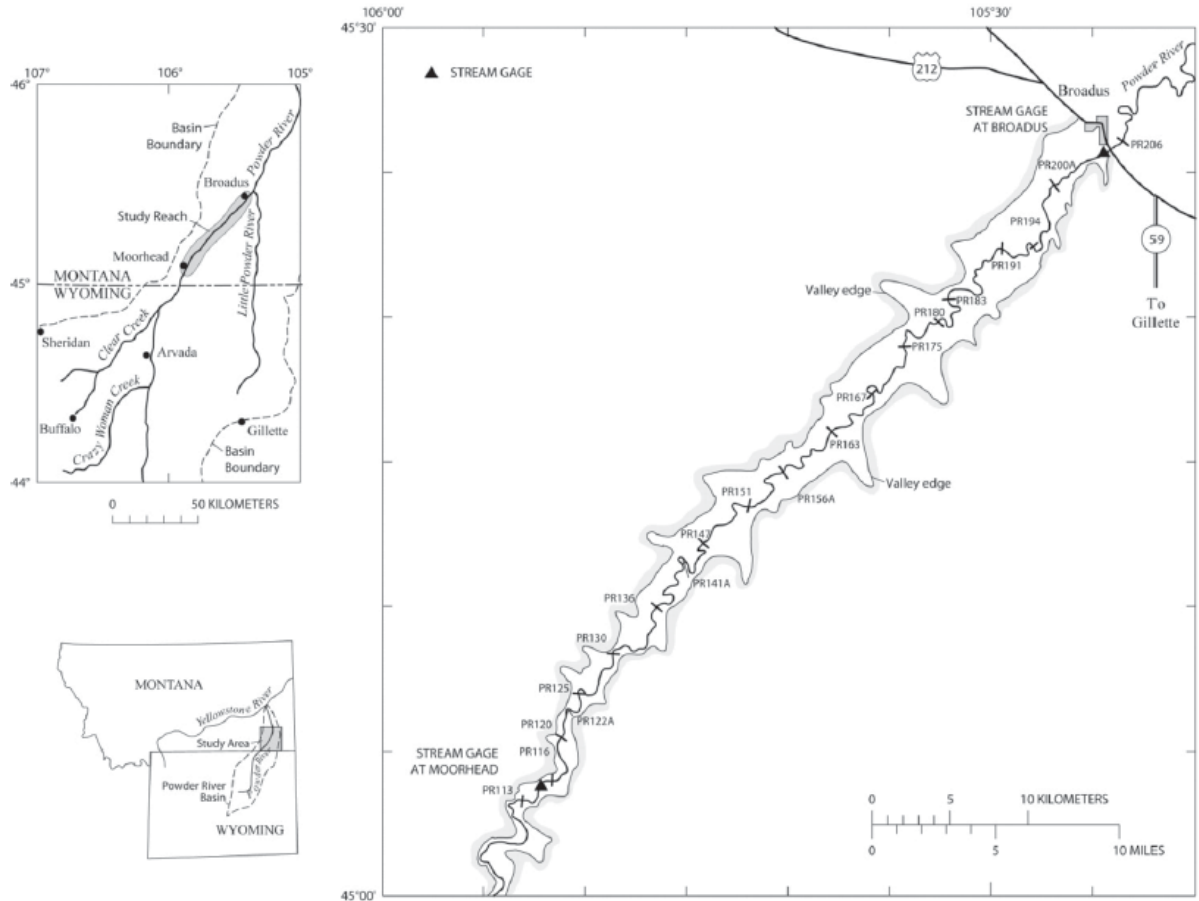


Figure 9: From (Moody and Meade, 2014). Location of Powder River southwest of Broadus, Montana.

CHAPTER 2

METHODS

2.1 Location of Ancient Point Bar Field Site

This study encompasses work in both ancient and modern point bar deposits. The first field site is located in the Steveville area of Dinosaur Provincial Park in Alberta, Canada (Figures 10 and 11). The highly dissected badland topography and sparse vegetation allow for excellent 3D exposure of ancient point bars. Field goals at this site include measuring detailed sections of accretionary bodies, conducting terrestrial LiDAR scans along two different amphitheaters of the same point bar, and performing preliminary architectural element analysis to aid in mapping on a 3D model. Matthew Palmer and I both worked this Steveville site and formed a common dataset to be analyzed for two differing purposes.

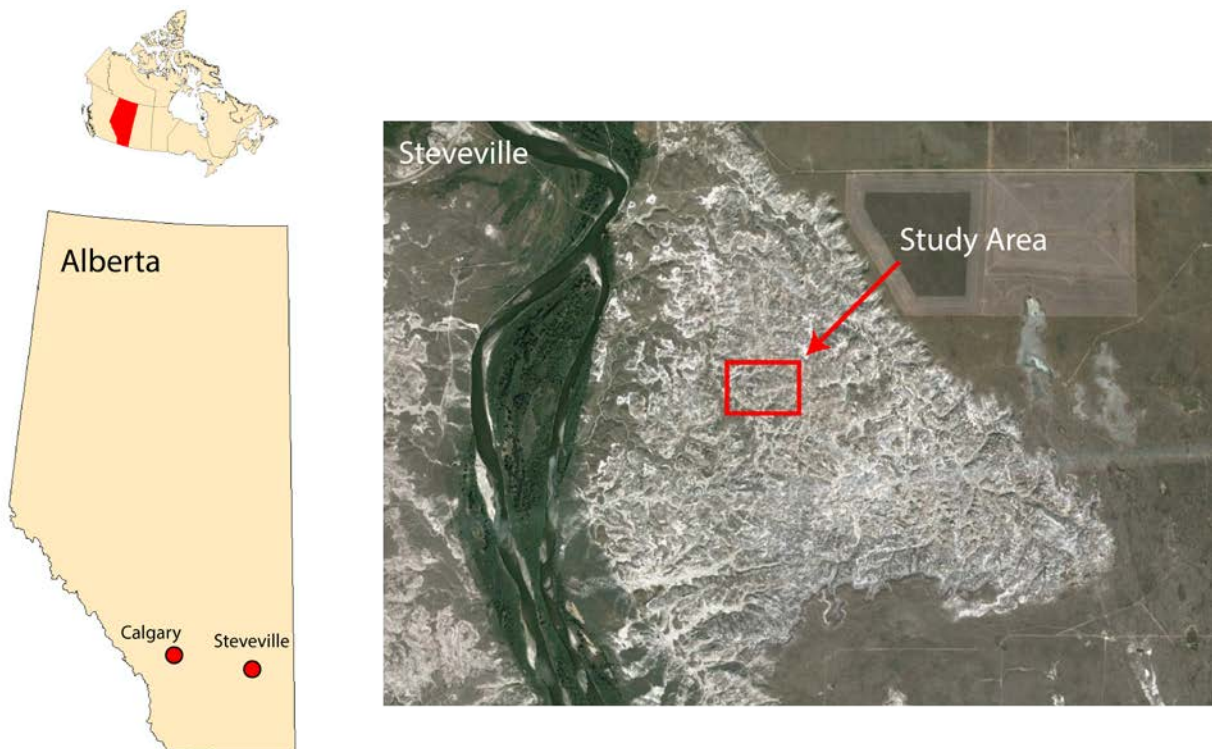


Figure 10: Map showing the location of Steveville area of Dinosaur Provincial Park in Alberta, Canada. Area outlined in red is the location of our study area.

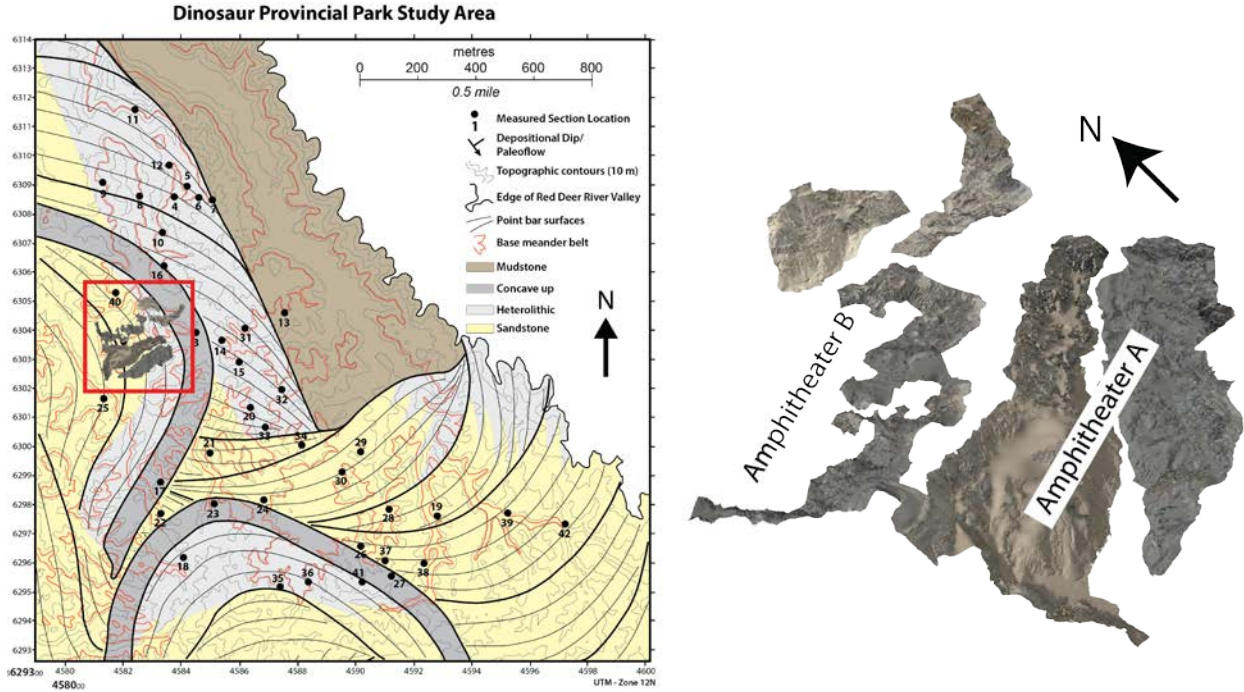


Figure 11: Modified from (Durkin et al., 2015). Geologic map (left) showing the location of point bar and section of point bar (outlined in red) of our study area. 3D model of exposed areas of point bar shown on right.

2.2 Stratigraphic Sections

We located two specific areas to measure sections within a single point-bar story (Figures 12 and 13). The areas we chose had clear, multiple, and-fully mappable accretionary surfaces. We measured six sections at one site and seven sections at the other, and we measured a section wherever a change in architecture occurred. Measured sections include lithology, color, sedimentary structures, grain size, sorting, roundness, and drape types along bounding surfaces.

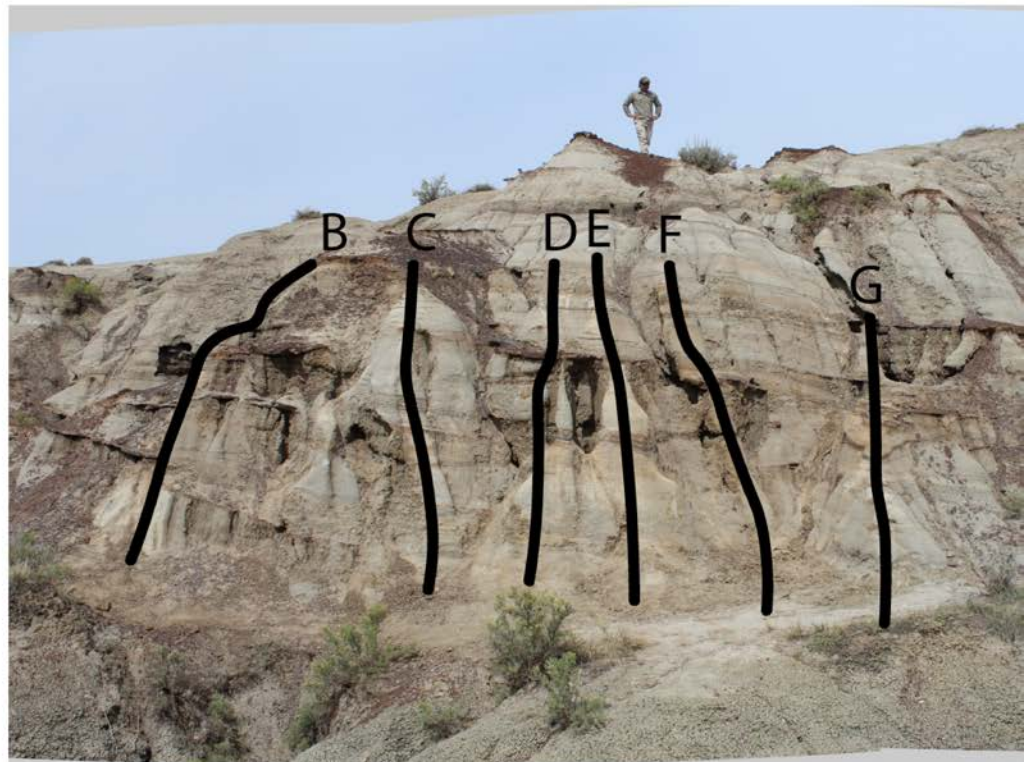


Figure 12: Locations of stratigraphic sections along Amphitheater A. Section A outcrops along strike and is 90° in orientation from sections B-G.



Figure 13: Locations of stratigraphic sections along Amphitheater B. Section A-D are over 90° rotated from sections E and F. Section E is not visible in photos.

2.3 Terrestrial Laser Scanning

We selected two amphitheaters to scan based on their exposure quality as well as ease of access to site with LiDAR equipment (Figure 11). Lionel White (University of Texas at Dallas) along with a team of two students provided the equipment and conducted the field scans. The equipment used for terrestrial laser scanning include:

- Riegl VZ-400 near IR LiDAR scanner
- Laptop to run the scanner
- Nikon D700 Camera with 85mm lens, mounted on top of the VZ-400
- 5 tripod mounted disk reflectors
- Topcon Hiper Lite GPS

The LiDAR scanner uses pulses of light that hit a target and reflect back at the scanner. The lasers that hit the outcrop do not affect the outcrop in any way. The scanner records the time it takes each pulse of light to return and uses this data to convert into XYZ coordinates. Reflectors act as points of reference to aid in stitching scans together.

We took multiple scans of each amphitheater at different locations and angles to decrease the likelihood of having holes in the data. We took six scans at Amphitheater A and four scans at Amphitheater B. During the scanning process, a camera mounted on top of the scanner took photos of the outcrops (Figure 14). We stitched together scans to construct a complete 3D model. Lionel and his team draped photos onto the model and the point cloud model was converted into a working TIN mesh 3D model that could be imported into ArcScene for architectural analysis. For detailed information about the steps taken from scanning in the field to creating a 3D TIN Mesh model see (Palmer, 2015).



Figure 14: Photo of Riegl VZ-400 LiDAR scanner with Nikon D700 SLR camera mounted above.

2.4 Architectural-Element Analysis

This study uses architectural-element analysis to map out both the ancient and modern point bar deposits. The GHVM GeoConstructor tools for ArcScene allow for mapping of surfaces on the 3D model. Tools built into Adobe Illustrator allow for mapping of surfaces onto panoramas for both ancient and modern point bar outcrops. Holbrook (2001) lists detailed steps to conduct architectural-element analysis and assign orders to bounding surfaces. The rules for conducting architectural-element analysis by Holbrook (2001) are:

1. Each surface is considered unique and laterally continuous until truncated, or deemed indiscernible.
2. A surface may truncate another, but surfaces may not cross.
3. Though surfaces may be diachronous, any location on a surface must be younger than the materials/surfaces it cuts, and older than the material/surfaces it binds.

The procedures to ranking orders to surfaces by Holbrook (2001) are:

1. Bedding surfaces bounding lamina sets are considered as 1st order.
2. Lower order surfaces will be bound by higher-order surfaces.
3. The order of a surface will be one order higher than the highest-order surface it binds, and may be of higher order where guideline 4 should be satisfied.
4. Surfaces truncate against surfaces of equal or higher rank.
5. Similar, but nested, surfaces may be treated as a set of boundaries of equal order, but the set should be ultimately bounded by a surface of higher rank.

2.5 Strike & Dip Measurements on a 3D Model

Strikes and dips of 3D bounding surfaces were measured at six locations to assess causes of bar fragmentation (Figure 15). I measured strikes and dips for each 3rd order surface along a vertical section at each location. Single-location measurement reduces the variation owing to changes in orientation along a convex shaped point bar. I recorded strikes and dips of mapped accretion surfaces using the GHVM GeoAnalysisTools Strike & Dip tool for Arcscene from strongly 3D sites. The tool calculates an average orientation and dip value, and outputs the values for both strike and dip as well as a projected plane of the averaged surface (Figure 16). I recorded strikes and dips for each location on an excel spreadsheet and imported into a free online stereonet program called Stereonet 9 by Rick Allmendinger. I generated six stereonets,

one for each location, and plotted the poles for all strikes and dips. I numbered poles in order from the oldest accretion surface to the youngest accretion surface to see if there were any patterns in the relationship of strike and dip for accretionary bodies.

All strikes and dips for each location are then averaged, as well as differences in strike and dip between each adjacent accretionary body. Lastly, I drew a series of arrows for each location that connected each pole in order of accretionary events. Arrows are colored as a gradient from light grey-to-dark grey to show the progression of older to younger accretionary events.

I plotted the length of each arrow with the amount of truncations seen in the model of each accretionary body to see if surfaces with larger changes in strike and dip are related to the number of truncations over a given area of exposed outcrop. To normalize the length of each arrow for all locations, I measured the number of degrees each pole deviated from the equator of the stereonet. For consistency, I only recorded truncations over a viewing length of 40m of exposed outcrop (20m left and right of vertical section where strikes and dips were measured). I plotted average length in degrees against number of truncations and took the average of values for each location.

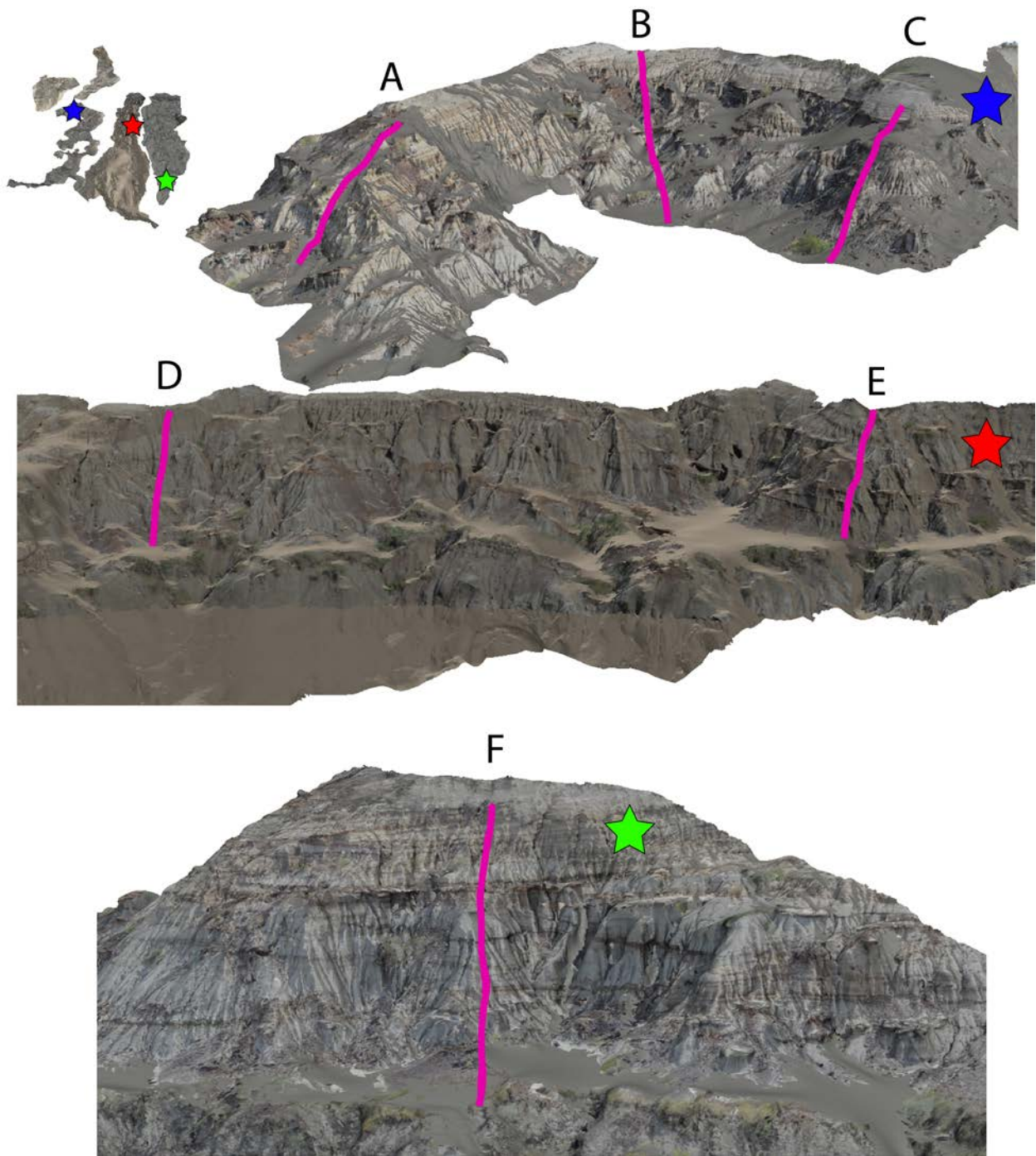


Figure 15: Locations where I measured strikes and dips of 3rd order surfaces. Sections are vertical to reduce error from orientation changes along a convex point bar. Locations A-C are measured along Amphitheater B while locations D-F are along Amphitheater A. Sections average approximately eight meters in height.

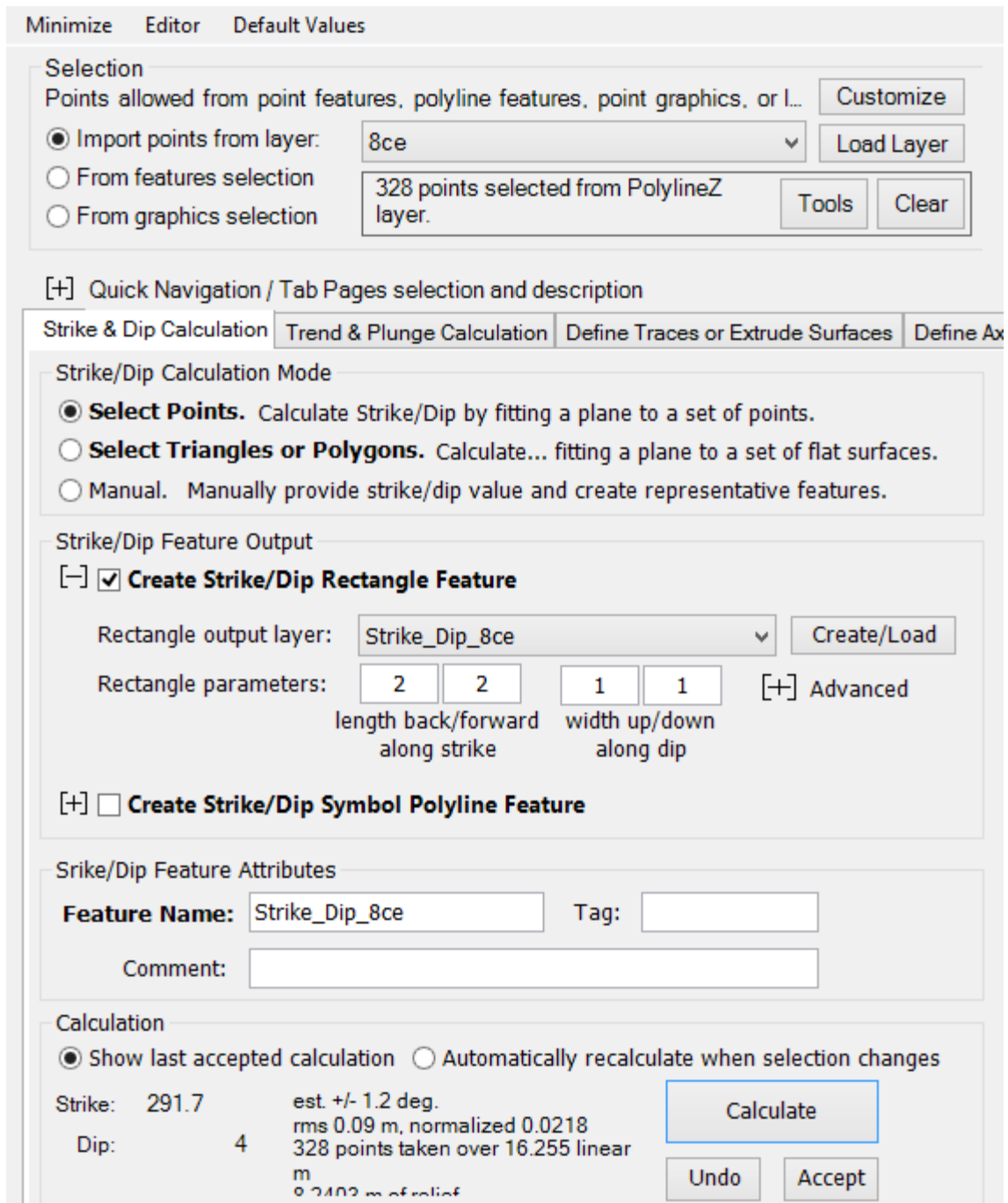


Figure 16: Strike and Dip Calculation tool tab from GHVM GeoAnalysisTools. Tool uses points from surfaces drawn and averages a strike and dip value. Example of strike and dip output is shown at bottom of figure.

2.6 Location of Modern Point Bar Field Site

The second field site is located on the Powder River near Broadus, Montana (Figure 17). Limited human influence on the growth and migration of the river make the Powder River an excellent site to study modern point bar processes. Field goals at this site include trenching point bar deposits and recording stratigraphic sections.

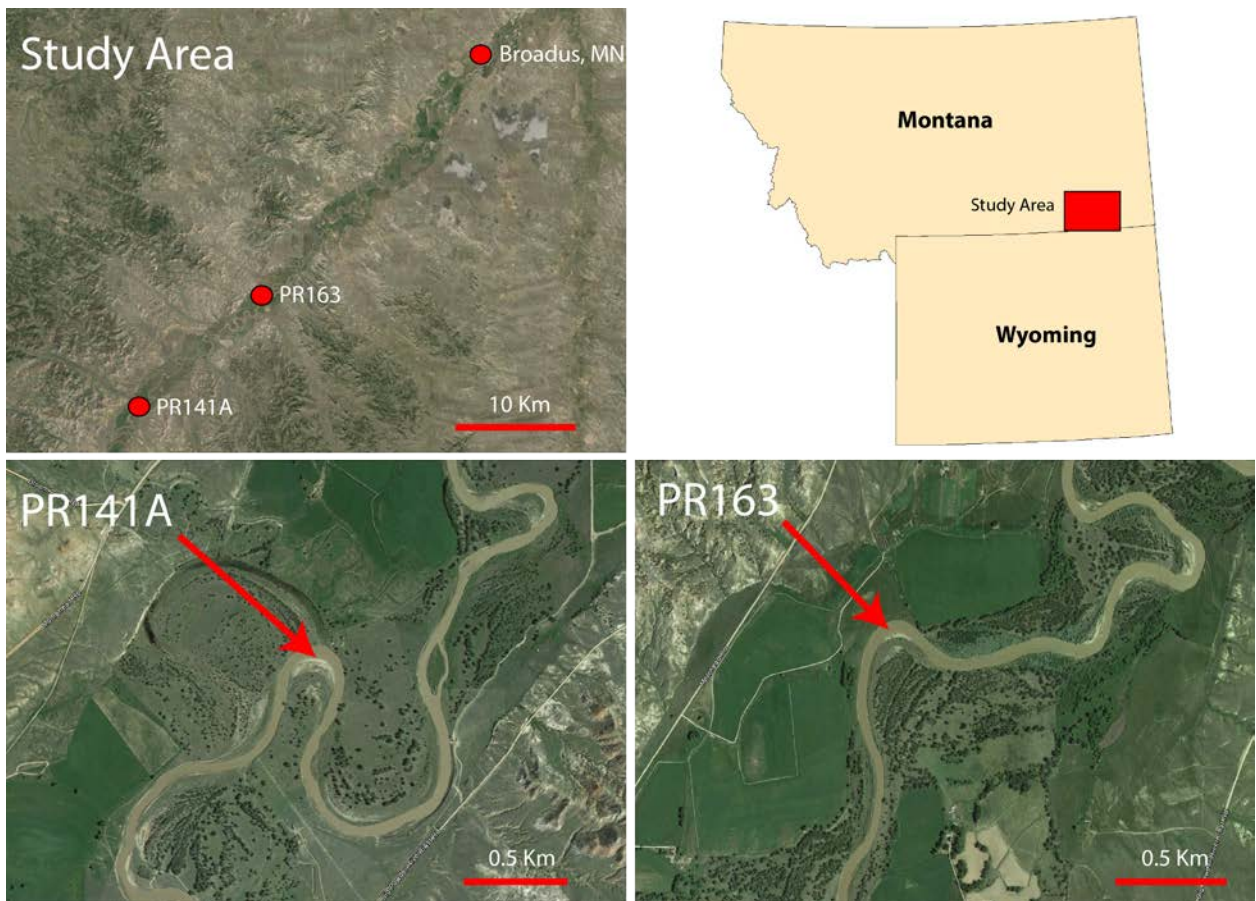


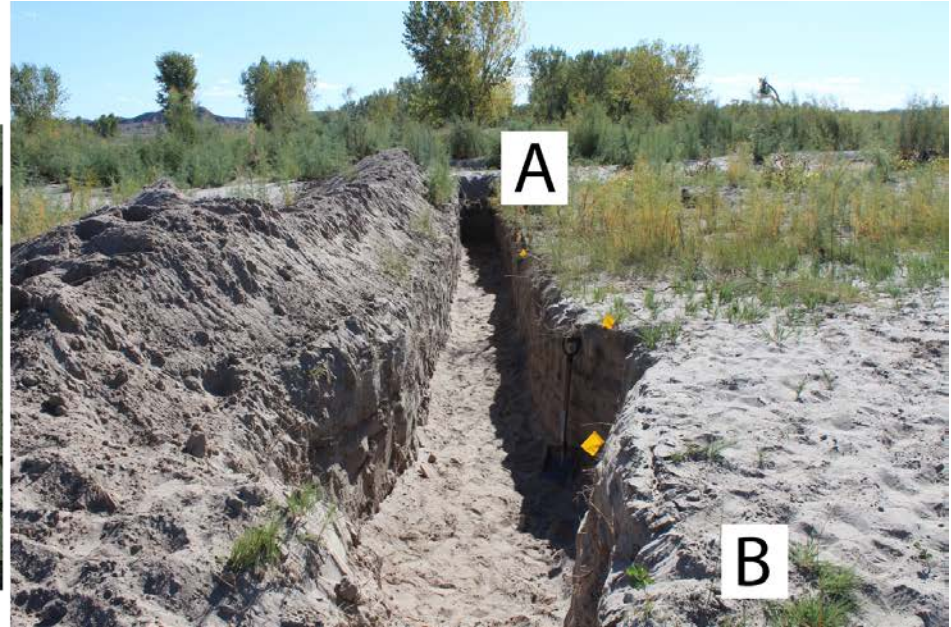
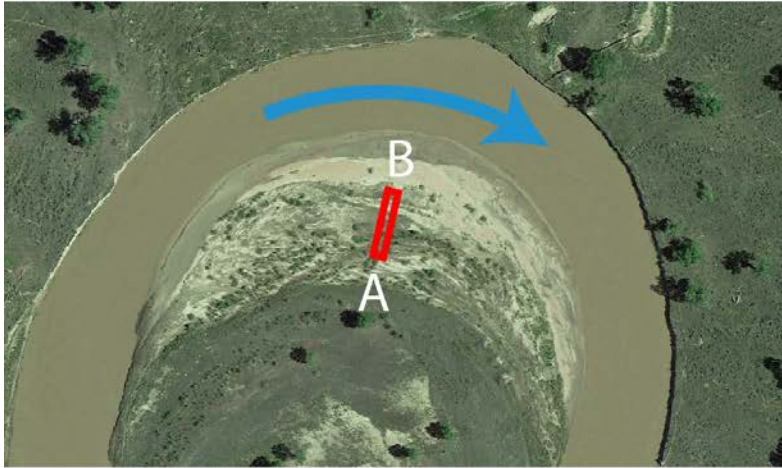
Figure 17: Maps showing relative location of PR141A and PR163 Point bar. Powder River has a general flow direction toward the northeast in this area.

2.7 Trenching a Point Bar, Correlating Yearly Surveys, and Analysis

Dr. Holbrook and I trenched two different point bar deposits on the Powder River. Owing to its fragmentary nature of deposition from yearly surveys we choose to trench point bar PR141A (Moody and Meade, 2014). We chose PR163, the second target point bar, because it

had a thick deposit from an extreme flood that occurred in 1978 allowing us to investigate the architecture of a known single flood event. Both point bars were trenched using spade shovels. We trenched PR141A a total of 17.5m in length, 1.5m in width, and 1.2-1.3m in depth. Due to difficulty trenching through more gravelly deposits in PR163 we trenched it 6.0m in length, 1.3m in width, and 1.46m in depth (Figure 18 and 19).

Moody and Meade (2014) have conducted yearly surveys of both PR141A and PR163 since the big flood event in 1978. This allows opportunity to constrain specific deposits within the trenches to different time intervals. Trenches are excavated two meters downstream and parallel to the survey line as to not disrupt the line for future surveys. In the location of interest, flags were placed every 5m along the survey line stations. At each flag, I measured the current elevation of the trench as well as the depth to the bottom of the trench. Using cross sections developed by Moody and Meade (2014) of the two trenches, I matched the elevations I recorded at each flag and located its position on the cross sections (Figures 20 and 21). I then matched the elevation of the tops of each survey year with the elevations within my trenches. Using Adobe Illustrator, I projected a line from flag to flag that would represent the time each survey was taken and draped it onto the panorama photo to constrain the position of the bar at each survey time.



PR141A Trench

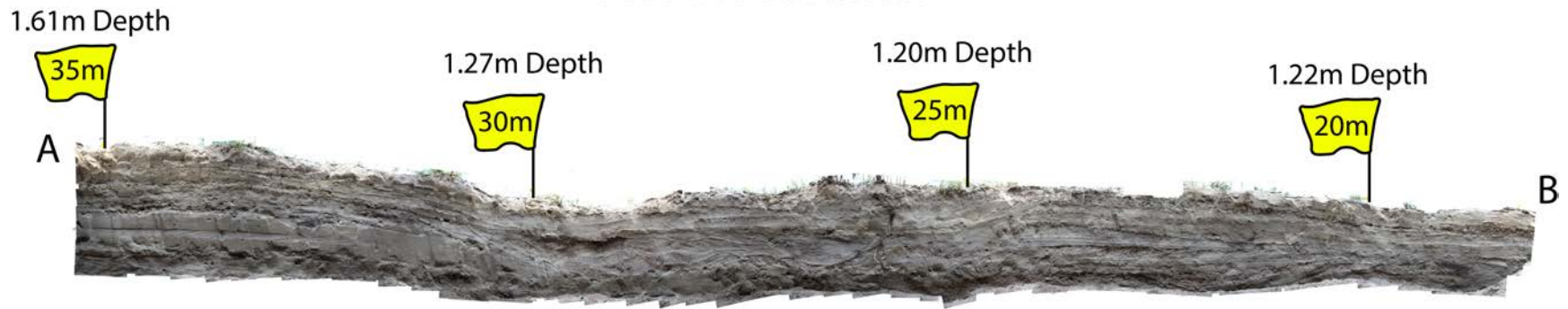
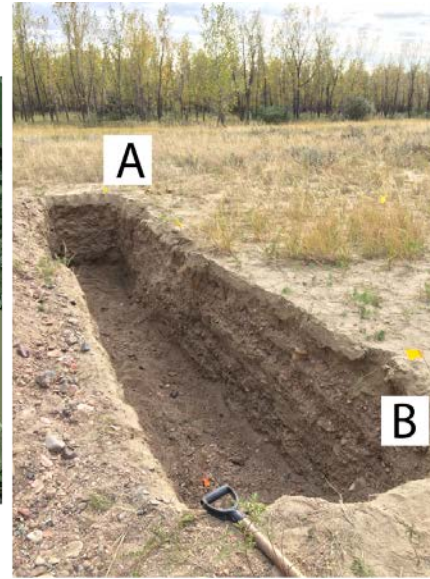
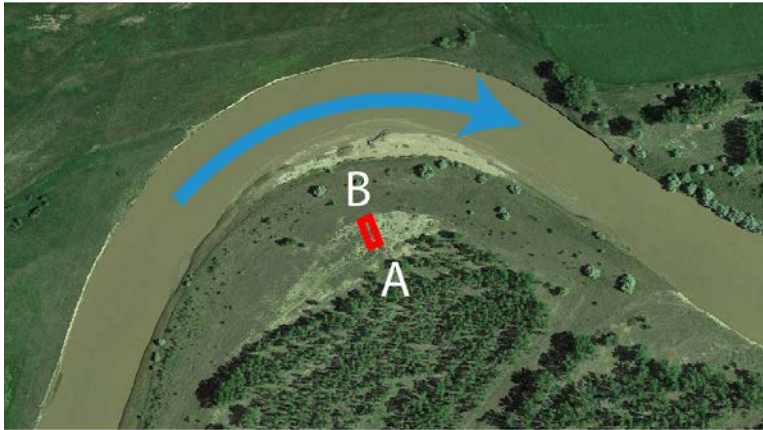


Figure 18: PR141A Trench. Location of trench shown in upper left photo. Easterly channel flow direction at PR141A point bar. Upper right photo shows a ground view of trench looking landward. Bottom image is panorama of PR141A trench. Flags mark specific points along survey line that represent the distance from a stationary pin.



PR163 Trench

1.46m Depth

25m



Figure 19: PR163 Trench. Location of trench shown in upper left photo. Easterly channel flow direction at PR163 point bar. Upper right photo shows a ground view of trench looking landward. Bottom image is panorama of PR163trench. Flag marks specific point along survey line that represents the distance from a stationary pin.

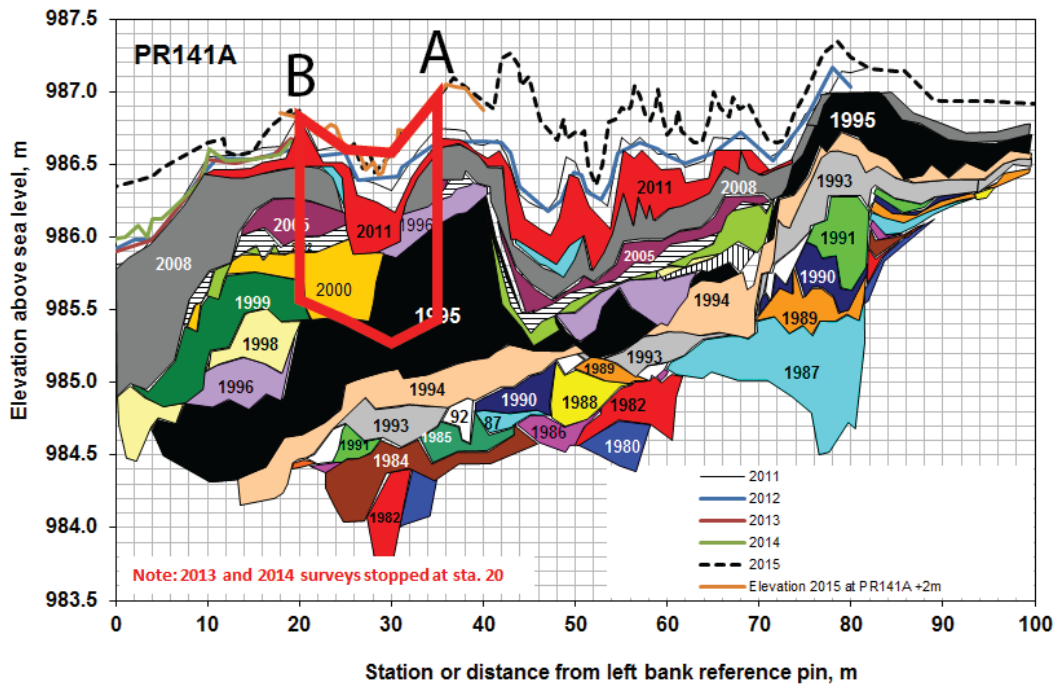


Figure 20: Modified from (Moody and Meade, 2014). Cross section of PR141A point bar from survey line. Portion outlined in red is the exposed area of trench in panorama. Trench is parallel and approximately two meters east of survey line. Flags along trenches correlate with distances from left bank reference pin.

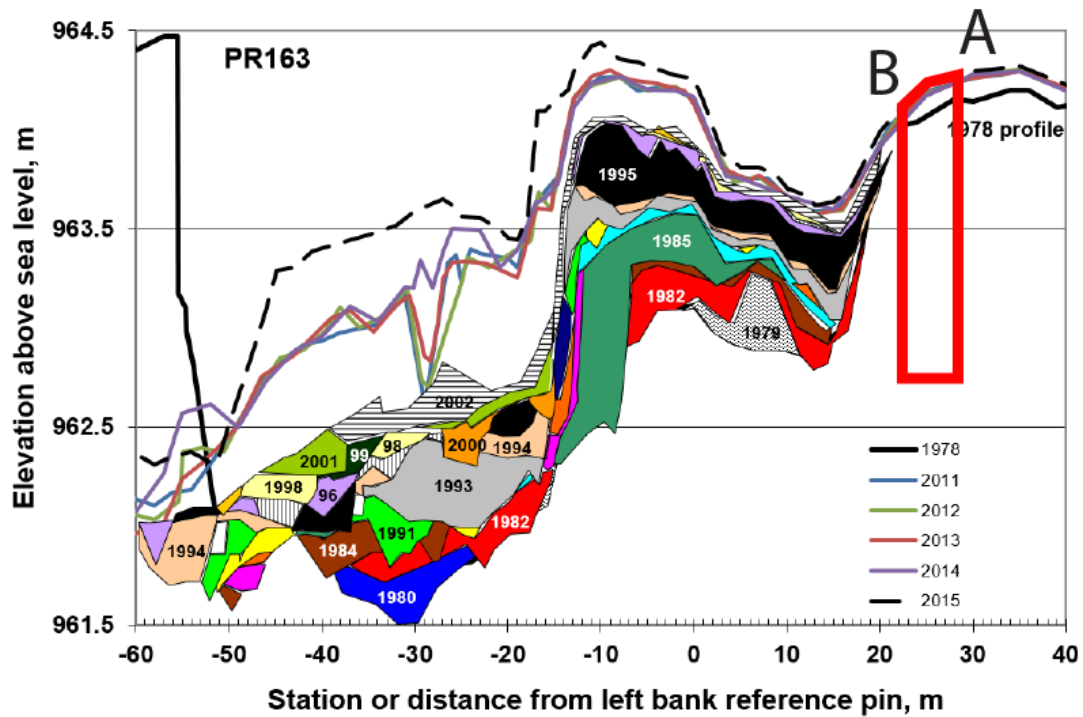


Figure 21: Modified from (Moody and Meade, 2014). Cross section of PR163 point bar from survey line. Portion outlined in red is the exposed area of trench in panorama. Trench is parallel and approximately two meters east of survey line. Flag along trench correlates with distances from left bank reference pin.

I measured stratigraphic sections at every flag station for the trenches. I recorded lithology, grain size, and sedimentary structures. I measured four sections at PR141A and two sections at PR163. After completing each section, I used an SLR Canon EOS Rebel T3i camera to document photos of each trench. Each wall of interest was flattened and brushed clean prior to taking photos to enhance the appearance of sedimentary structures. Beginning near the bottom corner of the trench I took a set of photos that followed the pattern left to right and then right to left until the entire trench was imaged. I also took a similar second set of photos that followed the pattern bottom to top and then top to bottom. I had approximately 40% overlap between each photo to improve photo stitching. Prior to photo stitching, I reduced the file size of all photos 30% to decrease the memory size of the panoramas. File size reduction did not interfere with observing fine scale architecture because of the short (~1m) photo distance. I imported photos into a software called PanoEdit for photo stitching. This software excels at stitching large batches of photos. A total of 356 photos were stitched together for PR141A trench and 146 photos for PR163 trench. Architectural-element analysis was then applied to these strata according to the procedures discussed above.

CHAPTER 3

RESULTS

3.1 Stratigraphic Sections Dinosaur Provincial Park

For the entire point bar story, we identified seven lithologies and five types of drapes. Lithologies consist of sand, siltstone, mudstone, peat, clayey peat, and composite soils from the floodplain beneath the point bar story and the floodplain capping the point bar above. Overall, the point bar story was sandy with a general fining upward trend. The finer scale stratigraphic sections focused on the point bar and each reveal similar lithologies.

3.1.1 Stratigraphic Sections of Point Bar Story

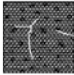
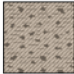




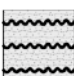




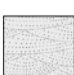



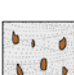
Below the point bar story is floodplain material. This composite soil material consists of blocky to angular peds, some organics, bone chips, and no sedimentary structures owing to heavy pedogenic reworking. Above this composite soil lies the base of the point bar. The surface separating the point bar and floodplain beneath is sharp and easily mapped across the study area. A buff colored, lower medium-grained, well-sorted, well-rounded, and somewhat poorly indurated sandstone dominates the lower portion of the point bar. Sedimentary structures within this sandstone include planar and trough cross sets, parallel planar laminations, and ripples. Siltstone to mudstone drapes discussed later commonly cap sandstone bodies.

The upper portion of the point bar changes to an abundance of thin interbedded fine sandstones, siltstones, and mudstones. Sedimentary structures include centimeter sized cross sets and an abundance of ripples and parallel planar laminations. Organics commonly drape sedimentary structures in this interval. Near the top of the point bar is an abundance of unconsolidated 6-14cm layers of silt, mudstone, claystone, and peat to peaty clay material. Capping the point bar is a composite soil that was not measured but is consistently over a meter

thick. The composite soil is composed of blocky to angular peds and an abundance of root casts (Figure 22).

3.1.2 Drape Types

We identified five different drape types that commonly cap sandstone bodies (Figure 23). Sedimentary structures seen within these drapes range from small-scale ripples to parallel planar laminations. The first and most common drape, Type A drape, ranges from silt to lower fine sand and is commonly a dark reddish rust color. Type A drape is poorly indurated. Type B drape is similar to Type A drape, but is well indurated with siderite cement. A single drape can vary laterally as a Type A or Type B drape. Type C drapes are composed of a poorly indurated light grey mudstone. Type D drape is similar in composition as Type C, but is cemented by siderite. A single drape can also vary laterally as a Type C or D drape. Lower plane bed laminations are the dominate sedimentary structure seen in Type C and D drapes. Type E drapes are made of very fine sand and are rich in interbedded organic layers. Type E drapes are commonly rippled or lower plane bed laminated.

-  Composite Soil. Blocky to platy Peds. Abundant root channels and carbonaceous material. 10 YR 6/3
-  Peaty Clay (50/50)
-  Well sorted, unconsolidated, very fine sand
-  Well sorted parallel laminated sand, ranging from very fine to lower medium sand with medium scale cross sets
-  Well sorted ripple laminated sand, ranging from very fine to lower medium sand with medium scale cross sets
-  Type E- Fine sand interbedded with organic rich laminations
-  Type E- Rippled fine sand with thin interbedded organic rich layers
-  Type D- Cemented and poorly sorted planar laminated (sometimes ripple laminated) silt to mud.
-  Type C- Poorly sorted and poorly cemented, planar laminated (sometimes ripple laminated) silt to mud.
-  Type B- Poorly sorted and cemented, planar laminated (sometimes ripple laminated) very fine sand to silt
-  Type A- Poorly sorted and poorly cemented, planar laminated (sometimes ripple laminated) very fine sand to silt
-  Well sorted planar laminated sand, ranging from very fine to lower medium sand with medium scale cross sets
-  Composite Soil No preserved sed structures. Blocky angular peds Gley 1 6/3 Scattered bone chips/sparse organics
-  Cross laminated sand with some organic rich laminations
-  Mudstone matrix with subrounded silty rip-up clasts
-  Sand with silty rip-up clasts

> > Organic rich sediment

8.25m

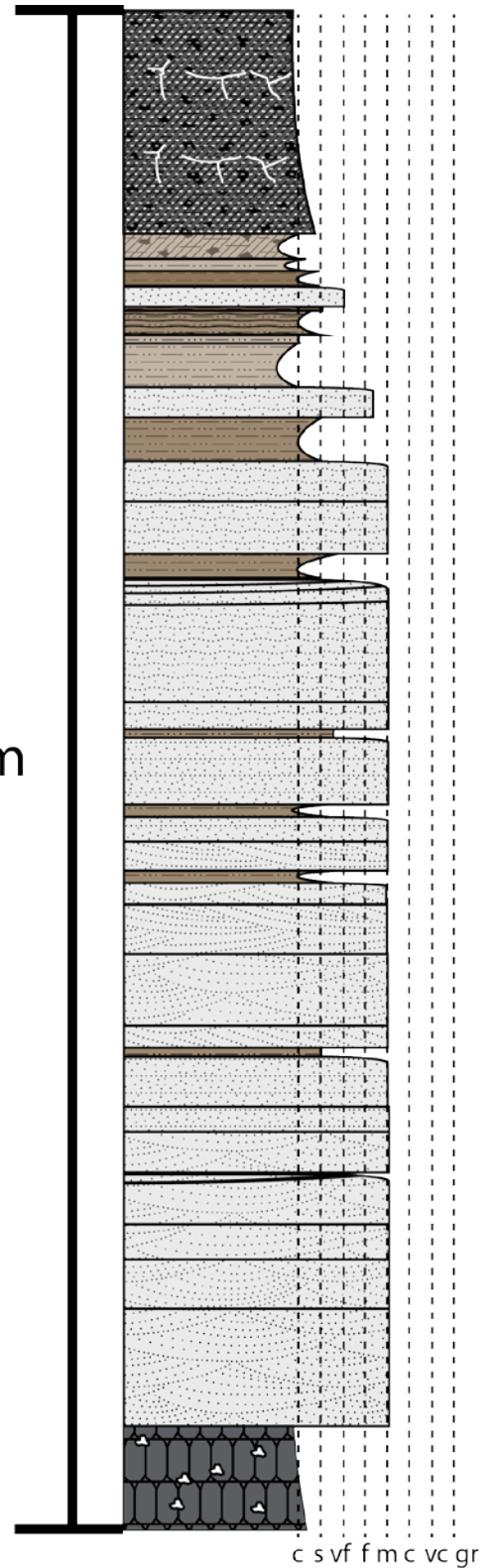


Figure 22: Modified from (Palmer, 2015). Legend and stratigraphic section of entire point bar story.

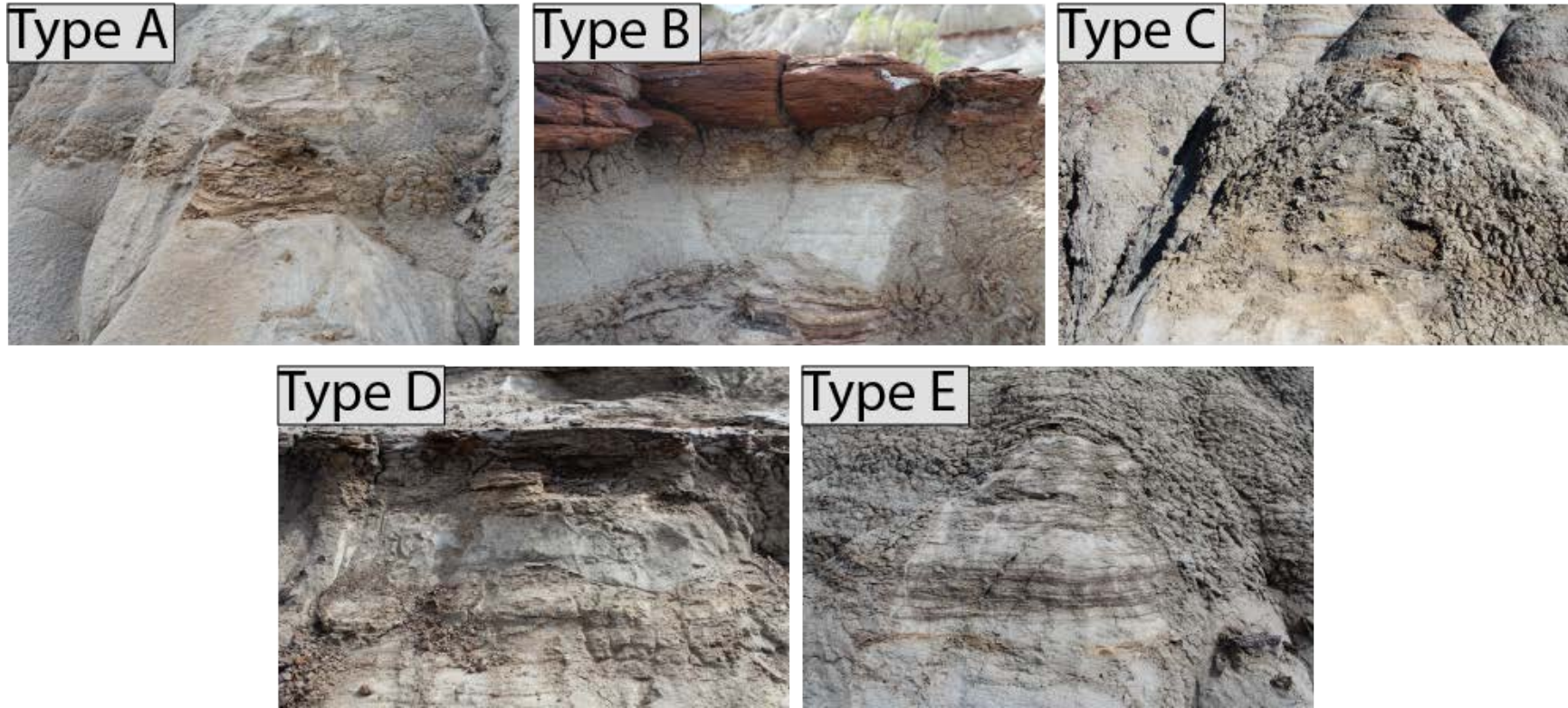


Figure 23: Examples of the five drape types seen in the field. Type A is a very fine sand to siltstone and poorly indurated. Type B is similar in grain size to Type A, but it well cemented by siderite. Type C is a poorly indurated grey mudstone. Type D is similar to Type C, but is cemented (note the bench of Type D in the lower left image). Type E is made of fine to very fine sand that is interbedded with abundant organic rich layers.

3.1.3 Stratigraphic Section of Accretionary Bodies

Chapter 3.1.1 discussed the general stratigraphy of the point bar. This section of the chapter focuses on the stratigraphy within single accretionary bodies bound by 3rd order surfaces. Near the base of an accretionary body is a surface that commonly scours into or onlaps the body beneath. Accretionary bodies range from medium-grained-to-fine grained sandstones. Type A through E drapes are present within the sandstone bodies as well. Although commonly found as a cap to the accretionary body, these drapes may appear at any location within a single accretionary body in a vertical section. Typically, accretionary bodies have a fining upward trend from lower medium-to-fine sandstone leading up to a drape. A single accretionary body, however, can contain a series of fining upward trends. Likewise, it is not uncommon for an accretionary body to be completely of one-grain size throughout and show no sign of fining upward.

Sedimentary structures include planar to trough cross sets that range in size from centimeters to tens of centimeters. Additional sedimentary structures include ripples and lower plane bed laminations. Typically, the pattern of sedimentary structures leading up to a drape in an accretionary body changes from cross laminae-to-ripples-to-laminations. However, there are instances where an accretionary body is of only one sedimentary structure or can vary from ripples to cross sets and back to ripples. It is also not uncommon for organics to drape individual laminae at any location of an accretionary body in a vertical section. Furthermore, some accretionary bodies contain an abundance of subrounded-to-rounded clasts of Type A drapes. These clasts are usually associated with a single cross set (Figures 24 and 25). See appendix for detailed view of sections.

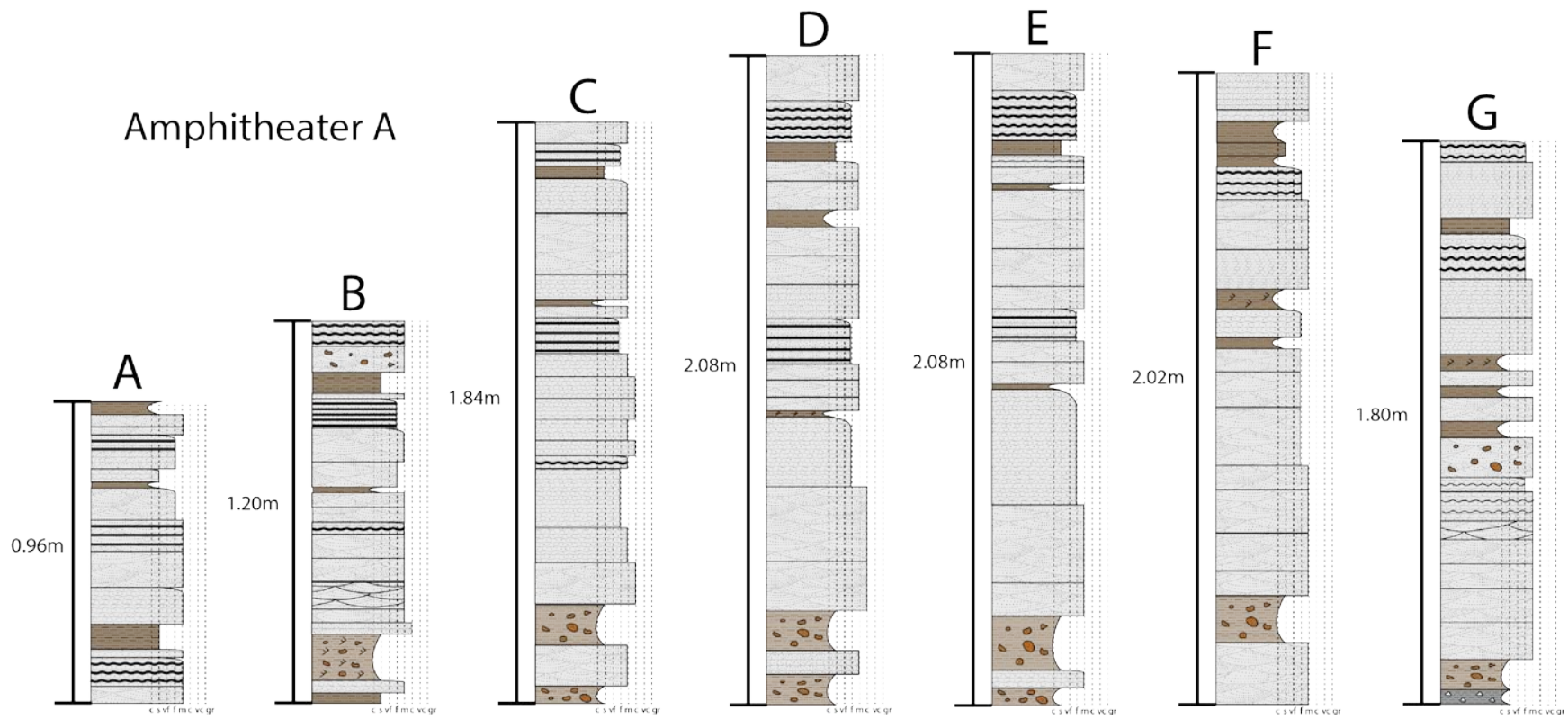


Figure 24: Stratigraphic sections A through G of accretionary bodies in Amphitheater A. Sections represent the lithology seen along the lower half of the lower point bar unit. Note the fining upward trends seen within accretionary bodies. Lithologies are marked along the vertical dashed lines and geologic swatches represent bedforms. See figure 11 for location of Amphitheater A and figure 12 for location of each section.

Amphitheater B

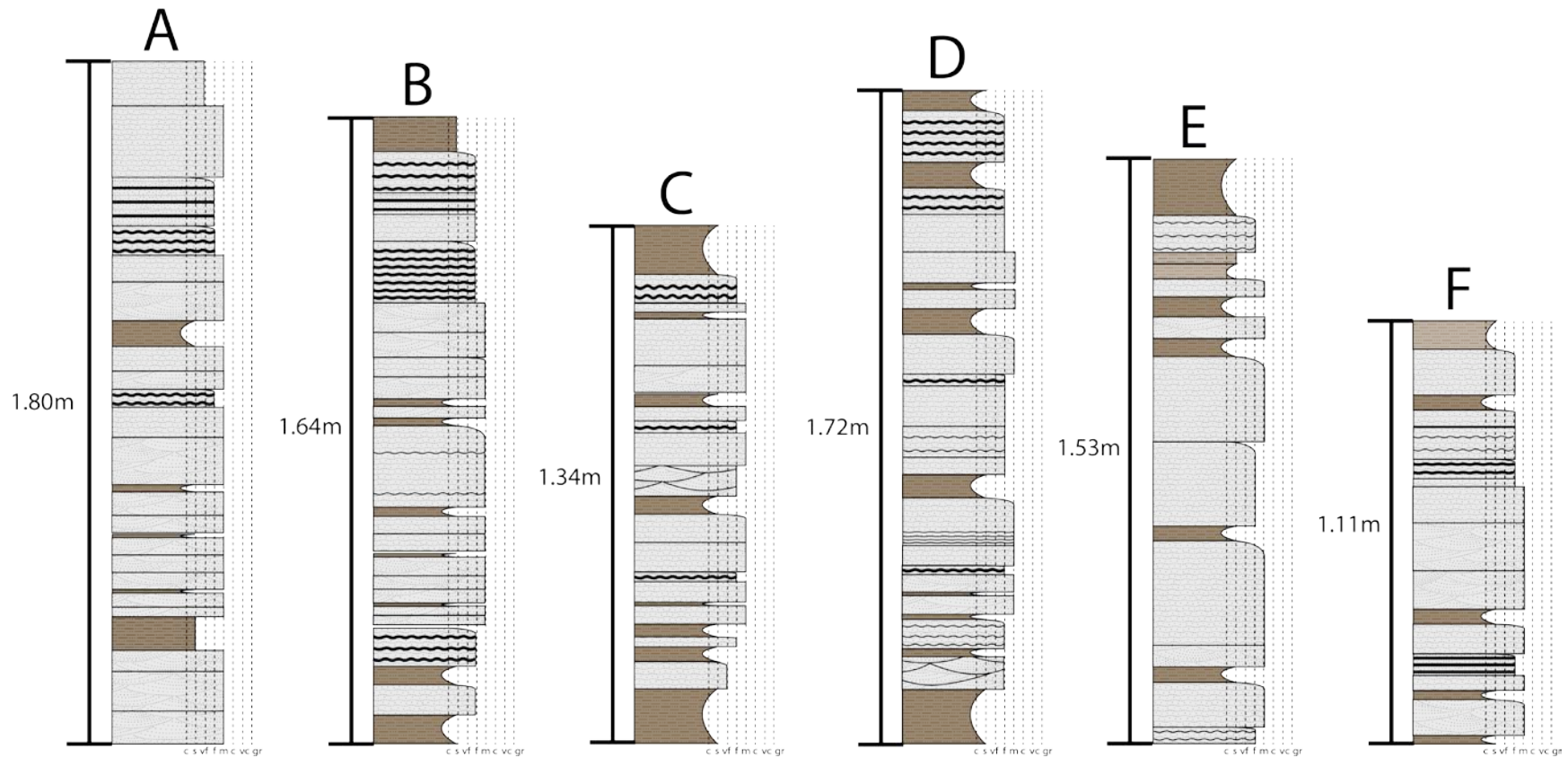


Figure 25: Stratigraphic sections A through F of accretionary bodies in Amphitheater B. Sections represent the lithology seen along the upper half of the lower point bar unit. Note the fining upward trends seen within accretionary bodies. Lithologies are marked along the vertical dashed lines and geologic swatches represent bedforms. See figure 11 for location of Amphitheater B and figure 13 for location of each section.

3.2 Architectural-Element Analysis

I performed architectural-element analysis along the entire 3D model, which is broken up into two amphitheaters (Figure 31). At each amphitheater, I performed fine scale architectural-element analysis to reveal architecture of additional orders unresolved by the model. My interpretation of the study area revealed seven surface orders.

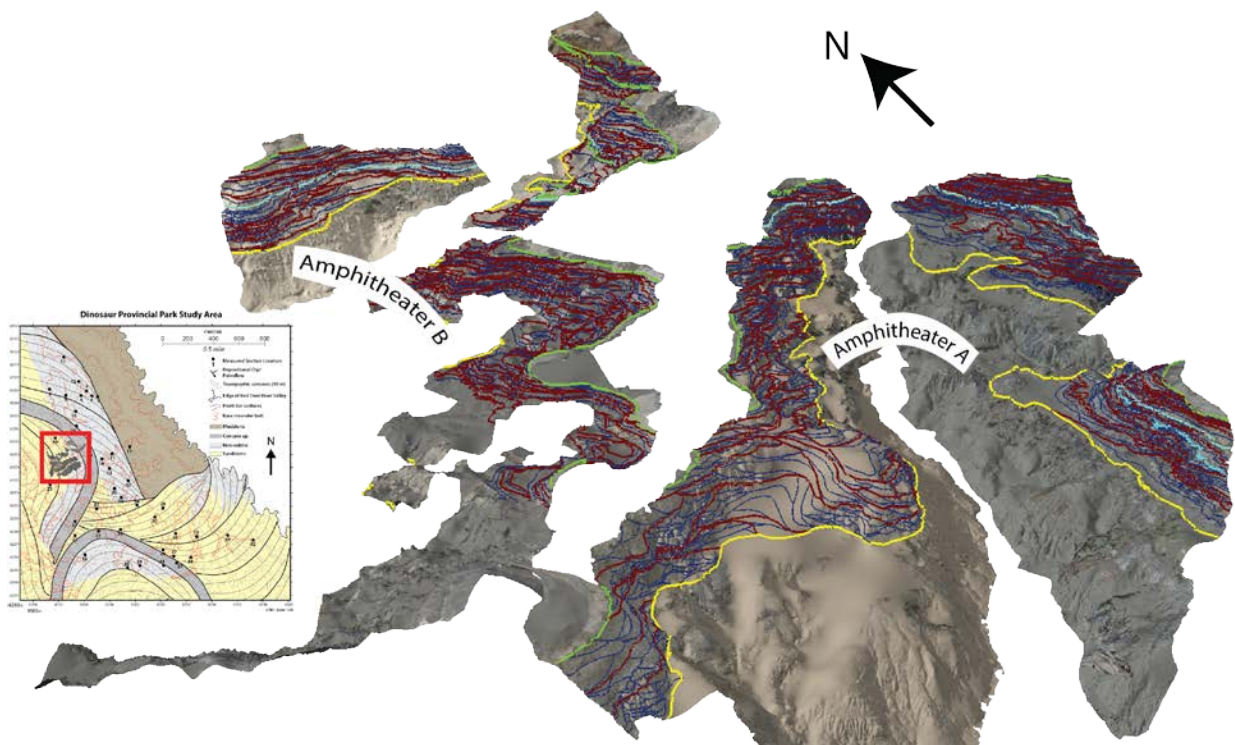


Figure 26: Full 3D model mapped using architectural element analysis. Sixth order surfaces are colored solar yellow. Fifth order surfaces are colored medium apple green. Fourth order surfaces are colored light blue. Third order surfaces are colored dark amber red. Second order surfaces are colored dark navy.

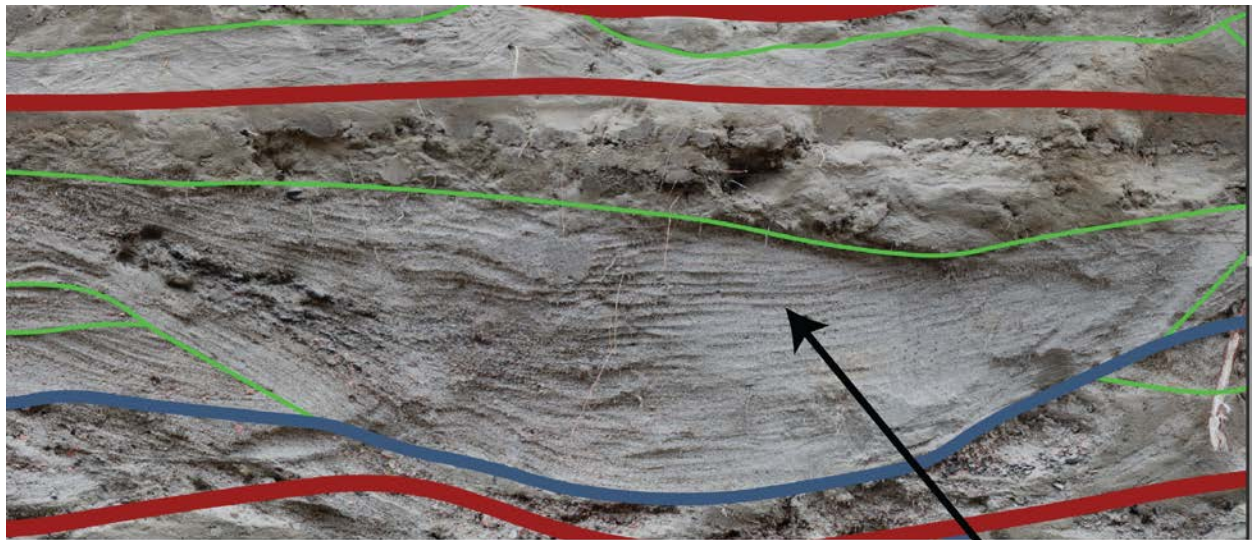
3.2.1 Zero Order Surface

The smallest of all architectural surfaces, the zero order surface, is bound by 1st order surfaces, but does not bind surfaces. Instead, these surfaces represent individual laminae (Figure 27). Even at this fine scale, it is not uncommon for clasts of coal and pebbles to line zero order surfaces (Figure 28). These zero order surfaces and their bounding 1st order surfaces are defined

as the initial surfaces for architectural order assessment by convention (Miall et al., 1985; Miall, 1986).

3.2.2 First Order Surface

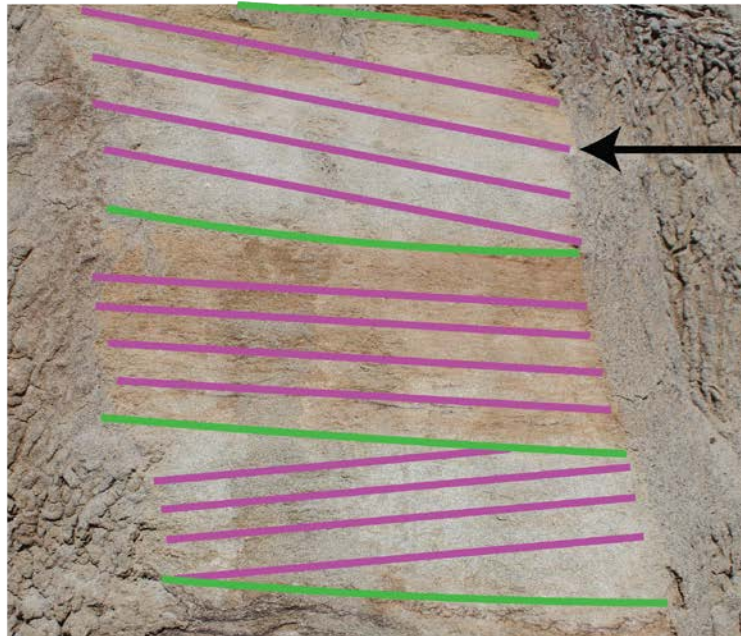
First and zero order surfaces are not present in the 3D model owing to lack of resolution. I used fine scale photos in the field to map and interpret these surfaces (Figure 27). 1st order surfaces bind zero order surfaces and map as a surface that binds either a set of planar cross laminae, trough cross laminae, or parallel planar laminations. It is rare for these surfaces to extend the entire length of a 2nd order surface before a younger surface cuts it off. First order surfaces are typically only a few meters in length. The zero order surfaces that are bound within 1st order surfaces are also indicators of paleocurrent flow of the point bar. Palmer (2015) provides a rose diagram of paleocurrent measurements of this point bar with an average flow direction of 107°.



First order
Cross Set #3

First order
Cross Set #2

First order
Cross Set #1



Zero order
surfaces

Figure 27: Close up images of 1st and zero order surfaces. First order surfaces are colored green and zero ordered surfaces are colored light purple. The upper image from PR141A trench shows a close up of a 1st order surface with parallel zero order surfaces within it. The lower image from the ancient point bar in Dinosaur Provincial Park shows three 1st order cross sets with zero order surfaces oriented in different directions.



Figure 28: Images of point bar platform. Upper image shows point bar platform lined with large pebbles along its surface. Lower image shows close up of point bar in lower portion of photo with pebbles scattered throughout.



3.2.3 Second Order Surface

Second order surfaces bind 1st order surfaces and make up accretionary bodies. Second order surfaces bind lobate bodies and are consistently cut by younger 2nd order surfaces as well as 3rd order surfaces. Bodies bound by 2nd order surfaces are thus highly fragmentary. Many of these surfaces do not extend the entire length of a single 3rd order accretionary body before being truncated by a younger surface. However, there are some instances where a second order surface does extend the length of an accretionary body. Surfaces range in length from meters to tens of meters. On average, second order surfaces are shorter than 3rd order surfaces. Sediments bound by 2nd order surfaces typically, but not consistently, have an overall fining upward trend. Similar to 3rd order surfaces, formation of 2nd order surfaces vary from composite constructional and single continuous surface (see Chapter 3.3).

3.2.4 Third Order Surface

Third order surfaces bind 2nd order surfaces and follow orientations of point bar accretion. Third order surfaces are consistently cut by younger 3rd order surfaces and typically have an elongated lobate geometry. Although some surfaces may be continuous for long distances, no single package of 3rd order surfaces extend along the entire bar (Figures 29-34). There are some surfaces that do downlap the 6th order surface above the floodplain beneath, but these do not extend upward for the bar thickness. Surfaces can range in length for meters to tens of meters, but are always cutoff by a younger surface at some point. Some surfaces follow the top of a drape while other surfaces may follow between sandstone bodies. Formation of these surfaces vary from composite constructional to a single continuous surface. Details of 3rd order surface construction features are expanded in Chapter 3.3. Although third order surfaces follow the general direction of

point bar accretion, there are differences in their orientations and dips. Chapter 3.4 describes orientation and pitch changes between these surfaces in more detail.

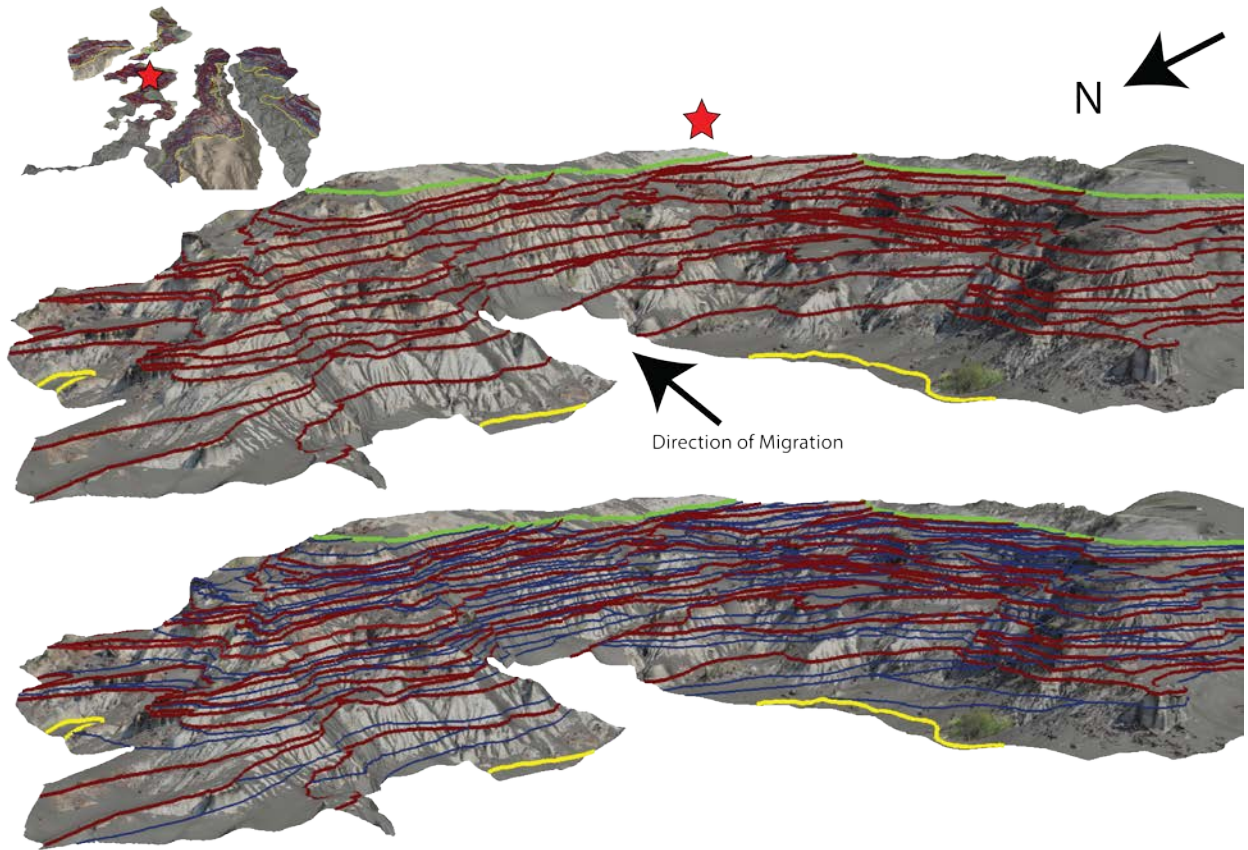


Figure 29: Broad scale view of 3rd order surfaces (upper image) as well as 3rd and 2nd order surfaces (lower image). Third order surfaces are colored in dark umber red and 2nd order surfaces are colored dark navy. General migration direction of 3rd order sets toward the east. Note how 3rd order surfaces do not extend the full length of the bar. Second order surfaces are lobate in geometry and there is no general direction of migration for these bodies.

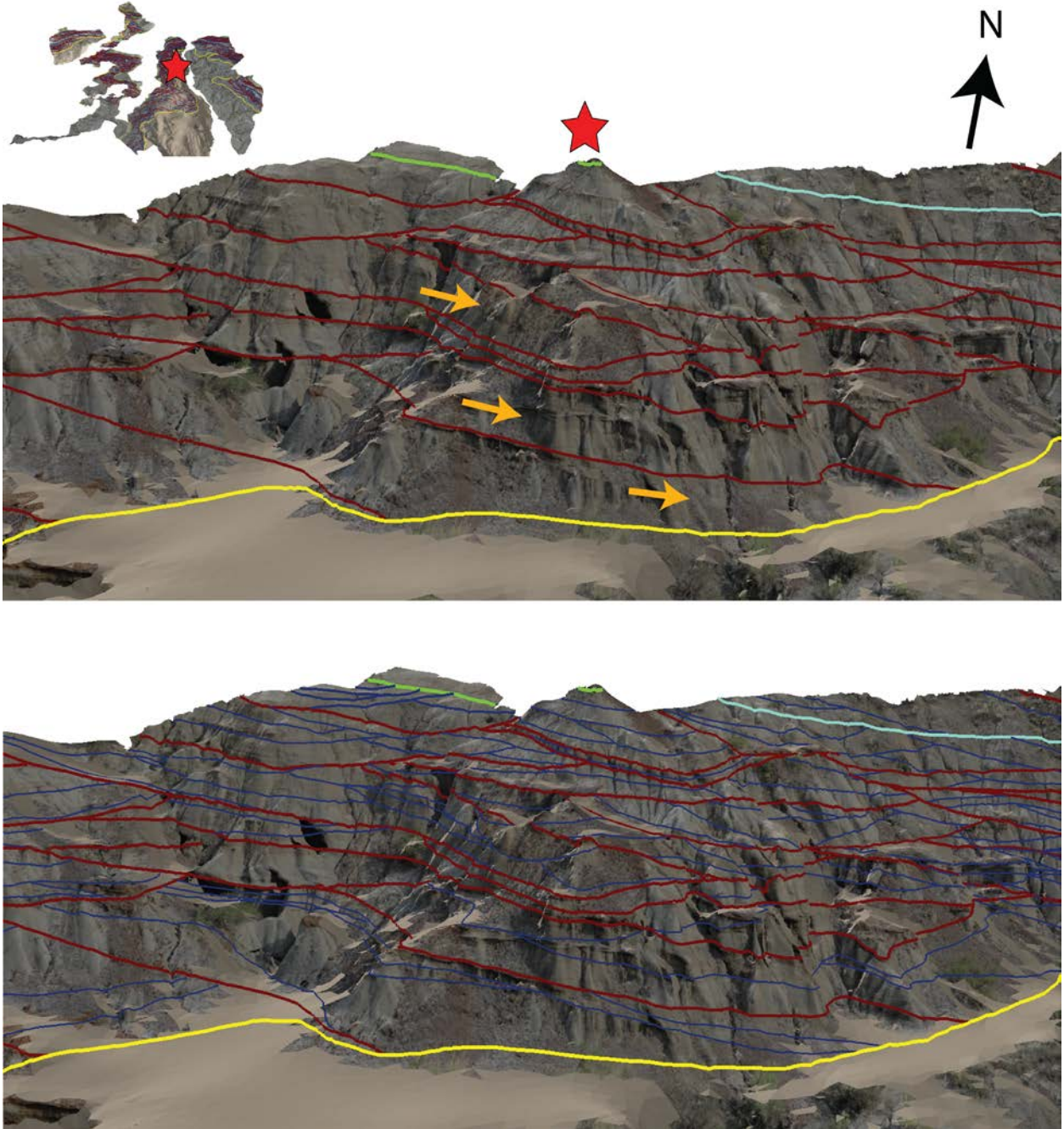


Figure 30: 3D model view of Amphitheater A where measured sections were taken. Third order surfaces seen in upper image as well as 3rd and 2nd order surfaces in lower image. Third order surfaces are colored in dark amber red and 2nd order surfaces are colored dark navy. General migration direction of 3rd order sets toward the east. Note how 3rd order surfaces do not extend the full length of the bar. Second order surfaces are lobate in geometry and there is no general direction of migration.



Amphitheater A

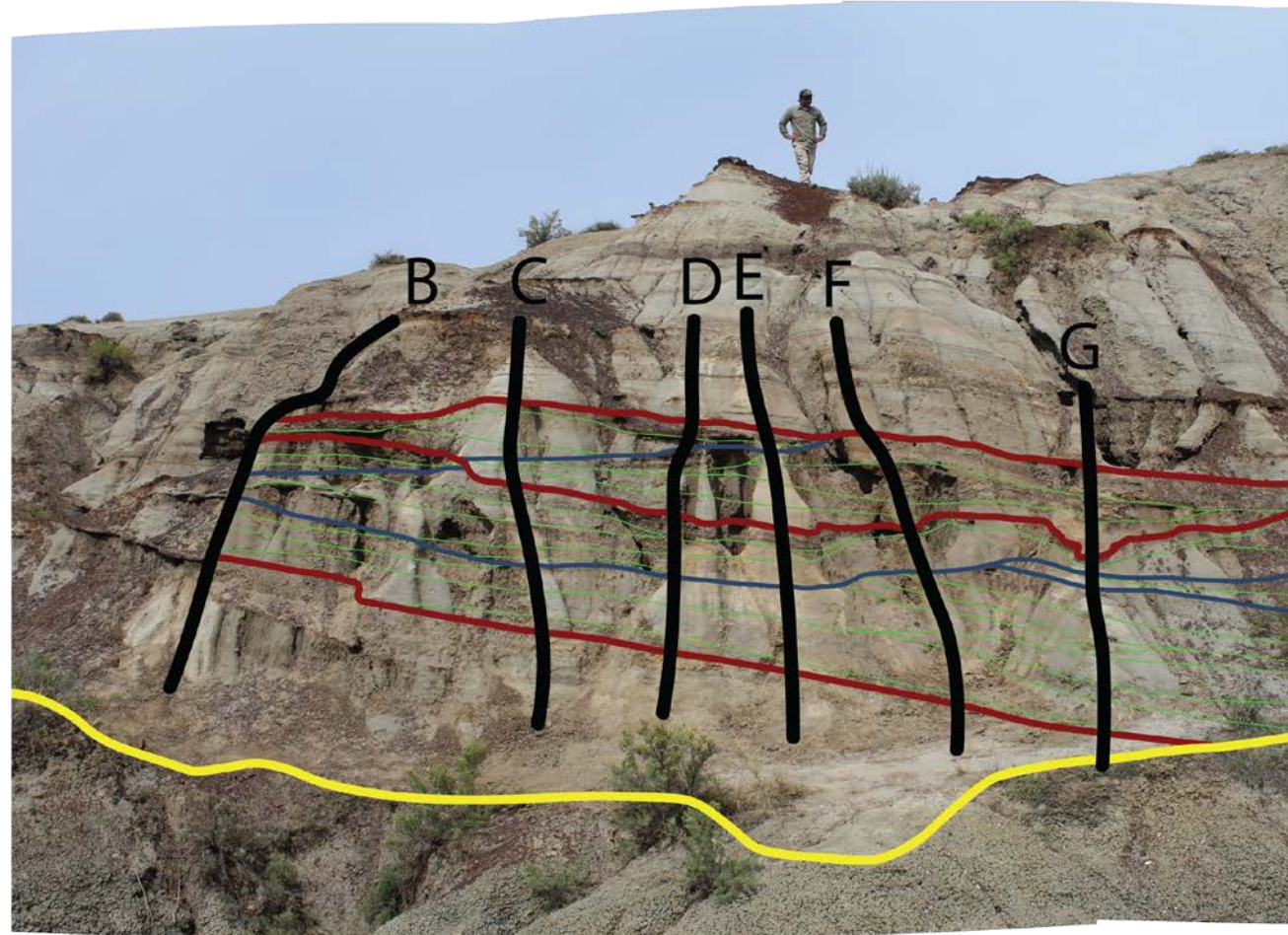
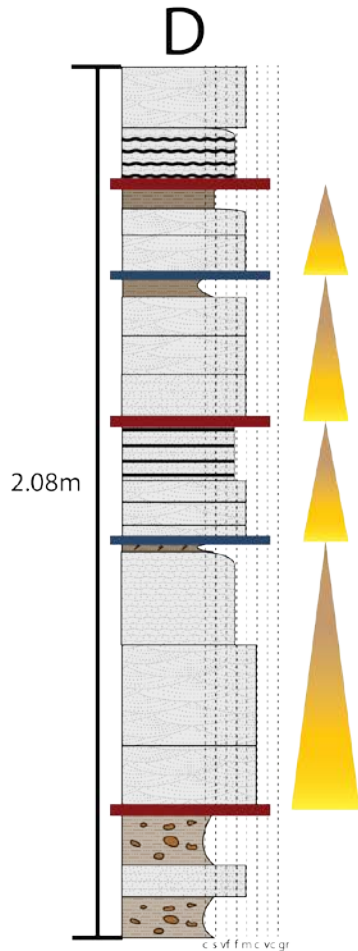


Figure 31: Photo of detailed sections in Amphitheater A. Close up of stratigraphic section D shows fining upward trends within 3rd order surfaces. Location of 3rd and 2nd order surface tops are marked on stratigraphic section. Fining upward trends are confined to individual 2nd order bodies that make up accretionary bodies.

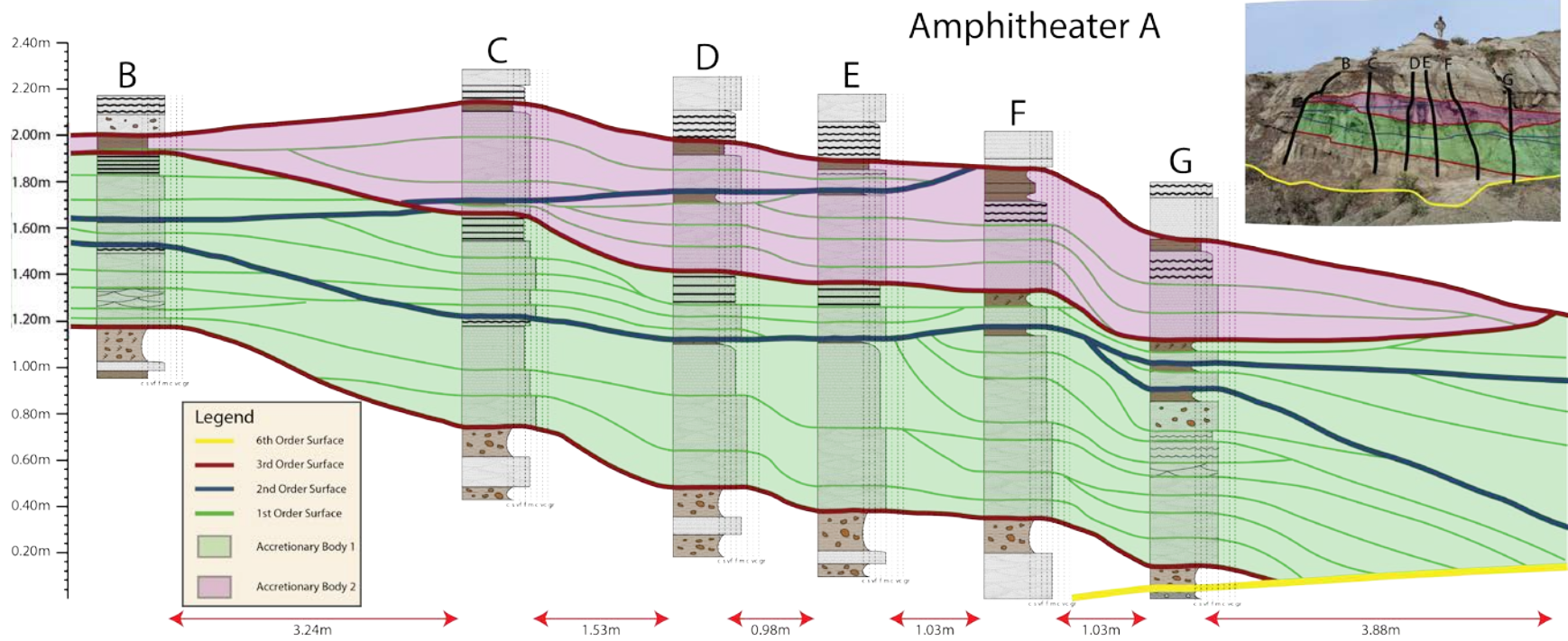
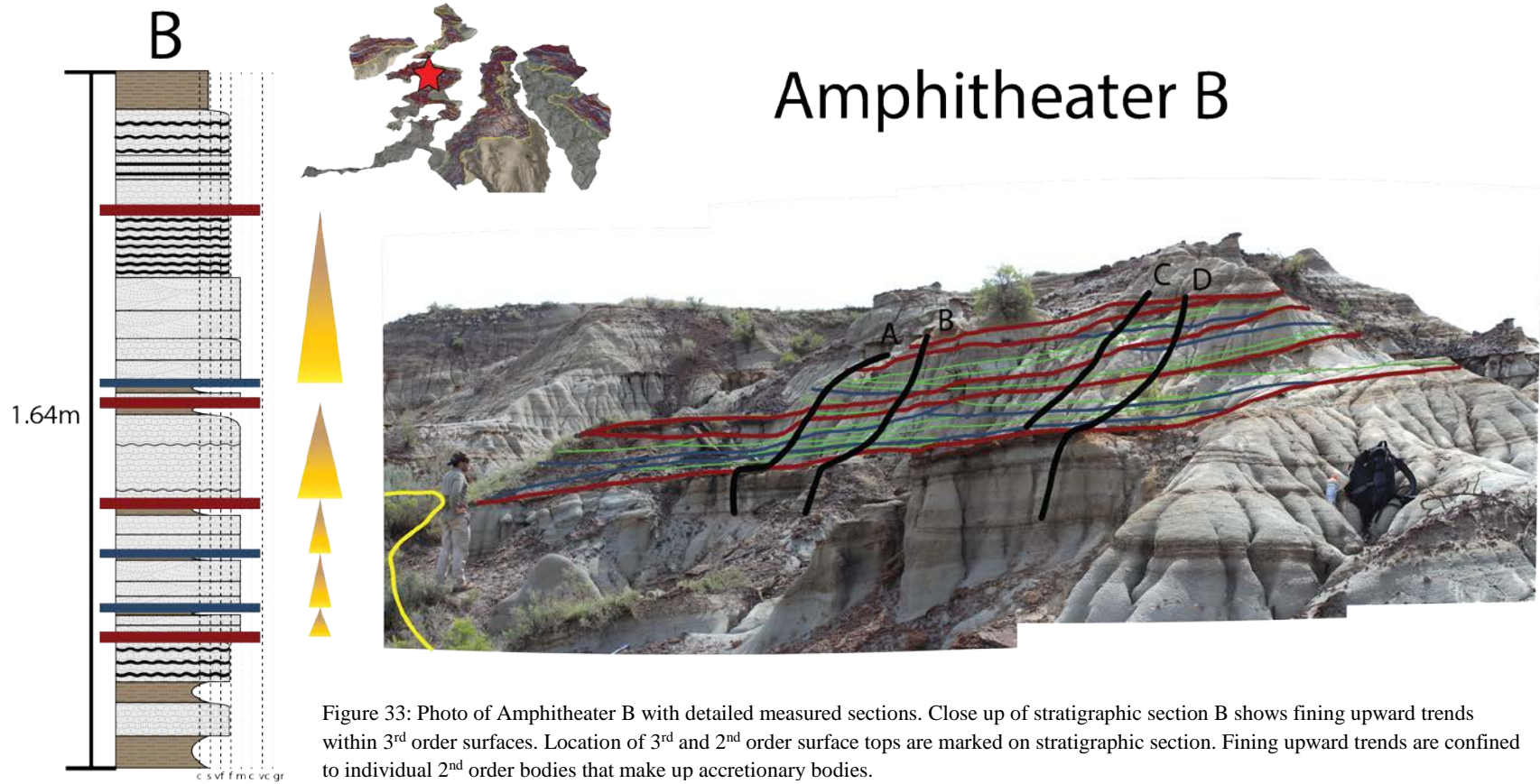


Figure 32: Correlation of Amphitheater A stratigraphic sections B-G in 2D. Each section contains two distinct accretionary bodies. Within each accretionary body are 2nd order unit bars. Accretionary bodies follow an easterly direction of migration. Second order unit bars are lobate in geometry and have no pattern in migration direction. Note how many of the unit bars show a fining upward trend. In some cases, unit bars may also show no fining trend.



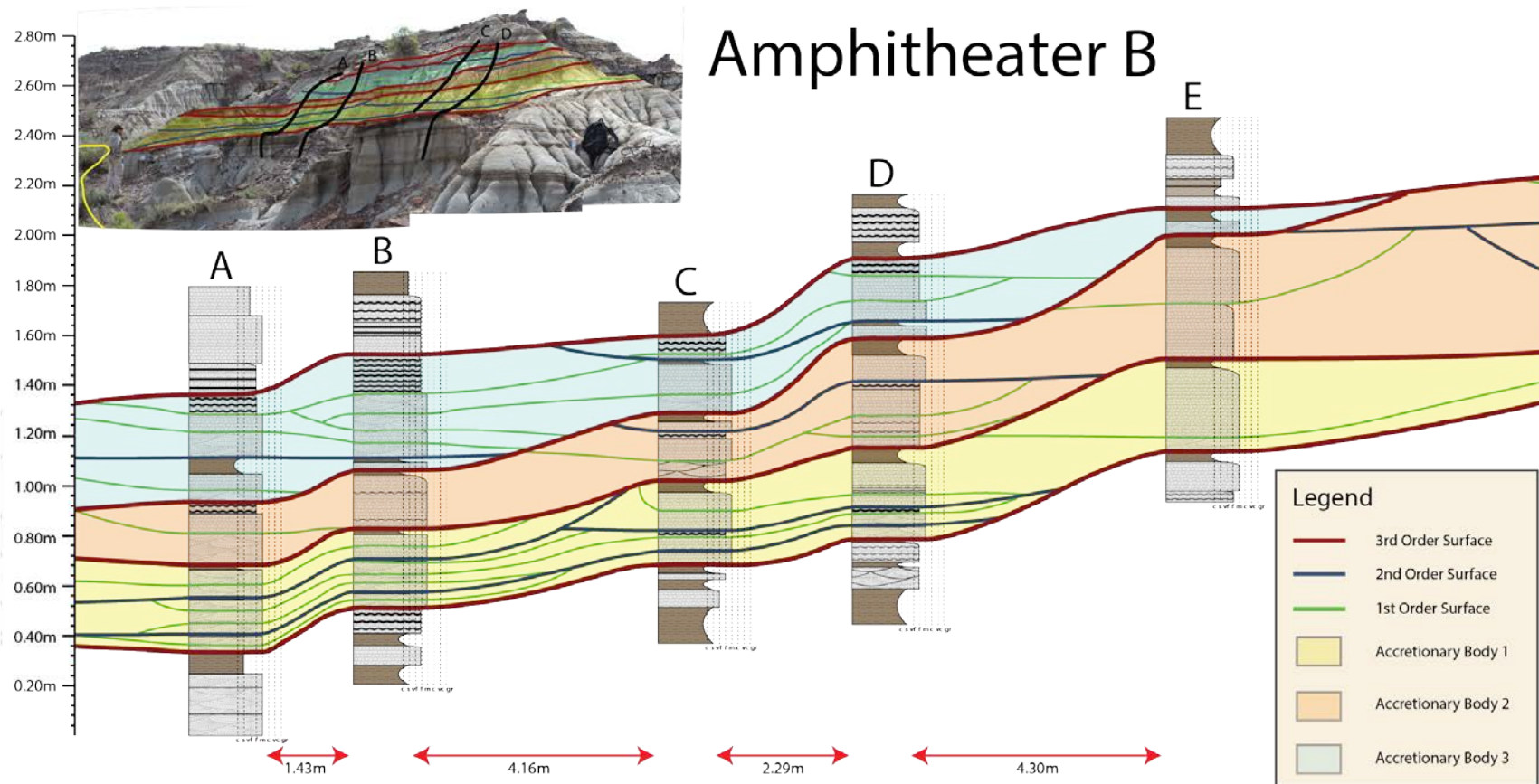


Figure 34: Correlation of Amphitheater B stratigraphic sections A-E in 2D. Each section contains three distinct accretionary bodies. Within each accretionary body are 2nd order unit bars. Accretionary bodies follow an easterly direction of migration. Second order bodies are lobate in geometry and have no pattern in migration direction. Note how many of the unit bars show a fining upward trend.

3.2.5 Fourth Order Surface

Fourth order surfaces bind 3rd order surfaces and map as a surface that separates a difference in accretion sets of the point bar. This surface maps as a boundary between the more sandy accretionary packages to more muddy accretionary packages. The basal 4th order surface maps near the channel at the termination of the point bar with several expressions at both amphitheatres (Figure 35).

3.2.6 Fifth Order Surface

Fifth order surfaces bind 4th order surfaces and map as a surface that separates the point bar from the floodplain material above and other bars of the same channel belt below (Figure 36). The top contact is of the same rank, but represents a gradational contact into the levee/floodplain deposits above rather than a surface. The basal surface crops out near the channel and separates the studied point bar from a separate bar story below. Beneath the 5th order surface are accretionary bodies that have a different orientation than the accretionary bodies above.

3.2.7 Sixth Order Surface (Master Surface)

The largest surface order, 6th order surface, binds the entire point bar story from top to bottom (Figure 37). This surface order maps as a sharp boundary between the base of the point bar and the floodplain beneath. Near the channel the 6th order surface binds the studied point bar as well as second bar story beneath. A similar basal scour for an overlying story is not present within the model owing to erosion. However, at other localities outside of the study area where more section is preserved above this does crop out.

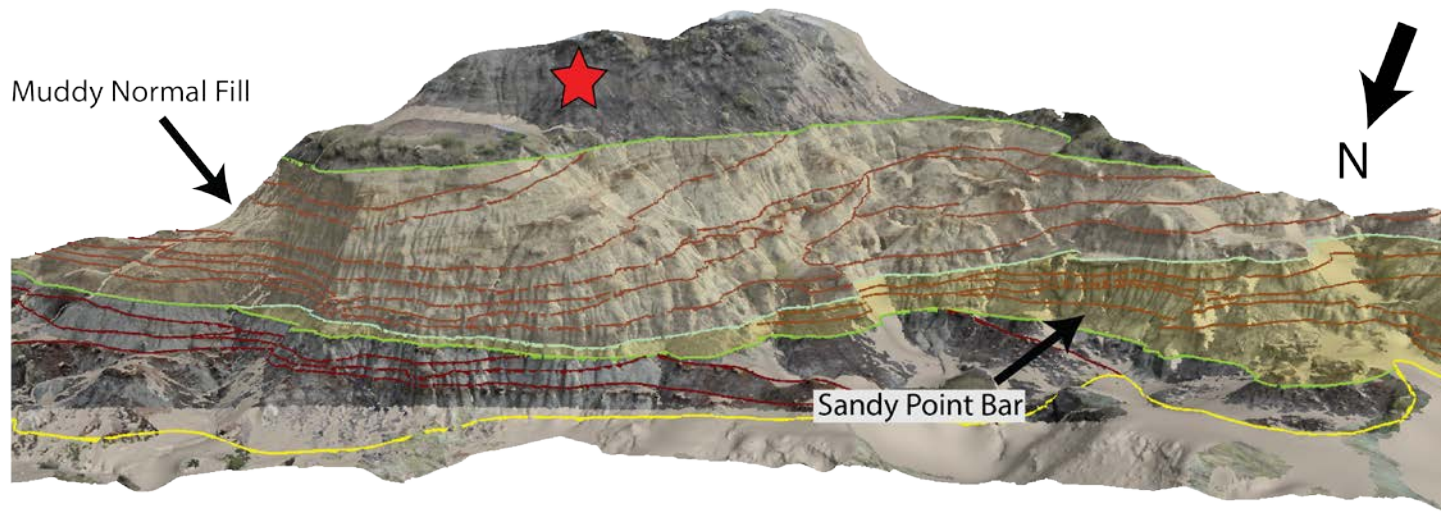
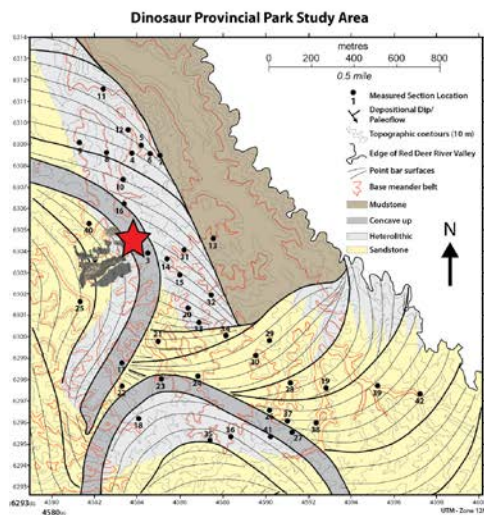


Figure 35: Fourth order surface marked in light blue. Accretionary bodies within the translucent tan fill show 3rd order accretionary bodies that are muddy. Accretionary bodies within the translucent yellow color fill show 3rd order accretionary bodies that are more representative of a sandy point bar. Red star marks a common point in this figure as well as figure 36.



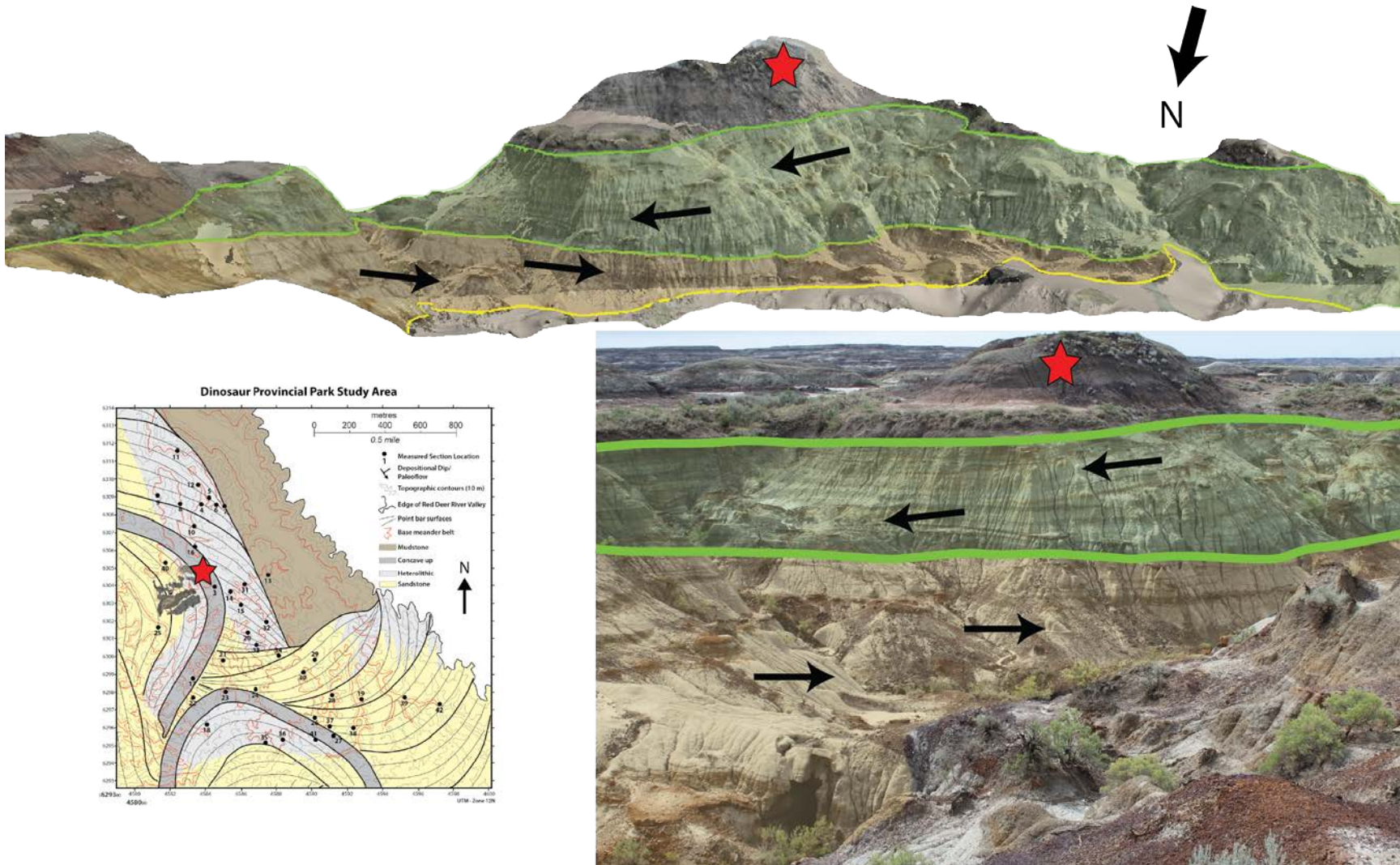


Figure 36: Fifth order surface marked in medium apple green. Accretionary bodies within the translucent green color fill show 3rd order surfaces migrating toward the east. Accretionary bodies within the translucent orange color fill show 3rd order surfaces migrating toward the west. Black arrows indicate the general direction of migration. Red star marks a common point for photos in this figure as well as figure 35.

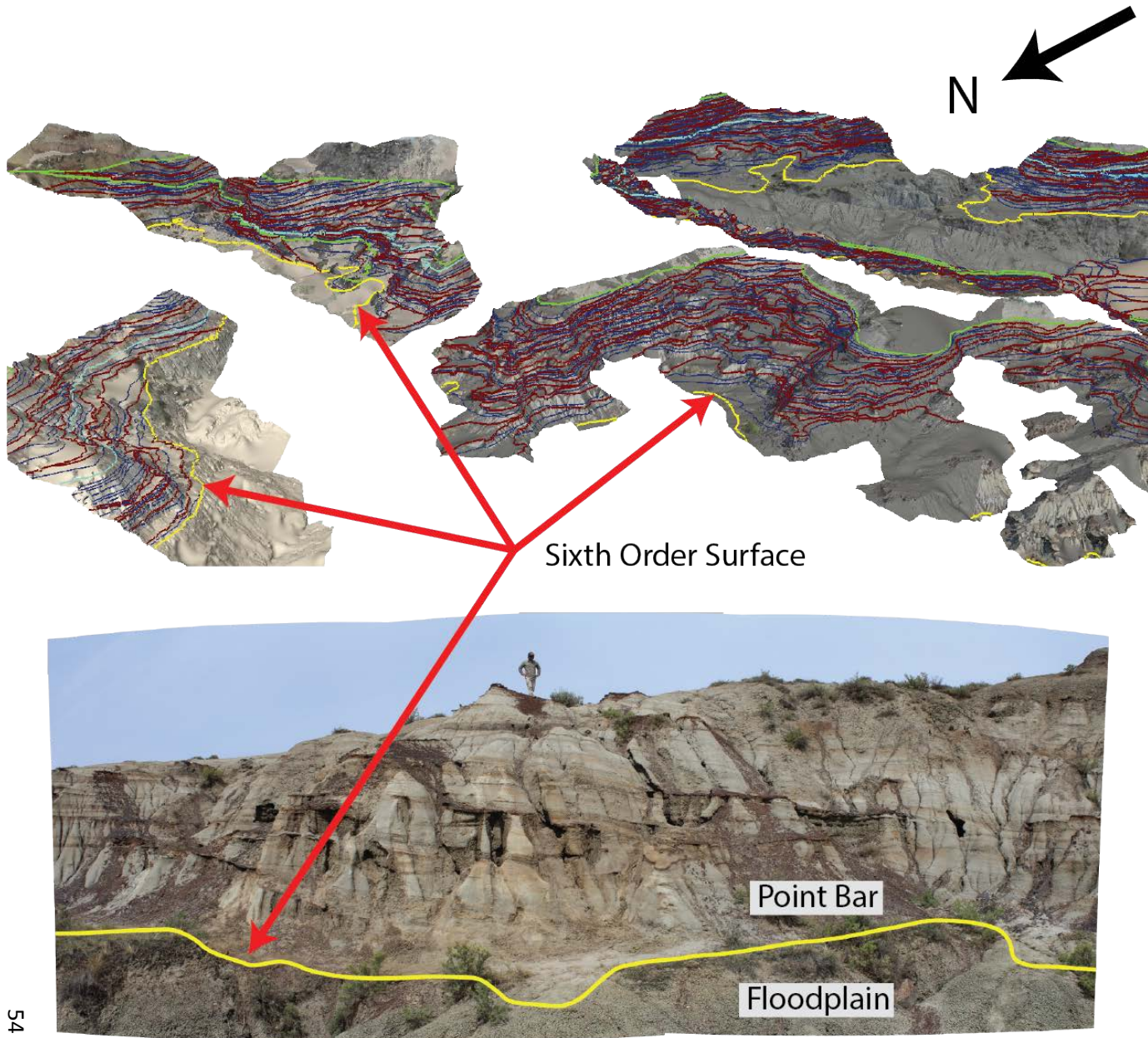


Figure 37: Sixth order surface marked in yellow. The upper sixth order surface is eroded out within the study area leaving only the basal surface exposed. I mapped this surface at all locations throughout the study area. Bottom image shows the sharp contact separating the floodplain beneath and the point bar above.

3.3 Characteristics of 3rd and 2nd Order Surfaces

Close up panoramas in both the modern and ancient reveal detailed patterns in architecture of individual 3rd and 2nd order surfaces (Figures 31-34). Observation of the 3D model and the panoramas reveal two different ways a 3rd order surface can form.

One is the composite constructional surface. In this case, a 3rd order surface is built over a series of scour or onlap events and is not synchronous. In the Cretaceous example, the surface commonly builds along one of the five drape types whereas the modern Powder River example lacks such drapes. Lack of synchronicity is based on cross cutting relationships between 2nd order units that are capped by the same 3rd order surface. Second order surfaces directly below 3rd order surfaces cut into older lateral 2nd order surfaces (Figures 38 and 39). The resulting 3rd order surface builds thus during multiple events controlled by 2nd order surfaces.

Other 3rd order surfaces form comparatively synchronously as a single continuous surface. In this case, below this 3rd order surface is a single 2nd order unit that spans the entire length of the 3rd order surface.

Similar to 3rd order surfaces, 2nd order surfaces can form as either a composite constructional or single continuous surface. For a 2nd order composite constructional surface, cross cutting relationships of 1st order surfaces show that this surface is diachronous and the 2nd order surface is built by a series of 1st order bodies. Composite constructional surfaces are the most common way a 2nd order surface is built with continuous surfaces being fairly rare. A continuous 2nd order surface forms when there is a single 1st order surface that extends the entire length of a 2nd order surface without being cross cut by a younger unit.

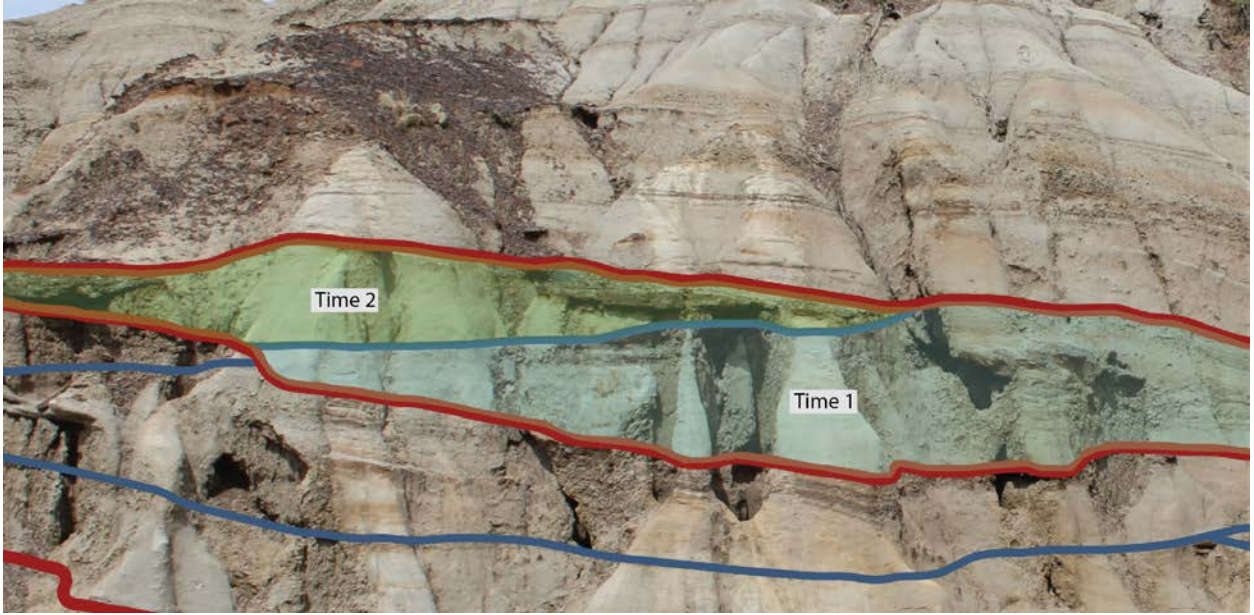


Figure 38: Example of composite constructional surface in the ancient. This image is taken in Amphitheater A along stratigraphic sections. Note how unit bar marked Time 1 (translucent blue color fill) is cut by unit bar marked Time 2 (translucent green color fill). Both unit bars share the same 3rd order surface in dark amber red above. Cross-cutting relationships show that this 3rd order surface must have been constructed during two different events and later preserved as a single surface. Unit bar at Time 1 constructed a portion of the surface during its deposition followed by unit bar at Time 2.

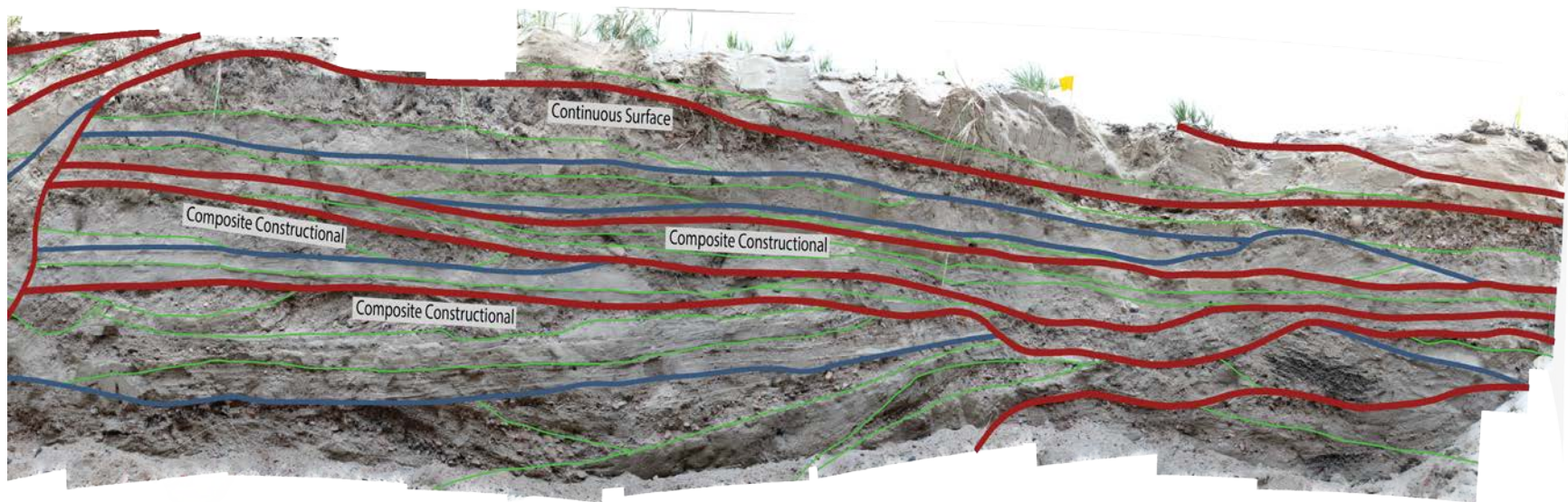


Figure 39: Close-up view of 3rd order accretionary surfaces (marked in dark umber red) within PR141A trench. Below each surface is a text box that identifies the surface type. The first three surfaces from the trench floor are all composite constructional surfaces. Note how there is more than one unit bar (surfaces marked in dark navy) that is present laterally along these surfaces. The uppermost marked surface is an example of a continuous surface. Only one unit bar spans its length and therefore a single event generated this surface.

3.4 Strike & Dip Measurements

Strike and dip measurements are recorded and plotted on a stereonet for each 3rd order surface in a vertical section at six dispersed locations throughout the model (Figure 15). I measured a total of 51 strikes and dips with an overall average strike value of 338° and dip of 6.8°. The change in strike and dip between each adjacent accretionary body averaged 31° and 3.4° respectively. Lastly, the length between each pole (in degrees) and number of truncations of an accretionary surface averaged 5.5° and two truncations (Table 1). Each measurement site is considered separately below (Figure 40).

3.4.1 Location A

Location A is close to the toe of the point bar near the channel. The vertical section runs through part of the accretionary bodies in Amphitheater B. The section encounters ten 3rd order surfaces, each of which was measured for a total of ten strikes and dips. Strikes range from 250° to 333° with an average strike of 306°. Dips range from 2.3° to 7.9° with an average value of 5.3°. Accretionary body five has the largest change in strike and dip with a pole departure of 5.6°, but generates no measured truncations. Accretionary body seven has the most truncations (four) with a pole departure of 3.3°.

3.4.2 Location B

Location B records ten strikes and dips and is located SW of Location A in amphitheater B landward from the paleochannel. Strikes range from 243° to 021° with an average strike of 335°. Dips range from 4.6° to 15.6° with an average dip of 8.2°. Accretionary body eight has the largest pole departure as well as the most truncations with an arrow length of 26.1° and four recorded truncations.

3.4.3 Location C

Location C records nine strikes and dips and is the most landward from the paleochannel of the three locations in Amphitheater B. Strikes range from 294° to 003° with an average strike of 326°. Dips range from 2° to 6.1° with an average dip of 4.3°. Accretionary body eight has the largest pole departure of 4.4° and three truncations. Accretionary body seven has the most truncations (three) with a pole departure of 3.3°.

3.4.4 Location D

Location D records six strikes and dips and is the most landward from the paleochannel of the three locations in Amphitheater A. Strikes range from 282° to 051° with an average strike of 347°. Dips range from 3.8° to 15.8° with an average dip of 9.6°. Location D has the highest average dip value of all locations. Accretionary body one has the greatest change in strike and dip with a pole departure of 13.8°, but has no truncations. Accretionary bodies four and five both have the most truncations (four) with a pole departure of 8° and 6.4° respectively.

3.4.5 Location E

Location E records nine strikes and dips and is near the toe of the point bar in Amphitheater A. Strikes range from 325° to 066° with an average strike of 010°. Dips range from 4.7° to 13.7° with an average dip of 9.2°. Accretionary body seven has the greatest change in strike and dip with pole departure of 11°, but only has one truncation. Accretionary body four has the most truncations (three) with a pole departure of 7.3°.

3.4.6 Location F

Location F records seven strikes and dips and is located on the downstream side of the point bar in Amphitheater A. Strikes range from 196° to 044° with an average strike of 356°. Dips range from 2.3° to 8.7° with an average dip of 5.0°. Accretionary body six has the greatest change

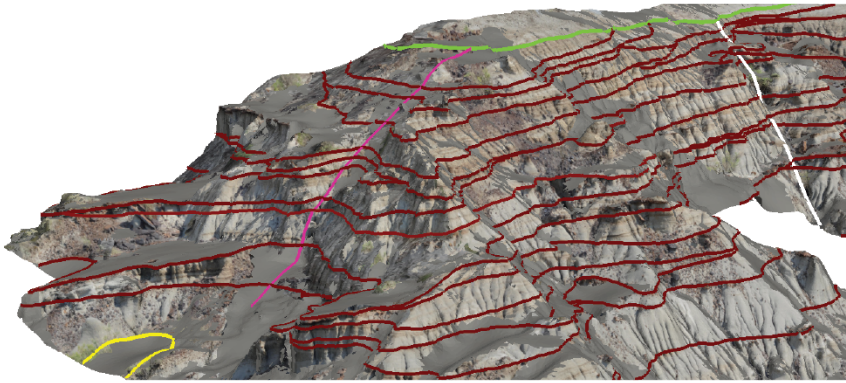
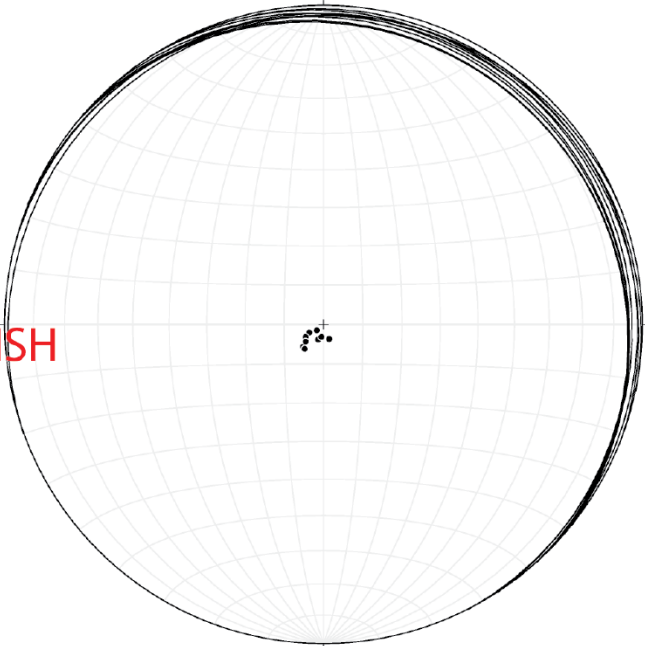
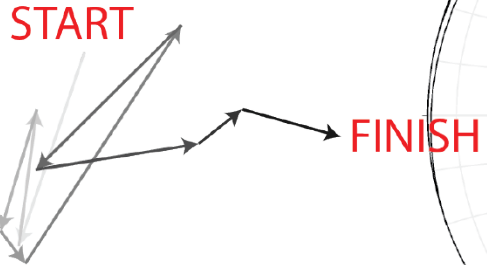
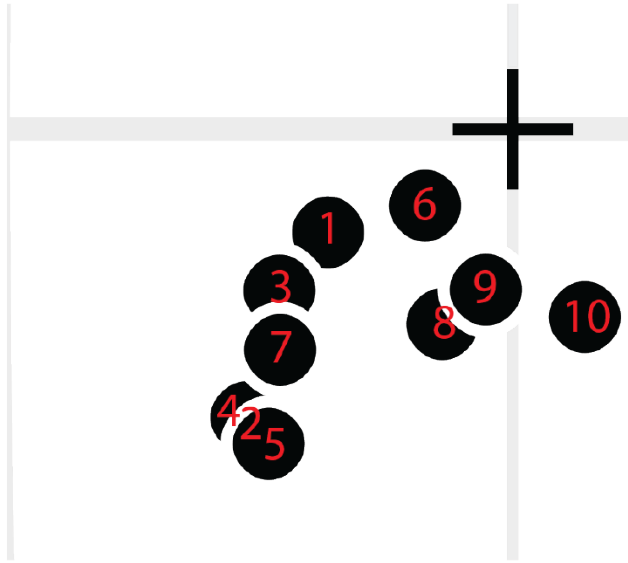
in strike and dip as well as number of truncations with a pole departure of 8.1° and three truncations.

.

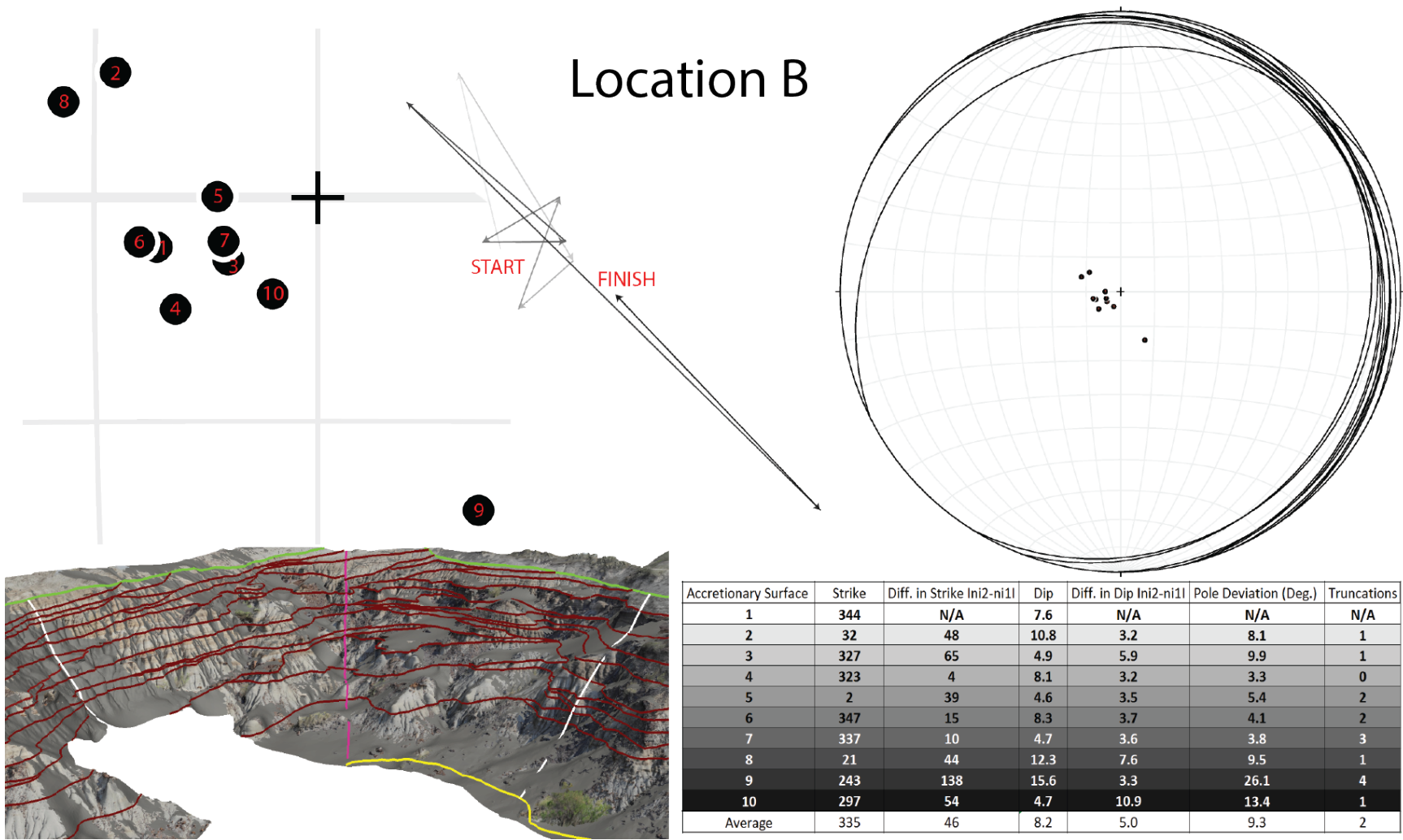
	Accretionary Surface	Strike	Diff. in Strike In2-n11	Dip	Diff. in Dip In2-n11	Pole Deviation (Deg.)	Truncations
Location A	1	333	N/A	4.2	N/A	N/A	N/A
	2	311	22	7.9	3.7	4	2
	3	327	16	5.6	2.3	2.7	3
	4	314	13	7.7	2.1	2.5	1
	5	309	5	7.8	0.1	0.8	1
	6	323	14	2.3	5.5	5.6	0
	7	318	5	6.3	4	4	3
	8	292	26	4	2.3	3.3	4
	9	282	10	3.1	0.9	1.1	0
	10	250	32	3.8	0.7	2	3
	Average	306	16	5.3	2.4	2.9	2
Location B	1	344	N/A	7.6	N/A	N/A	N/A
	2	32	48	10.8	3.2	8.1	1
	3	327	65	4.9	5.9	9.9	1
	4	323	4	8.1	3.2	3.3	0
	5	2	39	4.6	3.5	5.4	2
	6	347	15	8.3	3.7	4.1	2
	7	337	10	4.7	3.6	3.8	3
	8	21	44	12.3	7.6	9.5	1
	9	243	138	15.6	3.3	26.1	4
	10	297	54	4.7	10.9	13.4	1
	Average	335	46	8.2	5.0	9.3	2
Location C	1	3	N/A	4.7	N/A	N/A	N/A
	2	355	8	2.1	2.6	2.7	0
	3	316	39	5	2.9	3.7	2
	4	334	18	5.6	0.6	1.4	0
	5	308	26	4.2	1.4	2.8	2
	6	311	3	4.4	0.2	0.5	4
	7	330	19	4.2	0.2	1.4	1
	8	320	10	2	2.2	2.3	2
	9	294	26	6.1	4.1	4.4	3
	Average	326	19	4.3	1.8	2.4	2
Location D	1	282	N/A	11.5	N/A	N/A	N/A
	2	340	58	15.8	4.3	13.8	0
	3	320	20	13	2.8	5.7	2
	4	352	32	3.8	9.2	10	1
	5	51	59	9.2	5.4	8	4
	6	15	36	4.1	5.1	6.4	4
	Average	347	41	9.6	5.4	7.7	2
Location E	1	350	N/A	9.3	N/A	N/A	N/A
	2	1	11	7.3	2	2.6	0
	3	355	6	5.8	1.5	1.6	2
	4	325	30	13.7	7.9	9.1	1
	5	357	32	11.2	2.5	7.3	3
	6	33	36	10	1.2	6.7	1
	7	350	43	4.7	5.3	7.3	2
	8	66	76	11.1	6.4	11	1
	9	49	17	9.7	1.4	3.4	1
	Average	10	31	9.2	3.5	6.1	1
Location F	1	337	N/A	5.2	N/A	N/A	N/A
	2	16	39	5.4	0.2	3.6	0
	3	15	1	5.4	0	0.3	1
	4	44	29	8.7	3.3	4.9	1
	5	41	3	2.3	6.4	6.4	0
	6	42	1	6	3.7	3.7	1
	7	196	154	2.3	3.7	8.1	3
	Average	356	38	5.0	2.9	4.5	1
Total Average	338	31	6.8	3.4	5.5	2	

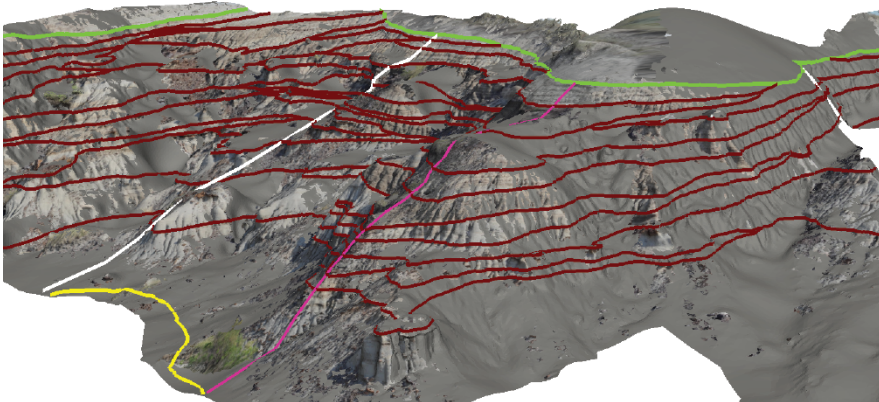
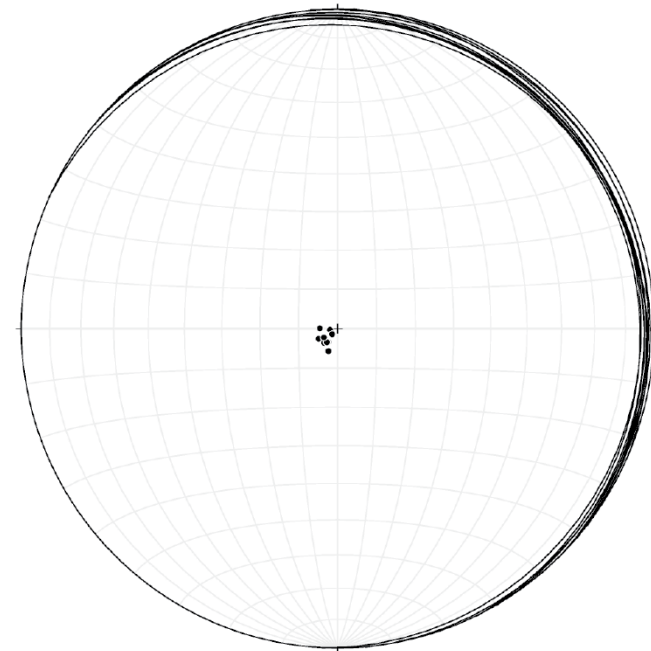
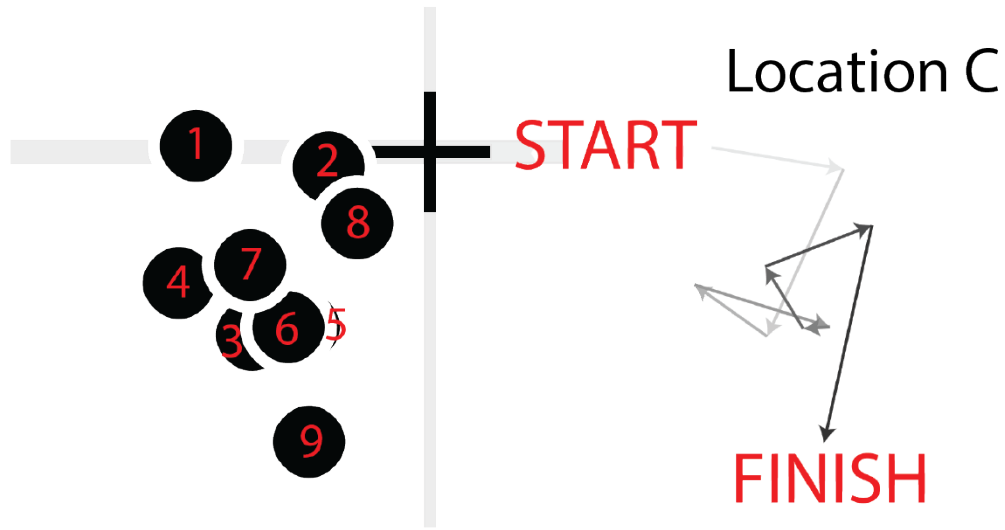
Table 1: Summary of strike and dip data collected. Each location is colored in a light grey-to-dark grey gradient to illustrate the progression of accretion (light grey being the oldest accretionary body and dark grey being the youngest accretionary body).

Location A

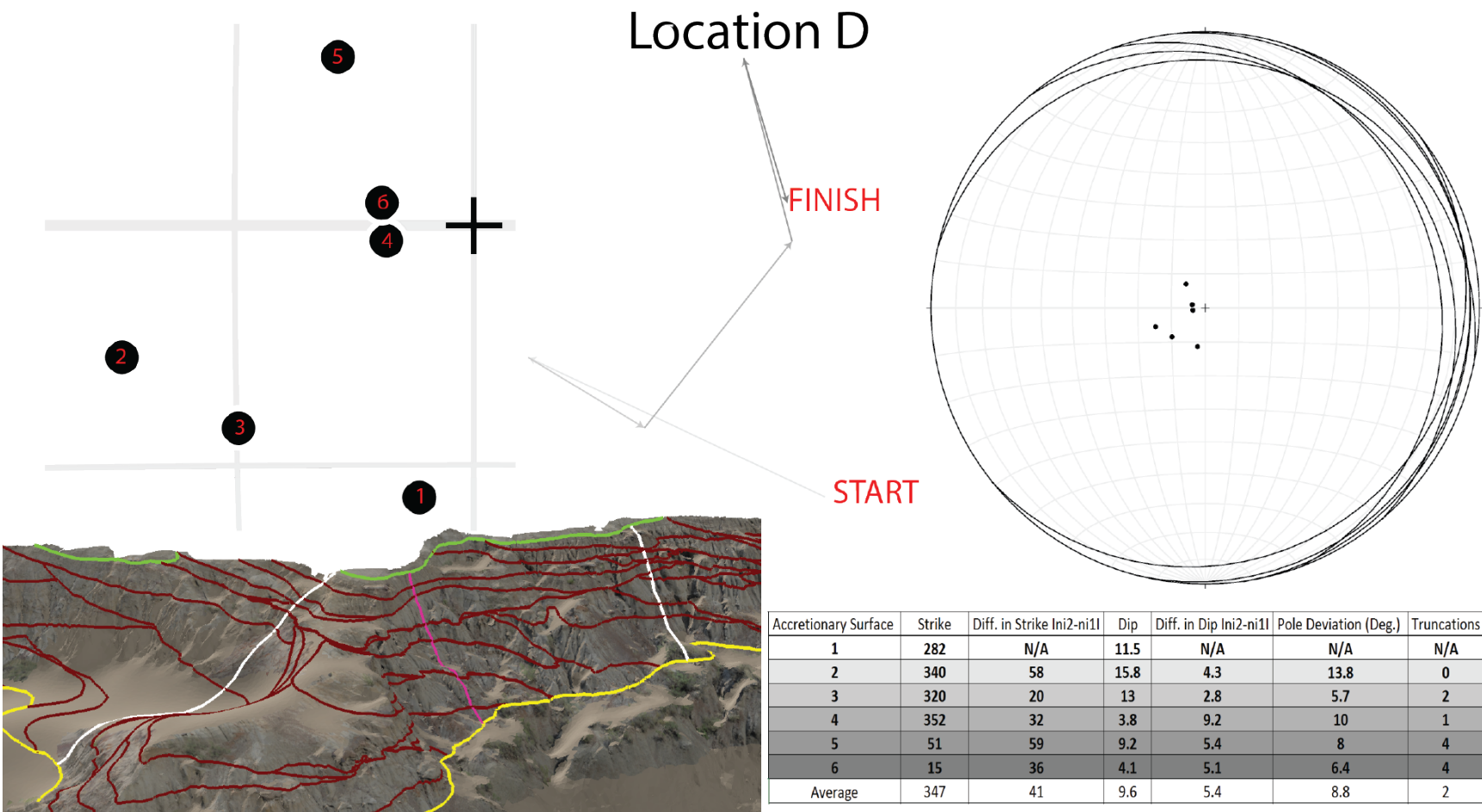


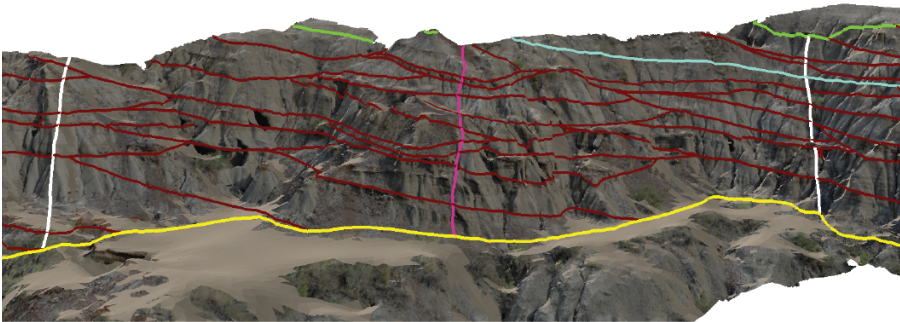
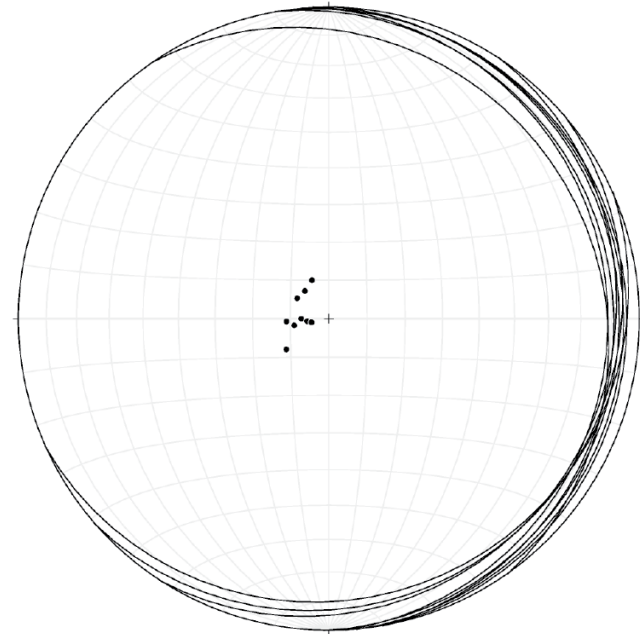
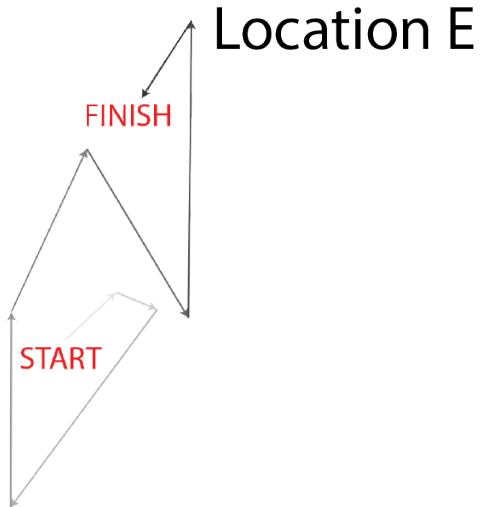
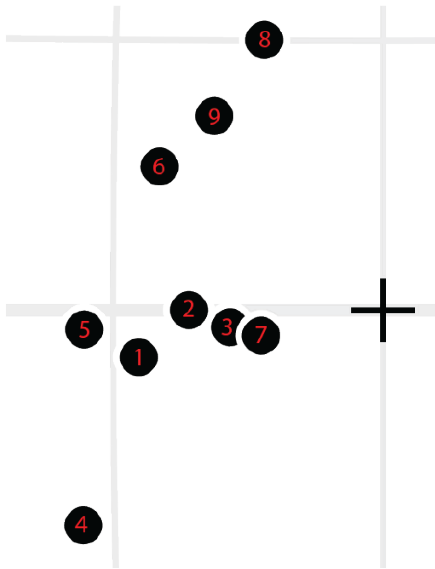
Accretionary Surface	Strike	Diff. in Strike Ini2-ni1l	Dip	Diff. in Dip Ini2-ni1l	Pole Deviation (Deg.)	Truncations
1	333	N/A	4.2	N/A	N/A	N/A
2	311	22	7.9	3.7	4	2
3	327	16	5.6	2.3	2.7	3
4	314	13	7.7	2.1	2.5	1
5	309	5	7.8	0.1	0.8	1
6	323	14	2.3	5.5	5.6	0
7	318	5	6.3	4	4	3
8	292	26	4	2.3	3.3	4
9	282	10	3.1	0.9	1.1	0
10	250	32	3.8	0.7	2	3
Average	306	16	5.3	2.4	2.9	2





Accretionary Surface	Strike	Diff. in Strike In2-ni1l	Dip	Diff. in Dip In2-ni1l	Pole Deviation (Deg.)	Truncations
1	3	N/A	4.7	N/A	N/A	N/A
2	355	8	2.1	2.6	2.7	0
3	316	39	5	2.9	3.7	2
4	334	18	5.6	0.6	1.4	0
5	308	26	4.2	1.4	2.8	2
6	311	3	4.4	0.2	0.5	4
7	330	19	4.2	0.2	1.4	1
8	320	10	2	2.2	2.3	2
9	294	26	6.1	4.1	4.4	3
Average	326	19	4.3	1.8	2.4	2





Accretionary Surface	Strike	Diff. in Strike In2-ni1l	Dip	Diff. in Dip In2-ni1l	Pole Deviation (Deg.)	Truncations
1	350	N/A	9.3	N/A	N/A	N/A
2	1	11	7.3	2	2.6	0
3	355	6	5.8	1.5	1.6	2
4	325	30	13.7	7.9	9.1	1
5	357	32	11.2	2.5	7.3	3
6	33	36	10	1.2	6.7	1
7	350	43	4.7	5.3	7.3	2
8	66	76	11.1	6.4	11	1
9	49	17	9.7	1.4	3.4	1
Average	10	31	9.2	3.5	6.1	1

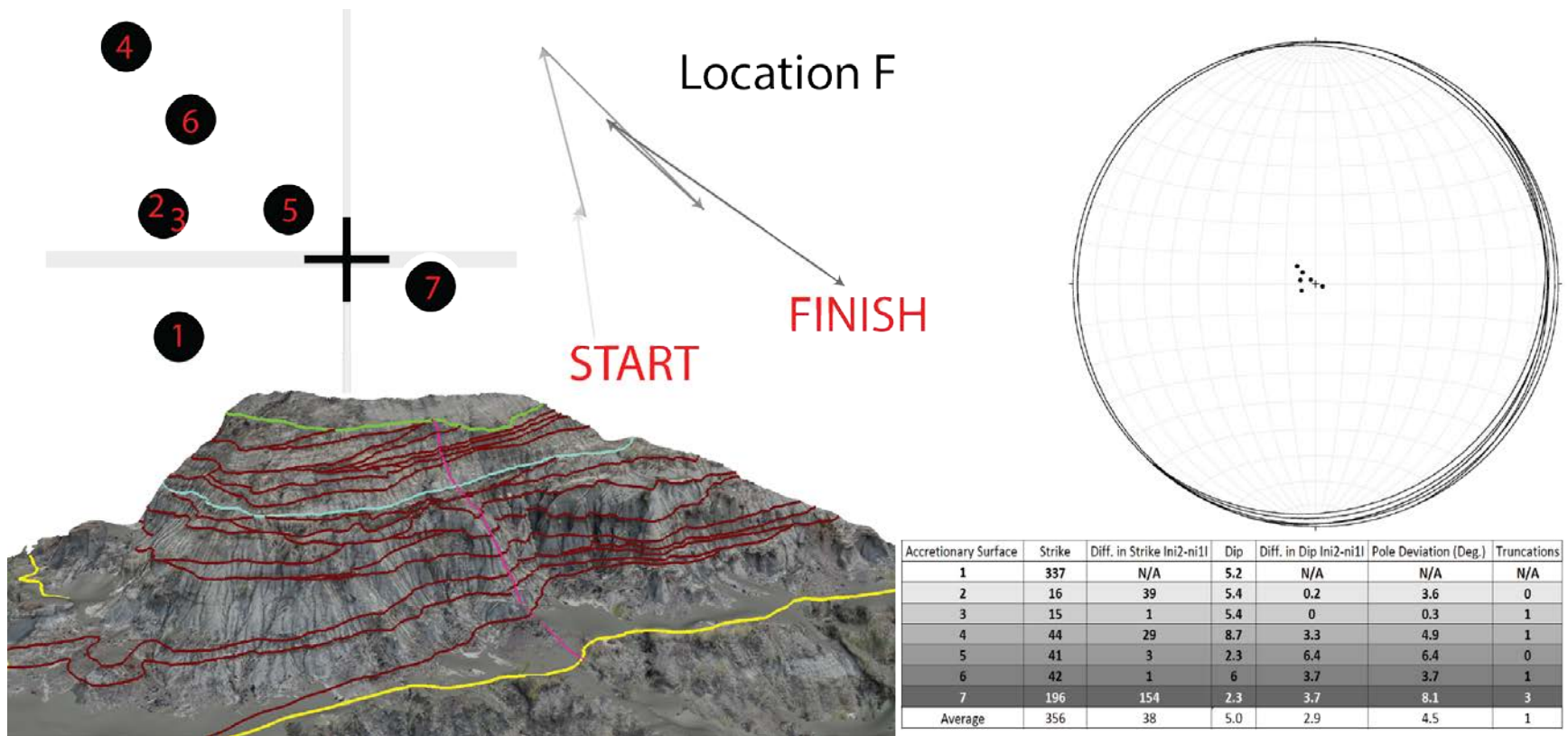


Figure 40: Summary of strike and dip data at Locations A through F. Accretionary surfaces are numbered from oldest to youngest. Accretionary bodies are colored in light-to-dark grey gradient with light grey being the oldest and dark grey the youngest. Upper right image is a stereonet with plotted strikes and dips as well as poles. Upper left image is a close up of stereonet with accretionary surfaces labeled as well as arrows that show the pole wander track because of changes in strike and dip over time. Lower left image is the location where I measured strikes and dips (marked by bright pink line) as well as number of truncations by each 3rd order surface of prior 3rd order surface. White lines mark boundaries where I picked truncations for accretionary surfaces. Lower right image is a summary of data and calculations.

3.5 Powder River Stratigraphic Section

I measured four stratigraphic sections along the trench in PR141A and one section at PR163. Below each trench is approximately 1.2m of vertical bar not recorded owing to the water table. Lithologies consist of sands, silts, and clayey silts. Overall, the entire point bar does show a fining upward trend stratigraphically similar to that of the Cretaceous point bar.

3.5.1 PR141A Stratigraphic Sections

Near the base of the point bar are light grey sandy bodies that range in grain size from fine sand to upper coarse sand. Many of the sandy accretionary bodies near the base have an abundant amount of rounded centimeter sized pebbles scattered throughout. The primary lithologies that make up the pebbles are clinker (burnt coal from surrounding hills), coal, Madison Limestone, and granite. The Madison Limestone and granite originate from the Big Horn Mountains (Moody and Meade, 2013). These pebbles, commonly clasts of coal, locally line laminae of zero order surfaces. Some bodies of sediment near the base fine upward into a fine sand while others show no stratigraphic trend. Trough and planar cross sets are the dominant sedimentary structures seen in the lower point bar.

The upper portion of the point bar is finer than the lower point bar. Sandy bodies in the upper bar range from fine sand to medium sand and pebbles are less abundant than in the lower point bar. Sediment bodies in the upper point bar also internally show fining upward from sand to silt or clayey silt. At all sections, rippled silt caps the very top of the point bar. Plant roots and bioturbation are common in the upper point bar. Primary sedimentary structures range from planar to trough cross sets, ripples, and lower plane bed laminations (Figure 41). See appendix for detailed descriptions of stratigraphic sections.

3.5.2 PR163 Stratigraphic Section

Most of the sediment deposited from PR163 originates from a single flood event in 1978. Deposits consist of light grey sands with an abundance of pebbles that locally line zero order laminae. Grain sizes of sands vary from upper medium to upper coarse. Sedimentary structures include planar and trough cross sets. Unlike the ancient point bar and PR141A, there is no sign of deposits fining upward (Figure 42). Rippled silts deposited during later years cap the flood of 1978 sediment.

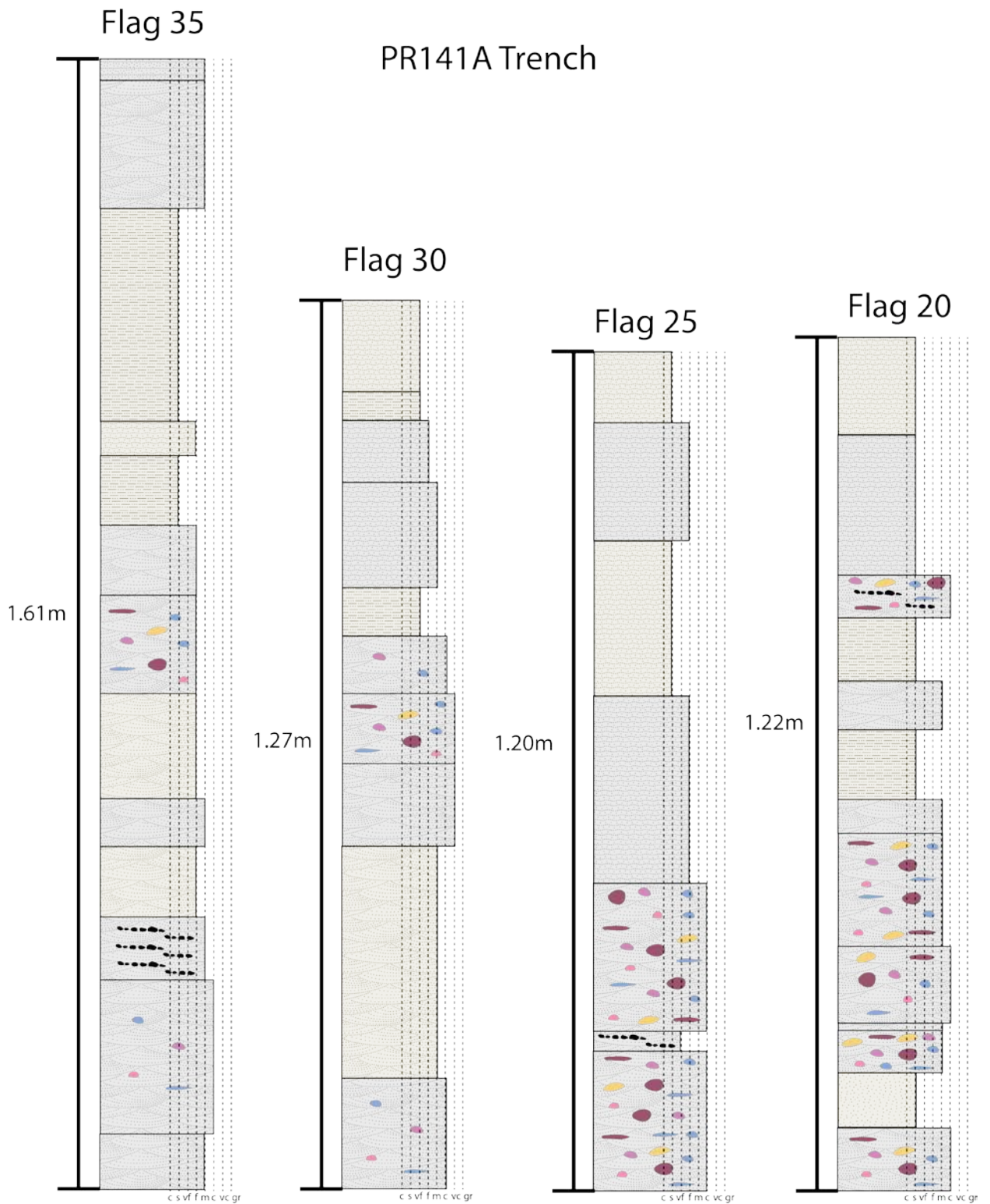


Figure 41: PR141A trench stratigraphic sections at flag stations 20m, 25m, 30m, and 35m. Overall lithology is coarser grained than ancient point bar. Fining upward trends are not as clear as in ancient example. Lithologies are marked along the vertical dashed lines and geologic swatches represent bedforms. Lithologies and pebbles are colored similar to their appearance in trench.

PR163 Trench

Flag 25

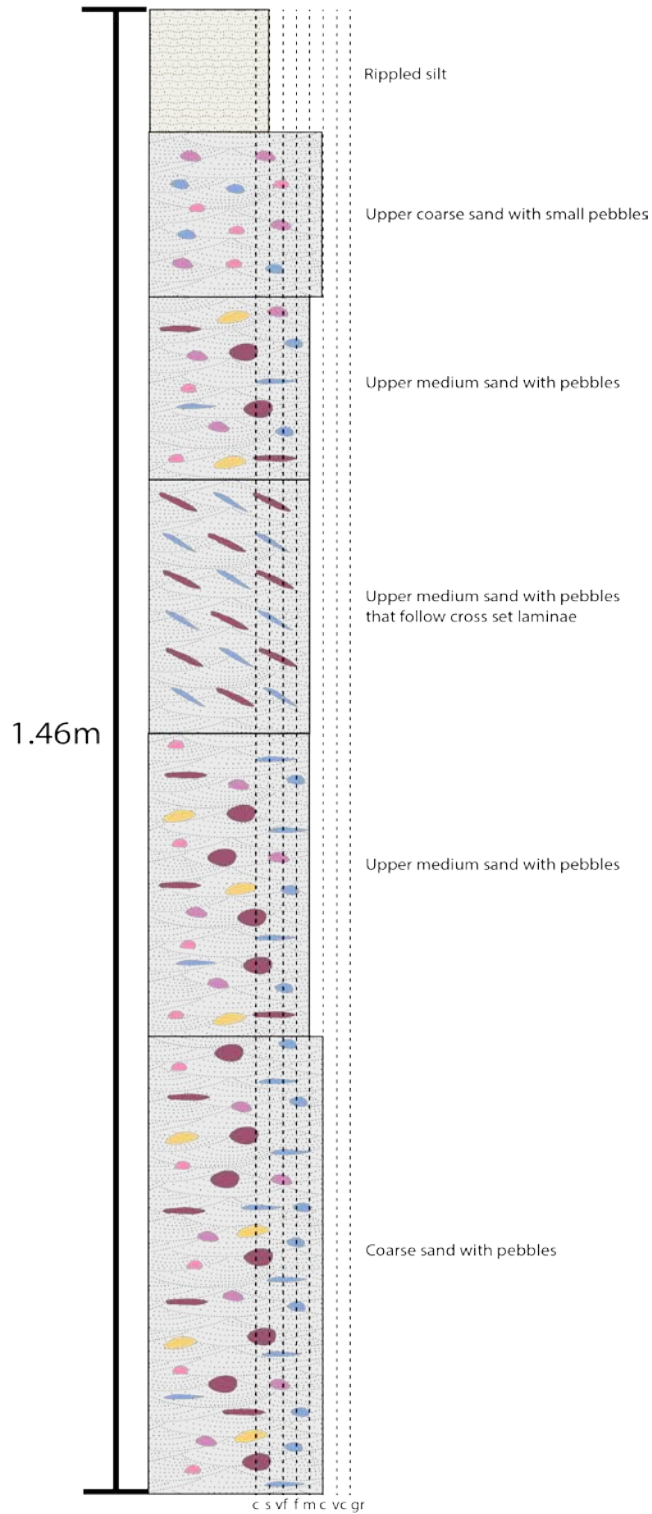


Figure 42: PR163 trench stratigraphic section at flag 25m. Overall lithology is coarser grained than ancient point bar. There are no fining trends seen in this trench. Lithologies are marked along the vertical dashed lines and geologic swatches represent bedforms. Lithologies and pebbles are colored similar to their appearance in trench.

3.6 Architectural-Element Analysis Powder River

Architectural-element analysis of trenches PR141A and PR163 expose four surface orders (Figure 43) that are similar in architecture and geometry to the ancient equivalent. Surface orders include 3rd, 2nd, 1st, and zero order surfaces. Zero order surfaces in the ancient behave similar to zero order surfaces in the modern. They represent individual laminae bound by 1st order surfaces. Zero order surfaces in the ancient commonly show draping of organics whereas pebbles and clasts of coal commonly line individual zero order laminae along the Powder River (Figure 28).

First order surfaces bind zero order surfaces. Planar cross laminae, trough cross laminae, and/or lower plane bed lamination sets make up strata bound by 1st order surfaces (Figure 27). These surfaces rarely extend the length of a 2nd order surface before a younger surface cuts it off. They are typically only a few meters in length. Zero order surfaces within 1st order surfaces record paleocurrent flow direction. For PR141A and PR163 the general flow direction of the channel at the apex of the point bar is toward the East.

Second order surfaces bind 1st order surfaces and are the units that make up accretionary bodies. Similar to the ancient point bar, 2nd order surfaces are lobate in geometry and may extend the length of a 3rd order surface. Most 2nd order surfaces are cut by younger 2nd or 3rd order surfaces. These surfaces extend meters, but none are seen extending more than ten meters in either trench. Bodies bound by 2nd order surfaces at PR141A may show fining upward trends (Figure 44). Fining upward trends are not as abundant as seen in the ancient. In fact, there are no fining upward trends between 2nd order surfaces at PR163. PR163 trench records sediment deposited during a single flood event in 1978. Second order bodies at PR163 trench only vary between upper medium and upper coarse sand. The geometry of 2nd order surfaces at PR163 trench is different than what is seen at both PR141A and the ancient point bar. These 2nd order surfaces follow the general

orientation of point bar accretion and behave similar to 3rd order surfaces although their internal architecture is different (Figure 45 and 46).

Third order surfaces bind 2nd order surfaces and follow the orientation of accretion of the point bar. Most third order surfaces extend for only a few meters before a younger event cuts it off. There is a 3rd order surface that does extend the full length of PR 141A (17.5m) and PR163 (6.0m). However, each trench only represents a portion of the point bar and more exposure is needed to determine the surface's full extent.

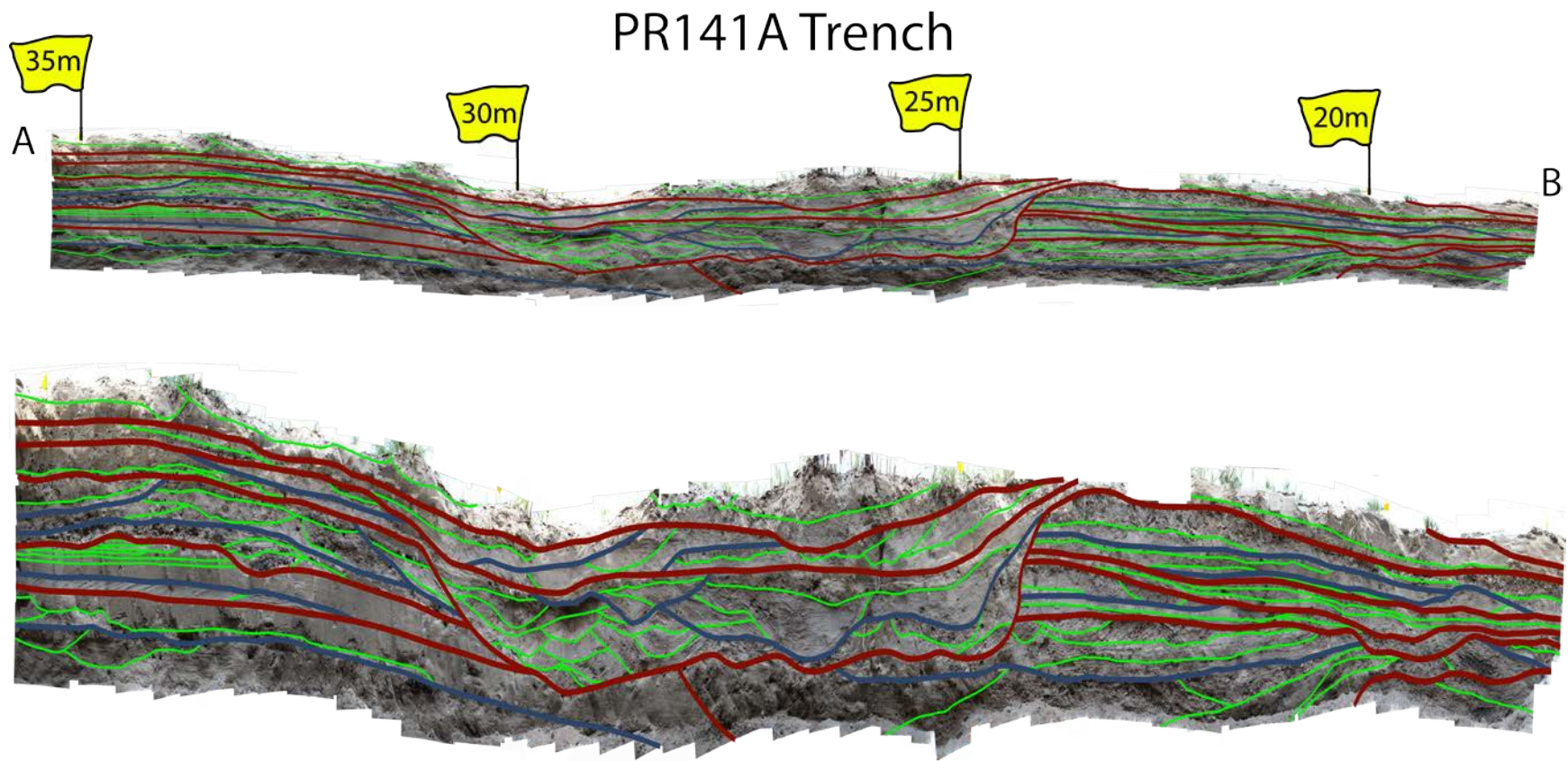


Figure 43: Interpreted PR141A trench (17.5m in length). Third order surfaces are colored dark umber red. Second order surfaces are colored dark navy. First order surfaces are colored neon green. Upper image is 1:1 scale and lower image is 200% vertically exaggerated to extenuate architecture. Architecture and geometry of surfaces in the modern are similar to the ancient.

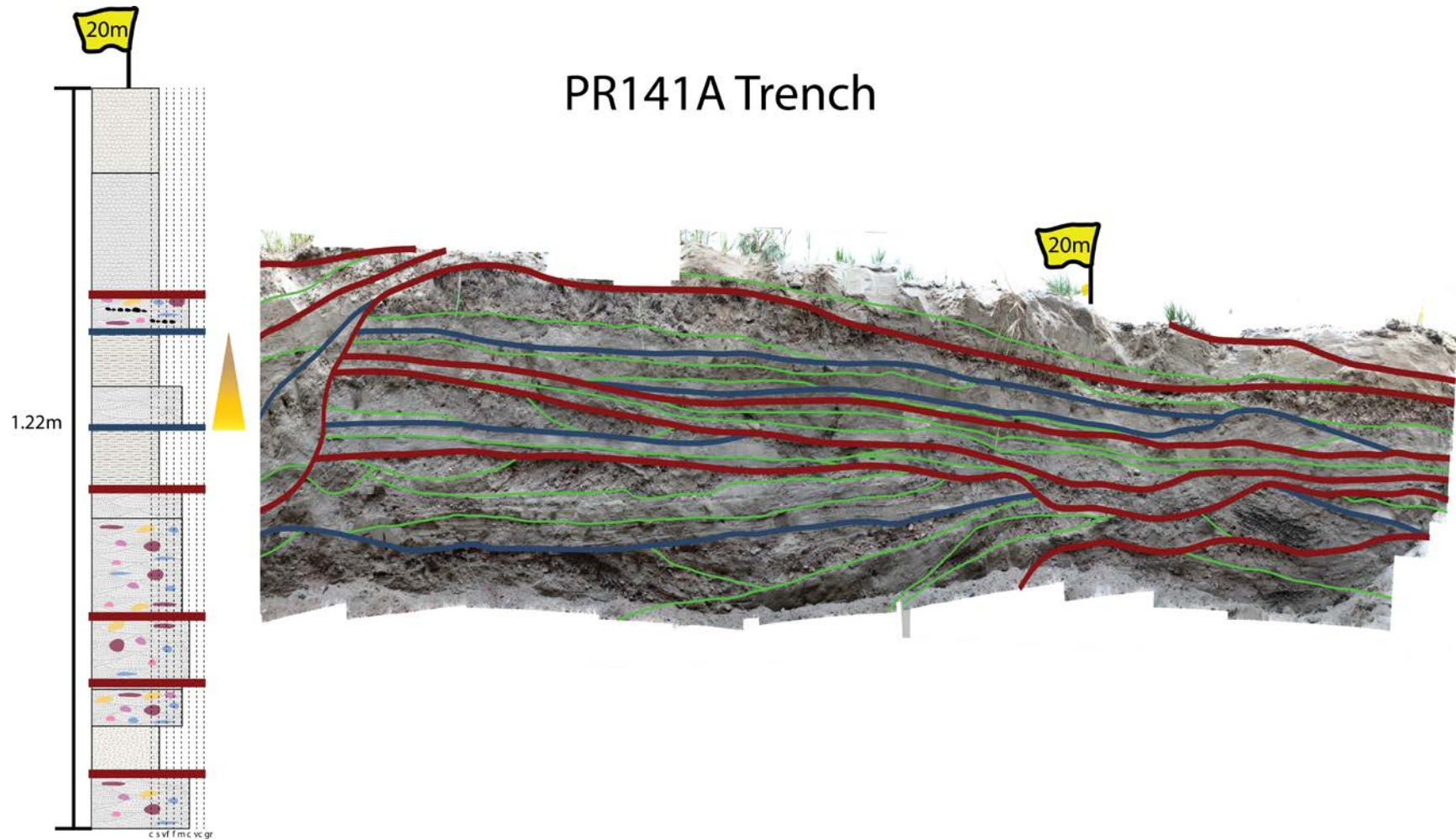


Figure 44: Close up of PR141A near flag station 20m. Stratigraphic section at station 20m shown on left to emphasize internal architecture of accretionary bodies and unit bars. Tops of 3rd order and 2nd order surfaces in trench are marked on stratigraphic section. Note there is only one accretionary body that shows a fining trend within it. Trench image is slightly exaggerated vertically.

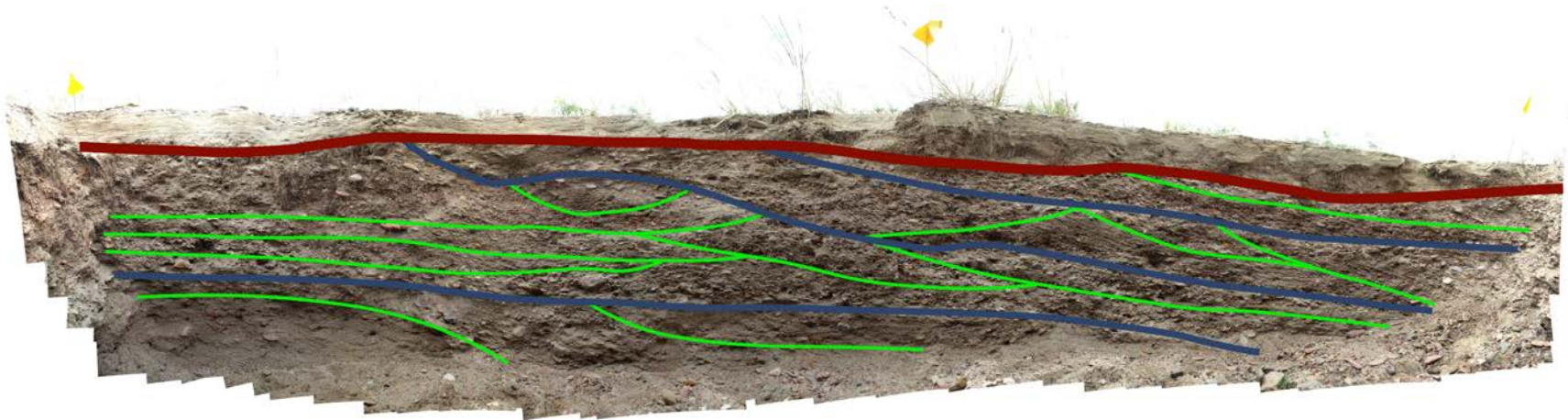


Figure 45: Interpreted PR163 trench (6.0m in length). Third order surfaces are colored dark umber red. Second order surfaces are colored dark navy. First order surfaces are colored neon green. Geometry of 2nd order surfaces in trench behave similarly to 3rd order surface geometry.

PR163 Trench

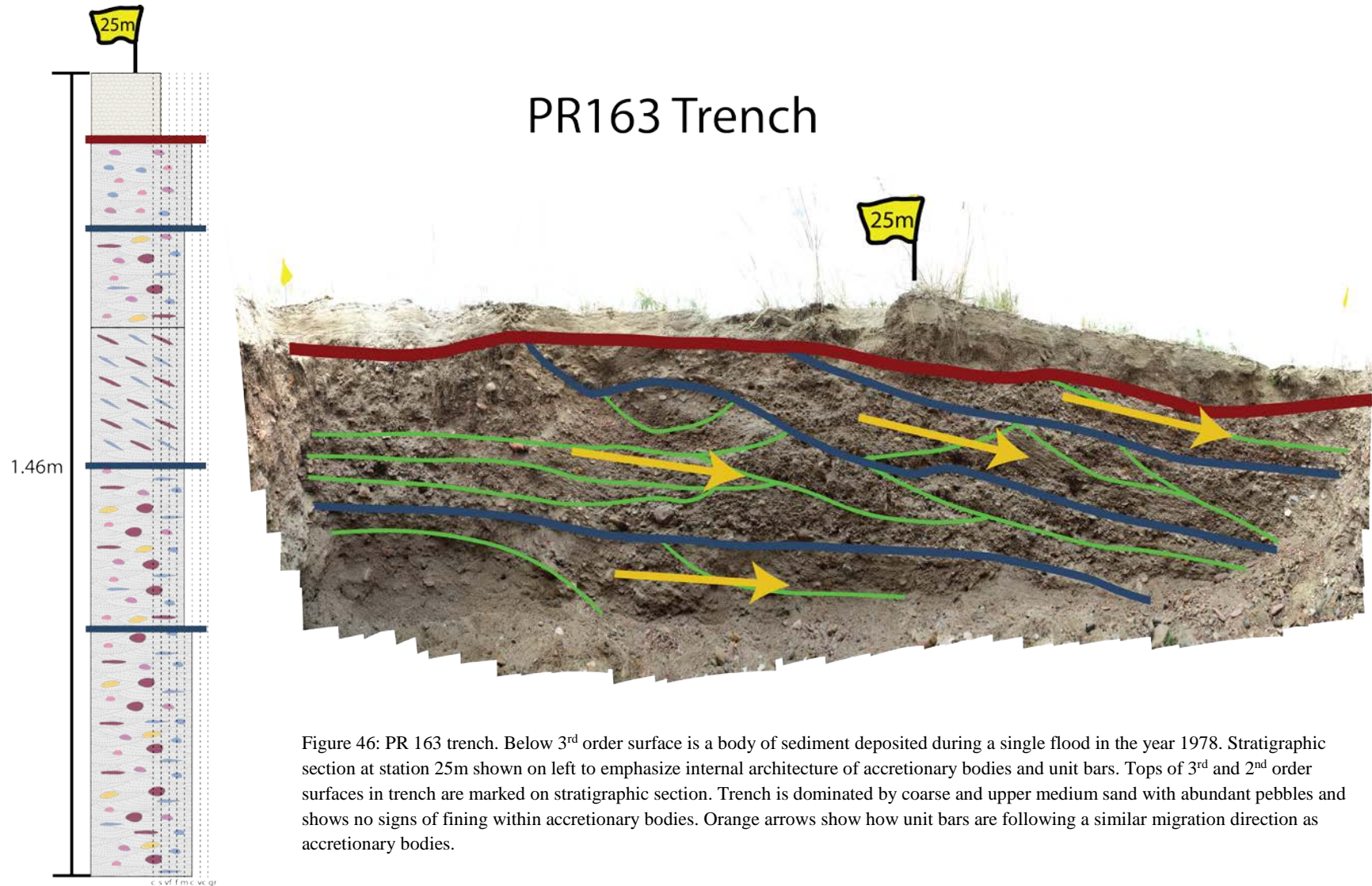


Figure 46: PR 163 trench. Below 3rd order surface is a body of sediment deposited during a single flood in the year 1978. Stratigraphic section at station 25m shown on left to emphasize internal architecture of accretionary bodies and unit bars. Tops of 3rd and 2nd order surfaces in trench are marked on stratigraphic section. Trench is dominated by coarse and upper medium sand with abundant pebbles and shows no signs of fining within accretionary bodies. Orange arrows show how unit bars are following a similar migration direction as accretionary bodies.

3.7 Comparison of Powder River Surveys

Moody and Meade (2014) conducted surveys on trench's PR141A and PR163 that record the elevation of the point bar platform along dip direction. Surveys were conducted from 1978-2015, but not all years were surveyed (Figures 20 and 21). I matched elevations of survey data at locations of stratigraphic sections and correlated survey data throughout the trench.

3.7.1 PR141A Survey Lines

Deposits of PR141A trench span from 1995 to October 2015. I projected eight survey lines onto the PR141A trench (Figure 47). On average, there is one accretionary body deposited any given year. Below are the dates of survey lines:

- October 2, 1995
- September 23, 1999
- September 26, 2000
- October 30, 2002
- September 28, 2006
- September 29, 2009
- October 12, 2011
- October 10, 2012

The first survey, October 2, 1995, accounts for a large portion of sediment at the southern end of the trench. The sediment beneath this survey line accounts for a portion of sediment deposited between September 23, 1994 and October 2, 1995. The architecture seen in these deposits are representative of a single year of deposition (Figure 48). Within that year, I recorded 3rd, 2nd, 1st, and zero order surfaces. The October 2, 1995 survey line closely matches the location of a 3rd order surface. There is a second 3rd order surface within this deposit showing that multiple 3rd order surfaces can form in a single year.

Between the September 23, 1999 and September 26, 2000 survey line is also approximately a single year of point bar deposition. However, the architecture is slightly

different. A 3rd order surface follows the September 26, 2000 survey line at some locations, but deviates at a slightly lower position in other locations. Not all 3rd order surfaces follow the exact positions of survey lines (Figure 49). In addition, the sediment deposited here does not have an additional 3rd order surface within it like the year 1995.

The October 30, 2002 and September 26, 2006 survey lines represent multiple years of deposition between them. Both survey lines match closely with the location of a 3rd order surface, but do not follow it exactly like some other survey lines. The body of sediment deposited here accounts for approximately four years of deposition, but there are only two 3rd order surfaces constructed during that time frame. Third order surfaces do not always follow a yearly cycle.

The September 29, 2009; October 12, 2011; and October 10, 2012 survey lines all closely match the location of a mapped 3rd order surface. Packages of sediment between these surveys all show 2nd and 1st order surfaces within them. The 3rd order surface associated with the September 29, 2009 survey line is unique and erodes through most of the 3rd order surfaces beneath it. This surface marks the base of a chute channel cutting into the point bar between station 25m and 30m. The location of the chute channel correlates well with the location of a swale (Figure 50).

3.7.2 PR163 Survey Lines

The PR163 cross section profile produced by Moody and Meade (2014) shows that sediment between station 22m and 28m is dominated by the flood of 1978. This flood marks the birth of PR163 as well as PR141A point bar. Following the flood, Moody and Meade (2014) conducted a survey of the point bar on August 30, 1978 to record the net gain in sediment following the flood. The architecture inside the PR163 trench is unique because it constrains to not only a single year of deposition, but also a single flood event. The 3rd order surface I mapped

marks the same location as the August 30, 1978 survey line. Below this 3rd order surface are deposits strictly from the flood of 1978. Both 2nd and 1st order surfaces are mapped within this deposit. However, the second order surfaces behave differently at PR163. Second order surfaces at this trench seem to follow the orientation and dip of lateral accretion of the point bar. Previously this pattern was only seen along 3rd order surfaces (Figure 45). Furthermore, the architecture within these 2nd order packages is somewhat different. Although both the ancient point bar and PR141A trench both show instances where a fining upward trend is absent, fining up still occurs. All 2nd order surfaces within the PR163 show no signs of upward fining. Cross sets between 1st order surfaces are almost completely one grain size throughout. As mentioned earlier, grain sizes from the flood of 1978 at PR163 only vary from upper medium to upper coarse with many rounded pebbles scattered throughout.

Survey Lines

- | | | | |
|-----------|--------------------|-----------|--------------------|
| ■ ■ ■ ■ ■ | October 30, 2002 | ■ ■ ■ ■ ■ | October 10, 2012 |
| ■ ■ ■ ■ ■ | September 26, 2000 | ■ ■ ■ ■ ■ | October 12, 2011 |
| ■ ■ ■ ■ ■ | September 23, 1999 | ■ ■ ■ ■ ■ | September 29, 2009 |
| ■ ■ ■ ■ ■ | October 2nd, 1995 | ■ ■ ■ ■ ■ | September 28, 2006 |

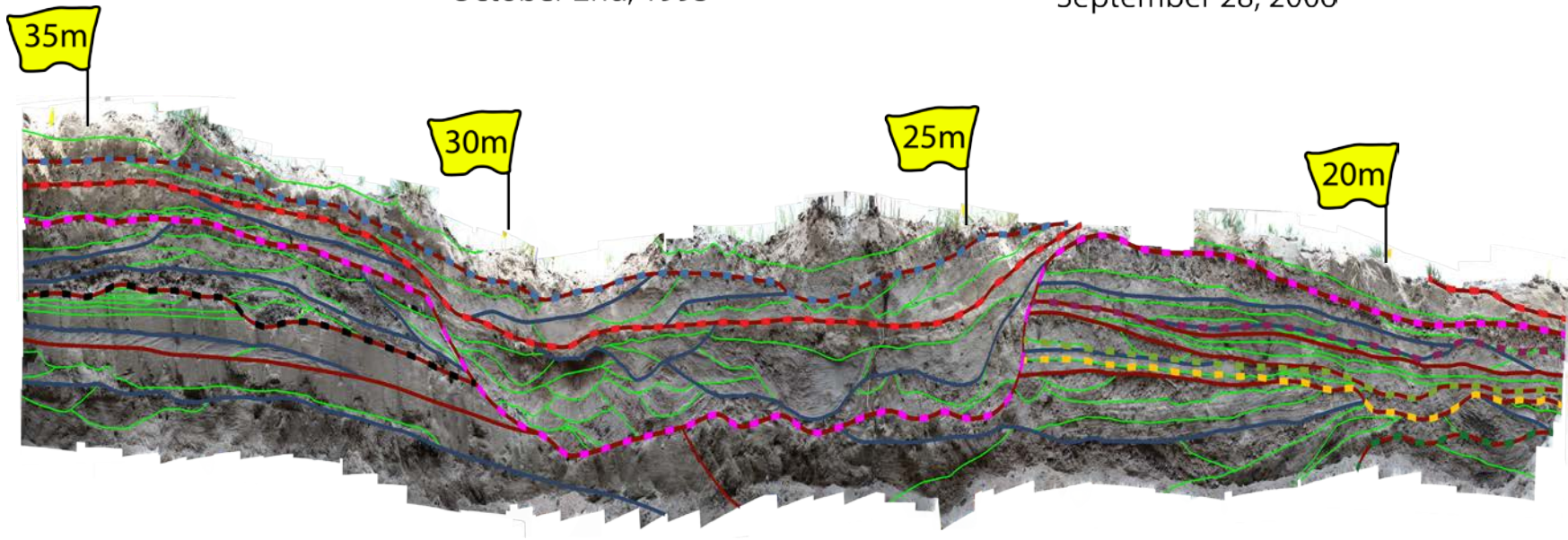


Figure 47: PR141A trench survey lines. Trench is 200% vertically exaggerated.

Survey Lines

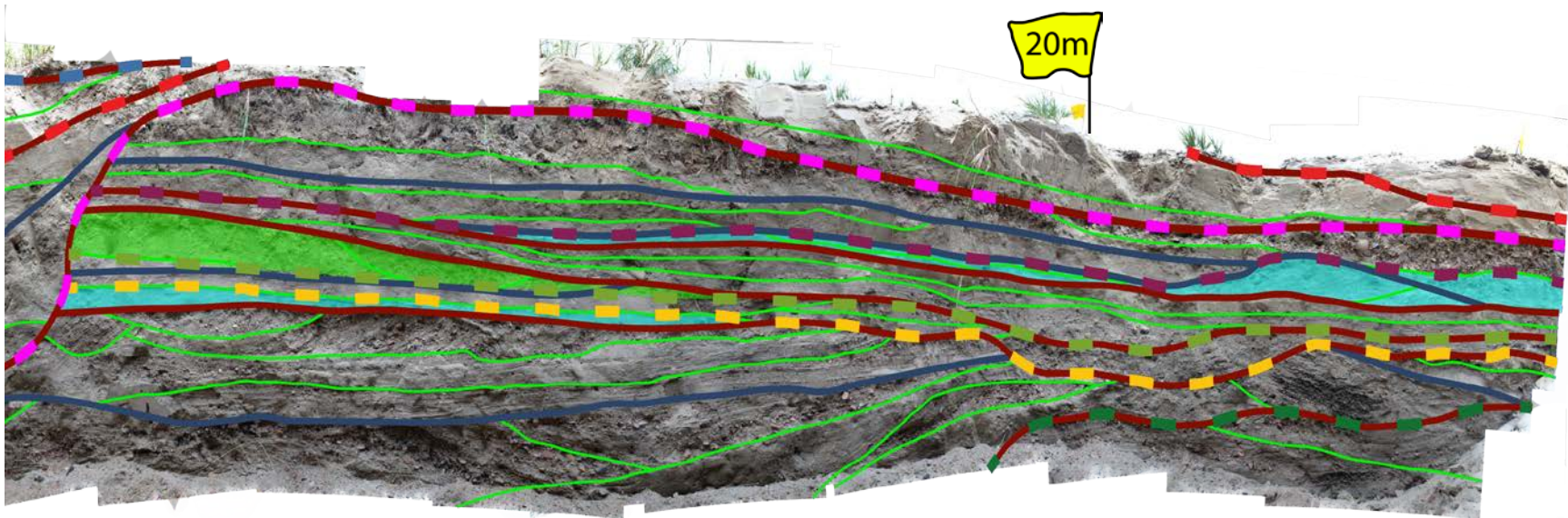
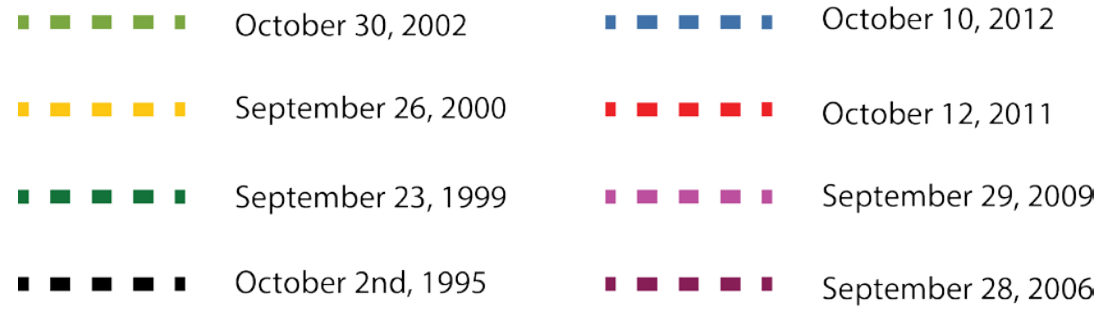


Figure 48: Survey lines overlain on 3rd order accretionary surfaces. Survey lines are marked as dashed lines and accretionary surfaces are solid dark umber red. Blue and green polygons show areas where survey lines deviate away from accretionary surfaces. Areas where a survey line deviates above an accretionary surface are marked in blue. Areas where a survey line deviates below an accretionary surface are marked in green.

Survey Lines

- | | | | |
|-----------|--------------------|-----------|--------------------|
| ■ ■ ■ ■ ■ | October 30, 2002 | ■ ■ ■ ■ ■ | October 10, 2012 |
| ■ ■ ■ ■ ■ | September 26, 2000 | ■ ■ ■ ■ ■ | October 12, 2011 |
| ■ ■ ■ ■ ■ | September 23, 1999 | ■ ■ ■ ■ ■ | September 29, 2009 |
| ■ ■ ■ ■ ■ | October 2nd, 1995 | ■ ■ ■ ■ ■ | September 28, 2006 |

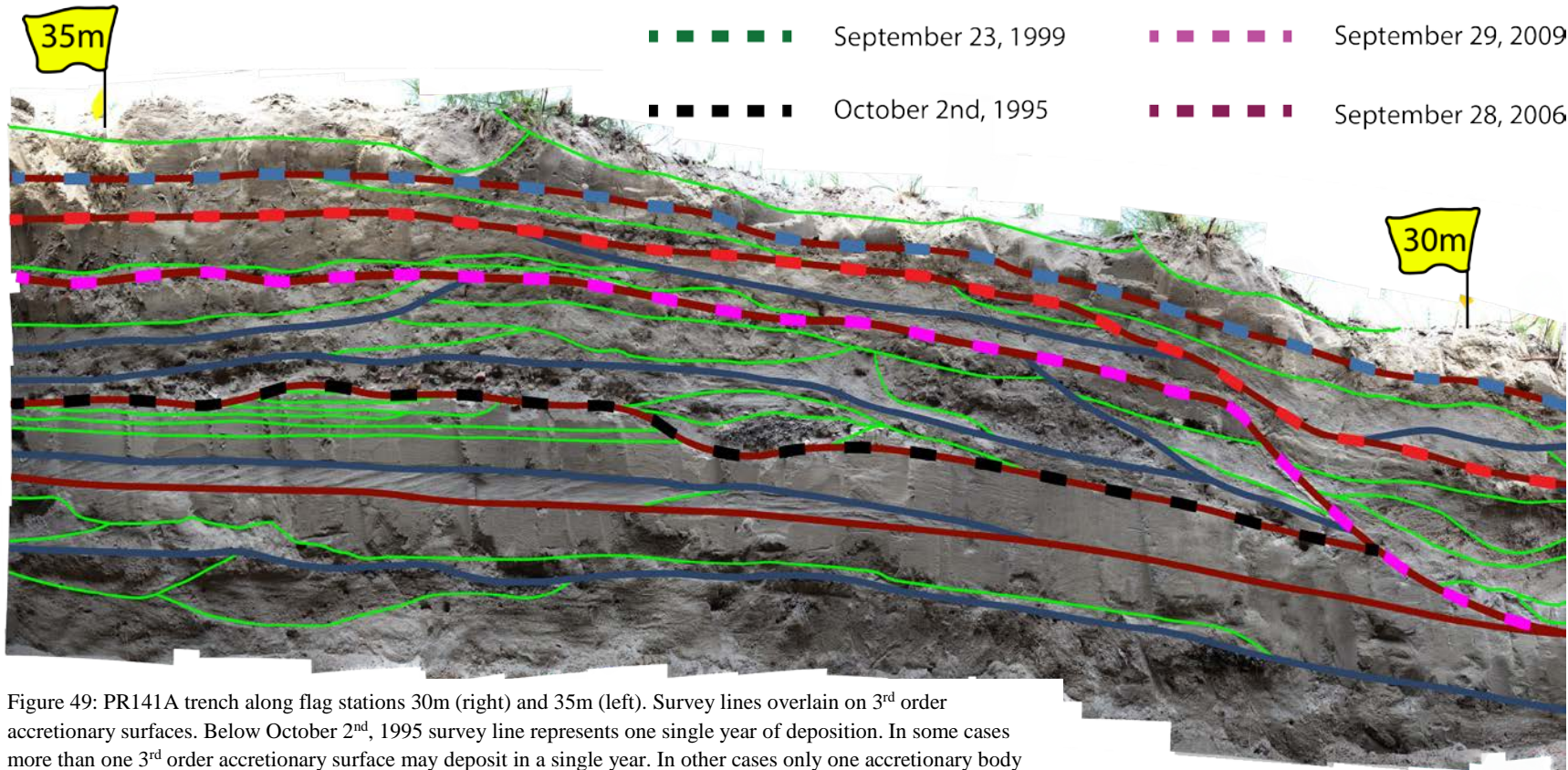


Figure 49: PR141A trench along flag stations 30m (right) and 35m (left). Survey lines overlain on 3rd order accretionary surfaces. Below October 2nd, 1995 survey line represents one single year of deposition. In some cases more than one 3rd order accretionary surface may deposit in a single year. In other cases only one accretionary body may deposit over a number of years. An example of this is seen between the 1995 and 1999 survey line.

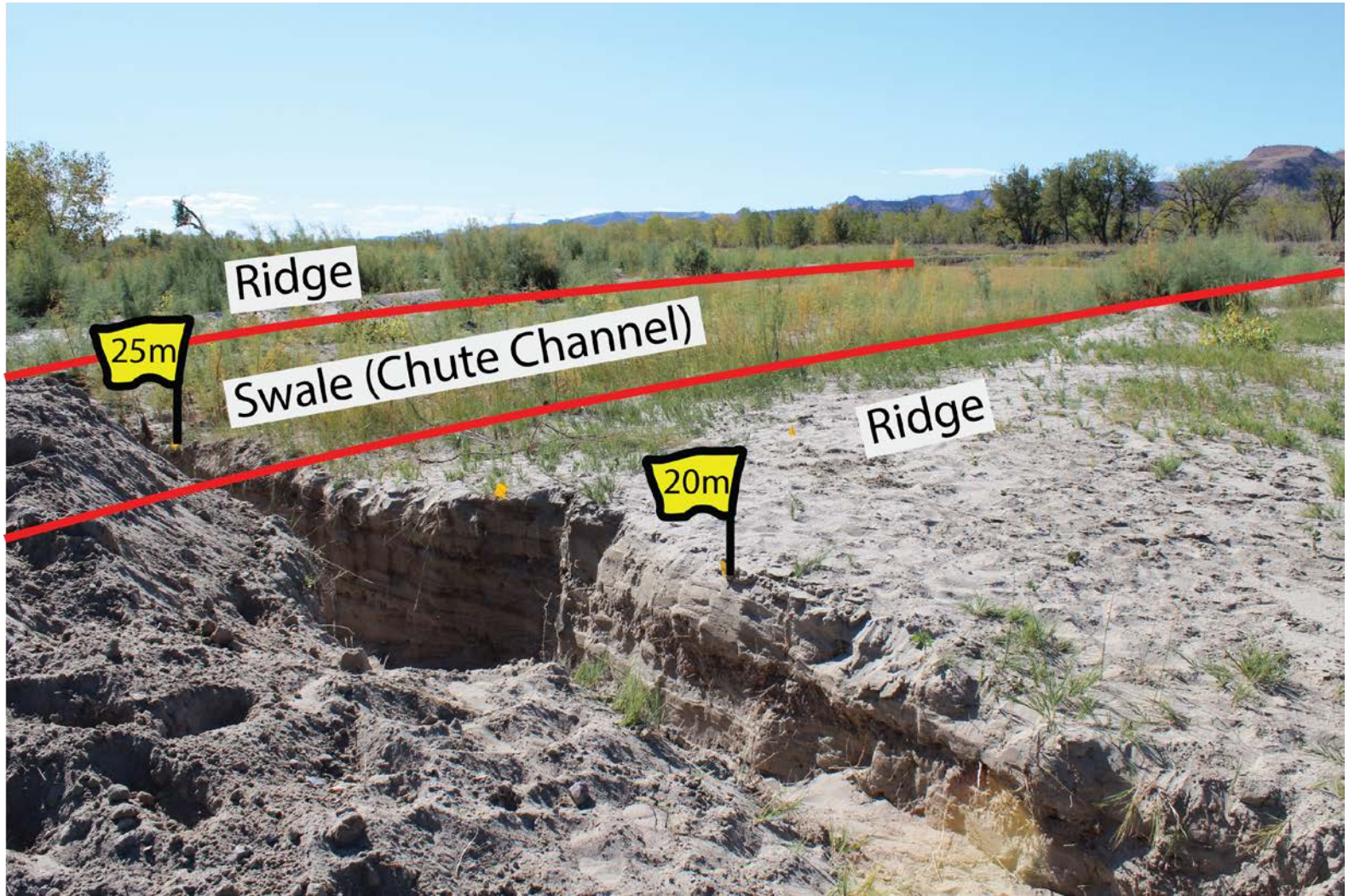


Figure 50: View of PR141A point bar outside of trench. Point bar topography is broken into ridges and swales. Area marked as swale represents a chute channel inside of trench.

CHAPTER 4

DISCUSSION

4.1 Interpretation of Fragmentary Bar Architecture

Architectural-element analysis plays a key role in understanding accretion of fragmentary point bars as well as their internal architecture. Each of the seven surfaces orders mapped is interpreted below.

4.1.1 Zero Order Surface

Zero order surfaces are the fundamental surface that represent the smallest architectural unit. Individual laminae characterize a zero order surface (Holbrook, 2001). These individual laminae record flow regime conditions and deposit as an individual ripple, planar or trough cross laminae, or lower plane bed lamination. Even at this scale, there is heterogeneity and fine-grained sediment rich in organics commonly drape zero order surfaces. This study supports Jordan and Pryor's (1992) interpretation that draping at the laminae scale occurs during periods of slackwater flow conditions at a similar frequency to laminae deposition.

4.1.2 First Order Surface Set

First order sets bind zero order surfaces (Figure 27). They represent sets of ripples, planar or trough cross sets, and lower plane bed laminations. First order sets elucidate flow regime and may constrain paleocurrent direction of the river channel. A 1st order set composed of ripples or lower plane bed laminations represents low shear stress and flow conditions and will likely deposit near the top of the point bar (Allen, 1965; Leeder, 1999; Bridge, 2003). Ripple marks may record a wider variation of flow direction. First order sets composed of lower plane bed laminations represent weak flow moving coarser grains (Allen, 1965; Leeder, 1999; Bridge, 2003). Both trough and planar 1st order cross sets are also part of a lower flow regime, but the

depth and shear stress to form these structures is greater. First order sets binding planar and trough cross laminae record the migration of individual dunes (Allen, 1965; Leeder, 1999; Bridge, 2003). Cross sets within a dune may indicate paleochannel flow direction, but measurements from multiple dunes are needed for accuracy as eddies can lead to a false channel flow direction.

4.1.3 Second and Third Order Surface Sets

Second and 3rd order surface sets have a strong interrelationship to each other and are accordingly interpreted here together. Third order accretionary bodies follow the direction of point bar migration and I interpret them as individual lateral accretion sets. Within a lateral accretion set are smaller 2nd order bodies that bind unit bars. In the ancient point bar these unit bars commonly fine upward and are capped by one of the five drape types discussed earlier (Figures 31-34). Unit bars in the modern also show instances of fining, but these trends are not as common as in the modern example. I interpret unit bars as pulses of sediment that form during floods. Drapes over the top of these unit bars record draping during intervening waning flow. Unit bars in the ancient and modern PR141A point bar commonly map as lobate bodies that do not behave as full lateral accretion sets, but are instead components that build lateral accretion sets. During a flood pulse unit bars will deposit into any void spaces on the bar surface, which may not match the pattern of migration individually, but form the pattern of migration collectively.

The main driver on shear stress during a flood event is water depth. During high stages of a flood, the deeper river has sufficient shear stress to carry and move larger grains of sediment. As water depth decreases during the waning stages of a flood event, the river loses shear stress and competence and deposits finer grains and drapes that preserve as a fining upward

trend. The modern and ancient examples here differ in that the ancient example more commonly has fining upward trends. These data infer that the Powder River near Broadus, Montana is less sensitive to changes in competence during waning flow conditions.

Point bar surveys along PR141A and PR163 reveal insights into the nature of 3rd order accretionary packages and how they form (Figures 45-49). These accretionary bodies can form as a unit during a discrete event or as a set of units deposited in phases. In the case of a discrete event driven accretionary body the yearly survey line will closely match the location of a mapped 3rd order surface. I interpret accretionary bodies that show this character as bodies that form during a discrete flood pulse event that deposits unit bars followed by a period of quiescence with little modification of the bar surface following a large event (Figures 47-49). On the other hand, there are times when the yearly survey does not match the exact position of a 3rd order surface, but instead deviates away from it in all or some locations. It is important to note that surveys are taken during the dry season when the river is likely to be more quiescent. Therefore, for cases where the survey line deviates above a 3rd order surface, I infer that sediment is depositing during small flood events in the offseason and a new accretionary body is in the beginning stages of construction. The accretionary body will continue to be constructed during later events. Therefore, the accretionary body constructs itself during phases of flood pulse events that occur at different times rather than a discrete event. For cases where the survey line deviates below a 3rd order surface, I infer that the accretionary body has not finished building at that location and continues to construct itself following the date of the survey.

These data argue for a preliminary relationship between flood pattern and the composite constructional and continuous surface. Composite constructional surfaces appear to form through a series of flood pulse events that deposit unit bars at different times during a single or multiple

floods. Unit bars will continue to fill void spaces and the wetted bar surface will continue to be reshaped during each flood pulse. Once all events are complete, a time independent composite constructional surface preserves and marks the end of the accretionary event. Continuous surfaces relate to discrete event accretion in their formation. For a continuous surface a single flood pulse deposits one unit bar and the surface is built during a single event with little to no modification of the surface following the event.

Results from the Powder River show that on average there is typically one accretionary body that forms per yearly flood cycle. However, there are instances where only one accretionary body forms over multiple years or more than one forms during a single year. These differences are likely a result of the hydrodynamic flow regime of the river. Typically, most years will have one large flood event that may be responsible for forming most of the sediment within an accretionary body. However, some years may not have a large flood event and it may take several years to build an accretionary body. Alternatively, one year may have multiple large flood events that build several accretionary bodies. Accretionary bodies commonly record the flood events on a yearly cycle, but variations in the hydrodynamic flow regime from other controls are also apparent and may lead to deviations from this cycle. Similarities in architecture of 3rd order and 2nd order surfaces in the modern and ancient suggest the formation and timing of accretionary bodies in the modern are also similar to the ancient. More investigation is required to match discrete accretion sets to discrete floods in the Powder River example, however, before more can be said of the relationship between accretion and flood events in the ancient.

4.1.4 Fourth Order Surface Set

The 4th order surface set is seen along the toe end of the fragmentary point bar. The basal 4th order surface maps as a U-shape that curves around the point bar. I interpret the 4th order set as channel fill deposits. The abandonment phase of this channel does not follow the traditional architecture of oxbow lake channel fill. Within this channel fill are lateral accretion sets that follow the same easterly direction of migration of the point bar instead of mimicking the shape of the channel itself. Toonen et al. (2012) shows similar examples of a diminishing flow channel fill near the Rhine Delta region that preserves barforms. These lateral accretion sets are muddier and more continuous than the sandier bar deposits and mark a transition in the depositional style of accretion (Figure 35). As the fragmentary bar abandoned it continued to deposit lateral accretion sets within the channel during flood events. However, a diminished flow regime leads to accretionary sets that are muddier than the sandier deposits of an active channel (Toonen et al, 2012). On the easternmost section of the channel fill are muddy accretion sets that migrate toward the west. I interpret these sets as accretion that occurs on the cutbank side of a channel when it begins to abandon. Once the bar fully disconnects from the newly active channel it gradually fills up with suspended load that spills over from the active channel during flood events (Toonen et al, 2012). There is no distinction of a channel “clay plug” from the surrounding floodplain deposits. Rather the composite soil that caps the channel fill is an extension of the floodplain and is marked by the upper 5th order contact.

4.1.5 Fifth Order Surface Set

A 5th order surface set binds a single point bar story. The channel area along Amphitheater B is the only location where the basal 5th order surface outcrops. Above the basal 5th order surface are surfaces that follow an easterly direction of lateral accretion. However,

below this surface are lateral accretion sets that migrate toward the southwest. These underlying lateral accretion sets represent an older bar story that the fragmentary point bar cuts into from above (Figure 36). The erosional contact between the two bars marks the location of the basal 5th order surface. This surface is also mapped in the geologic map by Durkin et al. (2015) showing the edge of the meander loop including the fragmentary point bar and channel fill cutting into what he identifies as a counter point bar beneath. The gradational contact above the point bar and channel fill that separates it from the floodplain above is not a discrete surface but is equivalent in order to a 5th order surface.

4.1.6 Sixth Order Surface Set

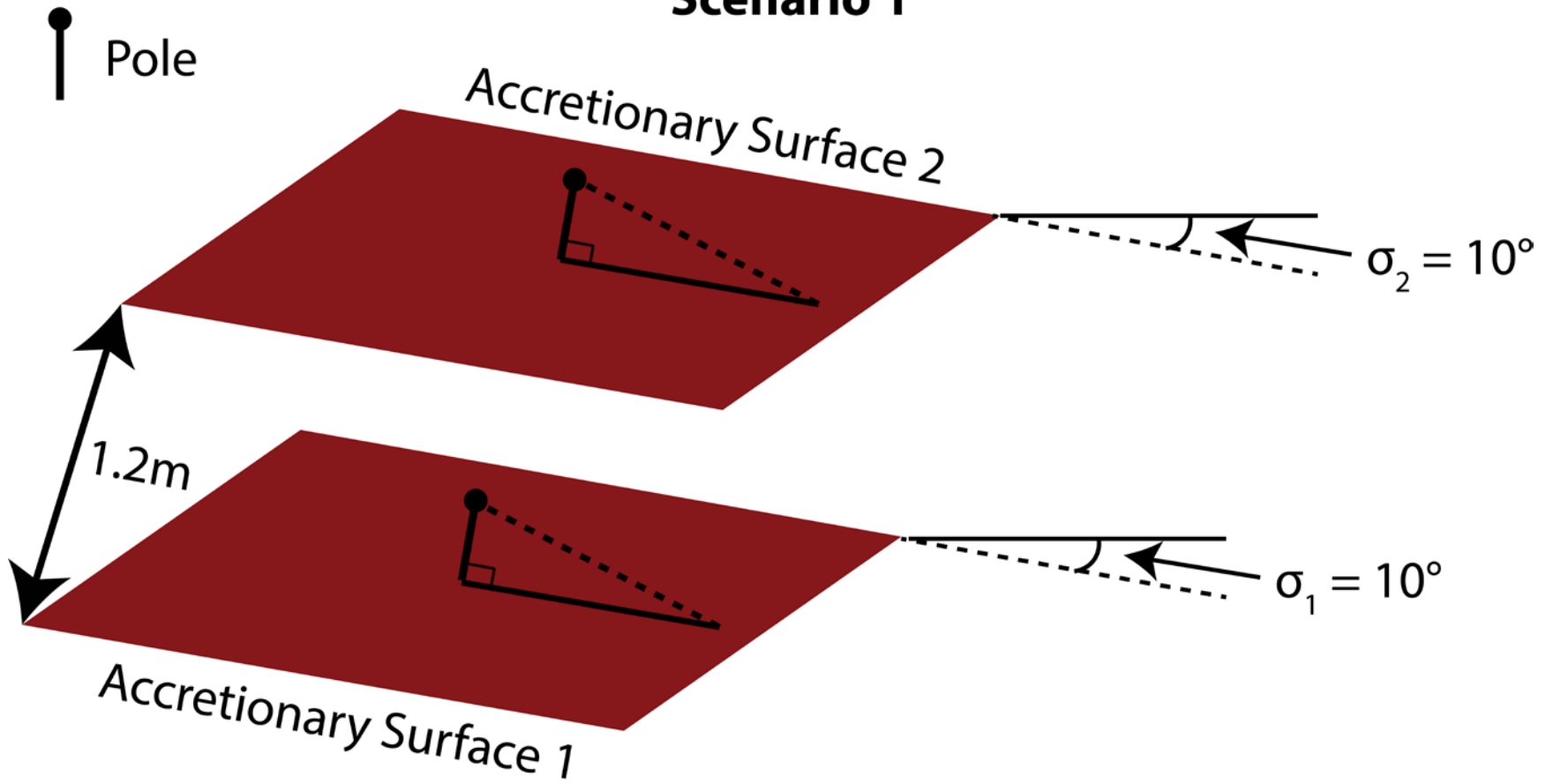
The 6th order surface set is the master surface and binds all surfaces seen in this study. Durkin et al. (2015) mapped this surface throughout much of the Steveville area of Dinosaur Provincial Park (Figure 37). This surface set represents a single channel belt from deposits below. It binds the basal point bar I am observing along with many other bars in the field site. The composite soil beneath this surface marks the floodplain deposit of the bars from an older channel belt.

4.2 How is a Fragmentary Point Bar Fragmented?

Detailed observation of the ancient Dinosaur Park Formation and modern Powder River point bars show that there is more than one way to build a point bar besides the widely accepted normal point bar accretion method. The alternative accretionary process introduced in this study is the fragmentary point bar. Discussion of fragmentary point bar architecture in Chapter 4.1 establishes that 3rd order accretionary bodies record individual lateral accretion sets. These 3rd order lateral accretion sets are also seen in normal point bars. However, the geometry of these sets are choppy in a fragmentary point bar and do not tend to extend the full bar length.

Changes in strike and dip, as measured by pole variation, between successive surfaces drives bar fragmentation. This is because fragmentation requires that an overlying surface truncates or onlaps an underlying surface and both surfaces do not continue the length of the bar. Parallel accretion surfaces extending the length of the bar will thus not result in fragmentation and will result in normal bar deposition with successive en echelon accretion surfaces. An ideal scenario of two successive accretionary surfaces that have no pole variation and are therefore parallel to each other. Assume a viewing area of 40m and an accretionary surface separation of 1.2m (the average separation of 3rd order surfaces measured in the Dinosaur Provincial Park field example). If successive accretionary surfaces deposit in this fashion, then the bar generated would model as a normal point bar. However, if the succeeding accretionary surface rotates its pole a minimum of 1.7° in any direction over a sample length of 40 meters, then the above surface will truncate the surface below resulting in fragmentation (Figure 51). Crossplots of Locations A through F in the Cretaceous Dinosaur Provincial Park example reflect the capacity of pole variation to drive fragmentation. Crossplots for Locations A through F compare the relationship between pole variation of accretionary surfaces, number of surface truncations, and accretionary surface number. A second set of crossplots with the same variables, considers the impact of these variables where extraneous surfaces introduced into the viewing area are removed (Figure 52). Truncations of underlying surfaces by overlying surfaces and pole deviations beyond the 1.7° minimum angle underlying are both common place.

Scenario 1



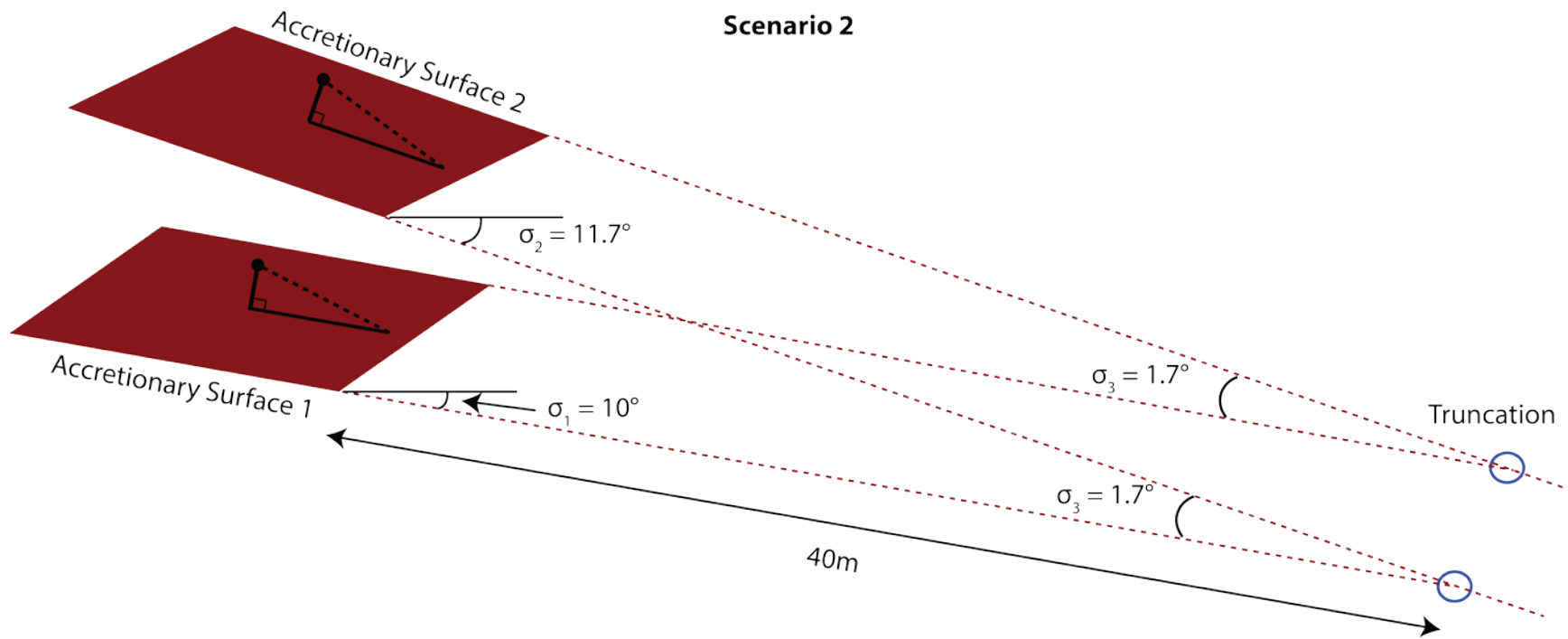


Figure 51: Scenario 1 shows two 3rd order accretionary surface planes (colored in dark umber) that are parallel to each other. Pole orientation is projected above each surface. Scenario 1 is characteristic of normal point bar deposition where surfaces lack pole variation and therefore accretionary bodies stack on each other. Both surfaces are inclined at a 10° angle and have a separation of 1.2m. Scenario 2 illustrates the minimum pole rotation angle needed for accretionary surface 2 to truncate surface 1 over a 40m distance. Note that a 1.7° rotation of surface 2 pole in any direction would result in a truncation.

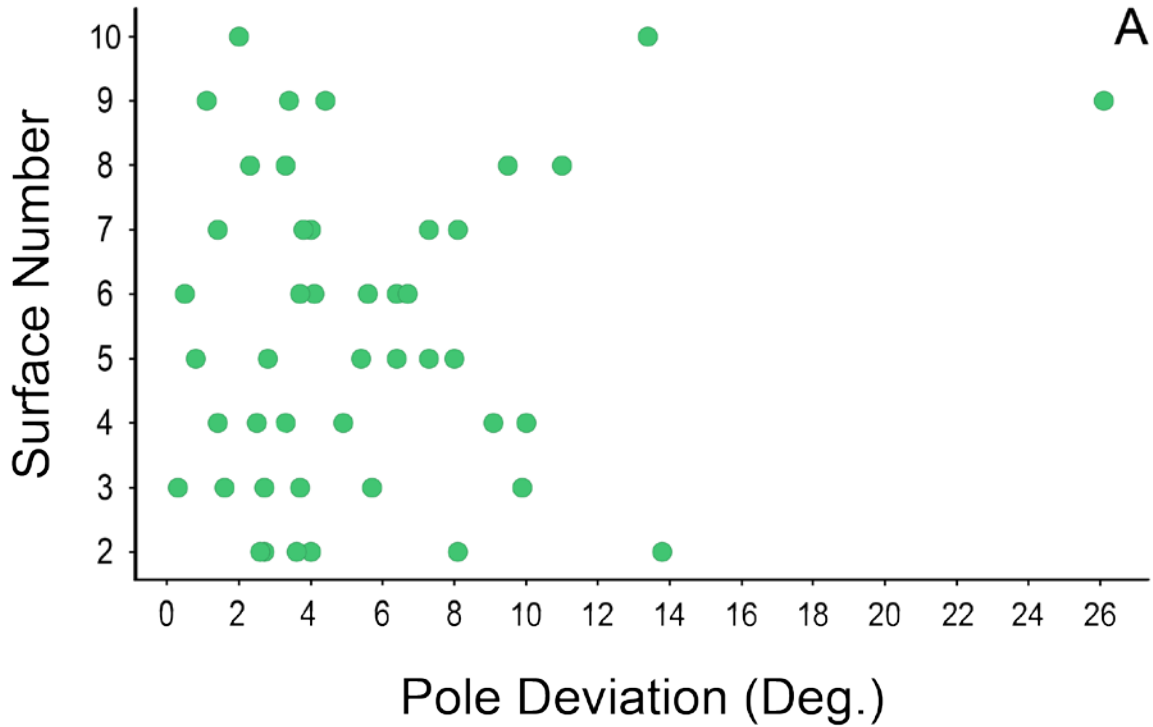
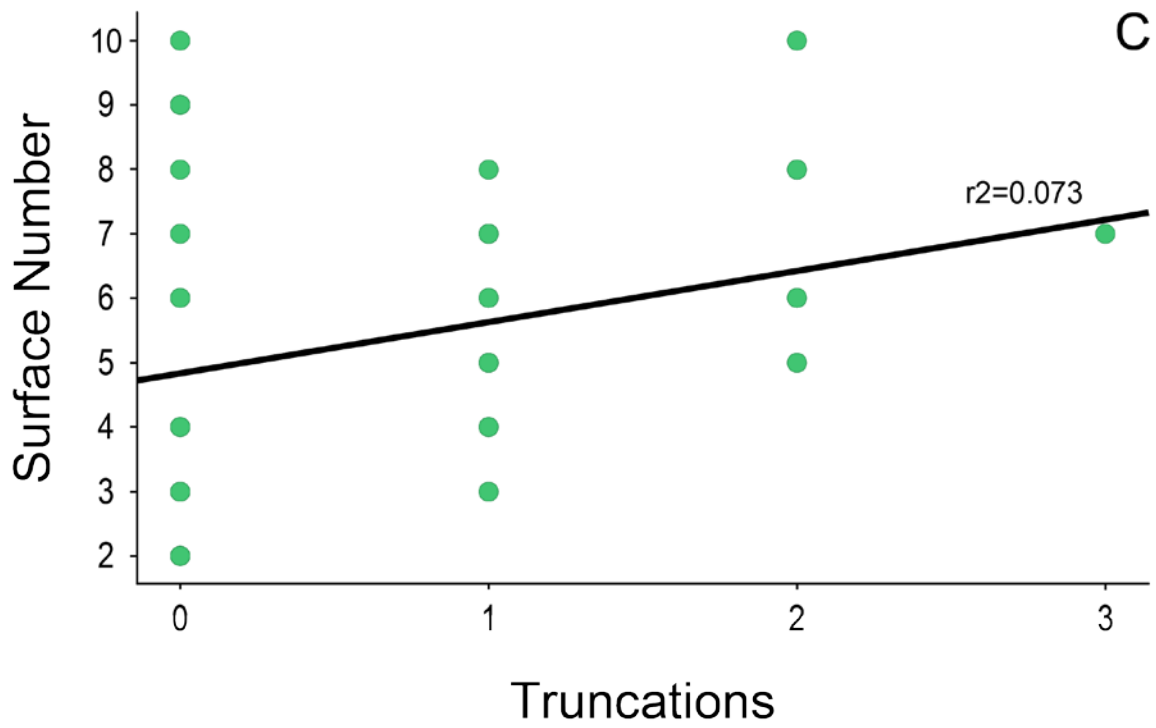
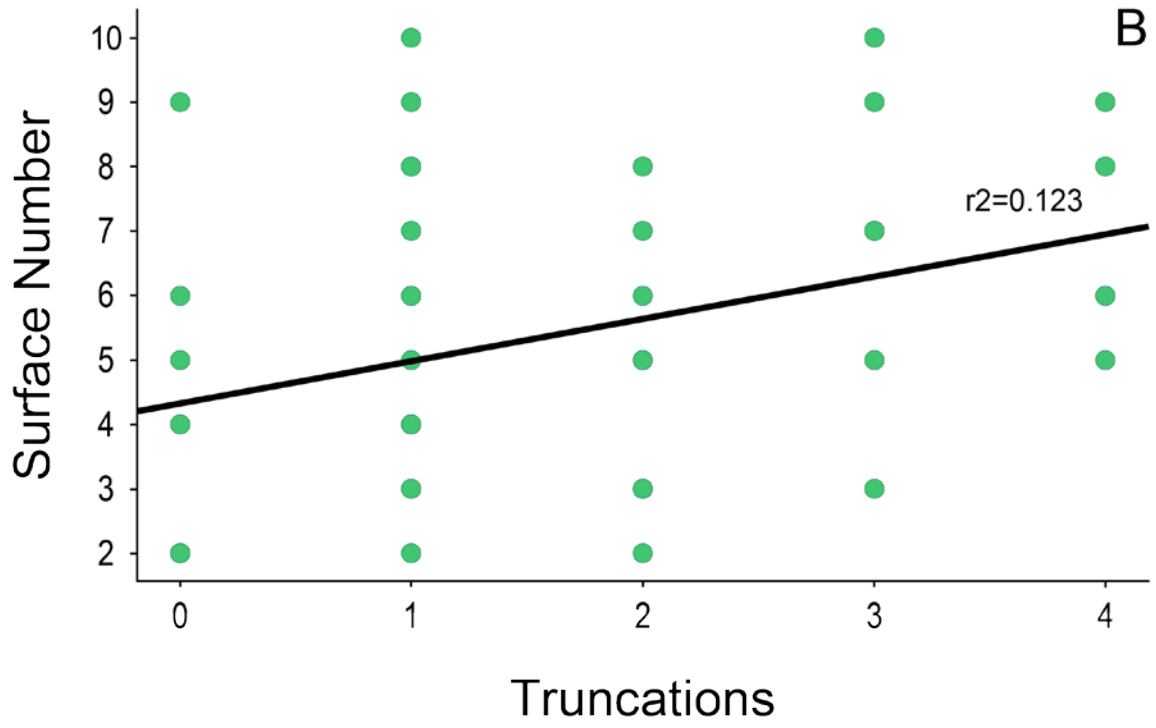
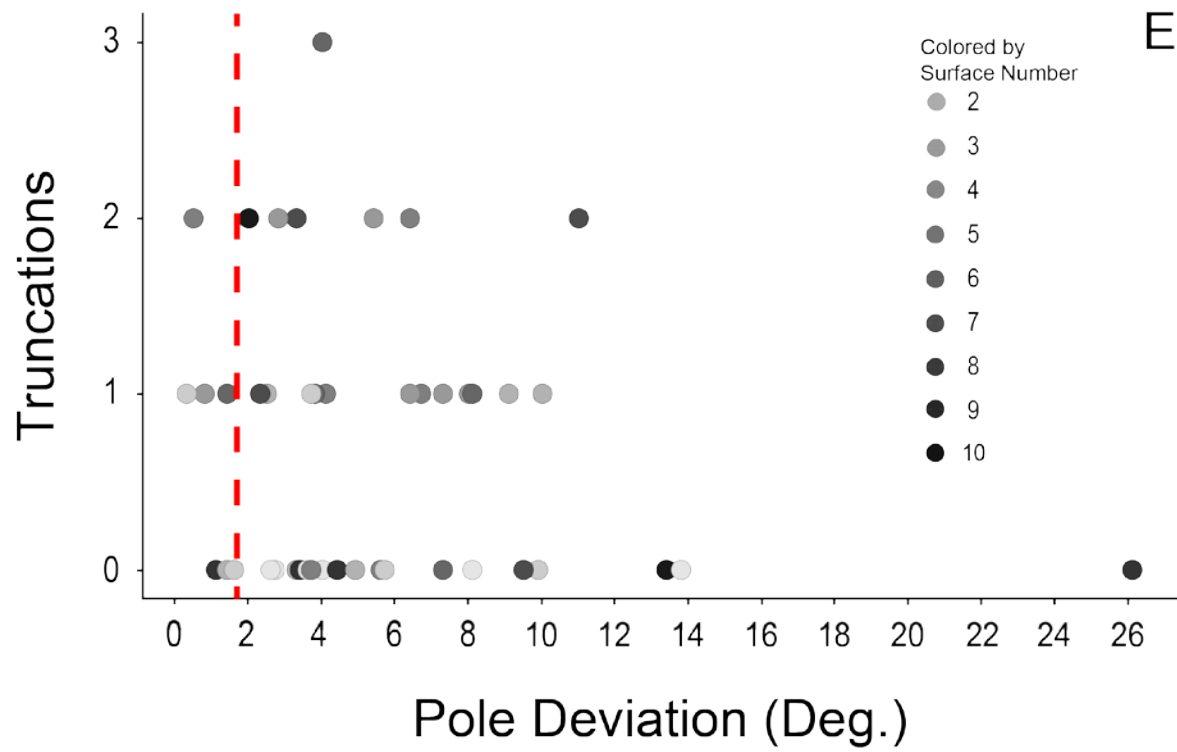
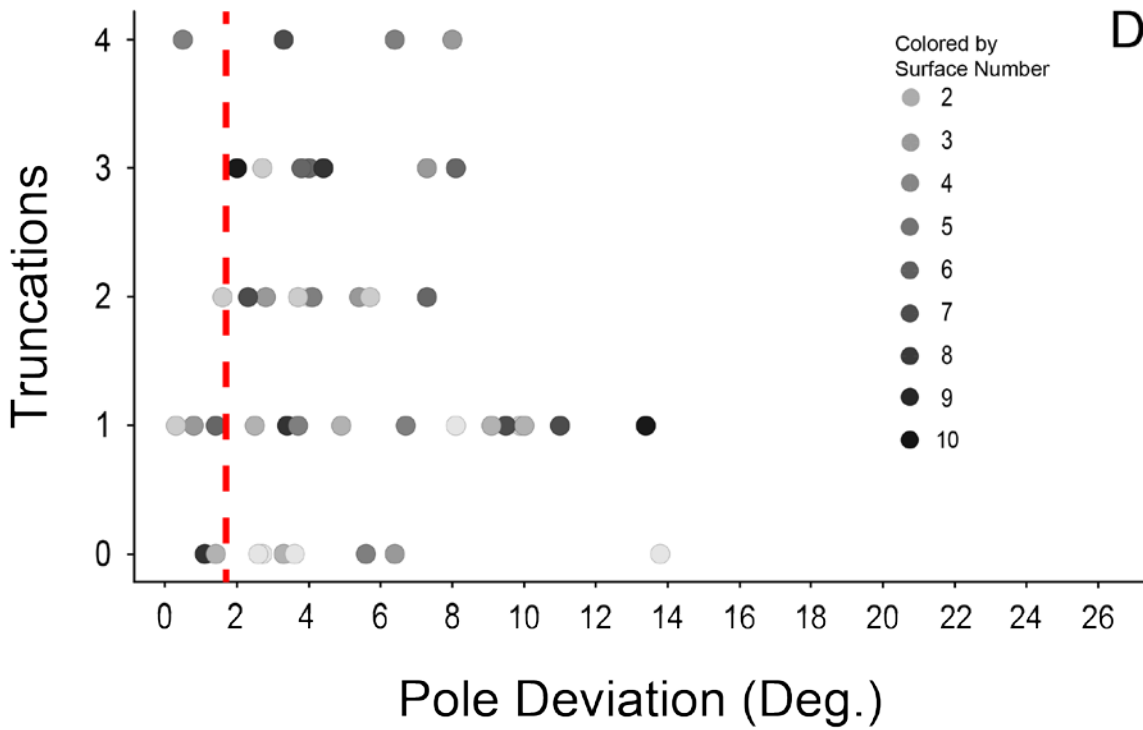


Figure 52: Crossplots A-E comparing pole deviation (degrees), accretionary surface number, and truncations. A) Lack of correlation between pole deviation and accretionary surface number. B) Weak correlation between number of truncations and the accretionary surface number. Crossplot includes all surfaces recorded. C) Excludes extraneous surfaces introduced into the 40m sample viewing area. Very weak correlation between number of truncations and the accretionary surface number. D) Lack of correlation between pole deviation, truncations, and accretionary surface number. The dashed red line shows the minimum required pole deviation (1.7°) for a truncation to occur on average between successive surfaces (see Figure 51). Note how most surfaces meet the average required minimum to truncate, and only a few that do not. E) Excludes extraneous surfaces introduced into the 40m sample viewing area. Lack of correlation between pole deviation, truncations, and accretionary surface number. The dashed red line shows the minimum required pole deviation (1.7°) for a truncation to occur on average between successive surfaces (see Figure 51). Similar to (D), most surfaces meet the average required minimum to truncate, and only a few do not.





In theory, a 1.7° pole rotation will lead to fragmentation of successive surfaces over the 40m Dinosaur Provincial Park viewing area summarized in Table 1. However, the data and crossplots show that the relationship between truncation and pole variation is more complicated and that additional observations are available. Crossplots reveal four key observations:

1. Pole variations neither decrease or increase further up the point bar (Figure 52A).
2. There is only a very weak correlation between the number of truncations and position of the surface within the point bar, whether or not extraneous surfaces are included (Figure 52 B,C).
3. There seems to be no correlation to pole variation and number of surface truncations (Figure 52 D,E).
4. There are instances where surfaces truncate yet have a pole variation that falls below the required 1.7° angle for truncation. There are also instances where surfaces have no truncations yet fall above the required angle for truncation (Figure 52 D,E).

Complications in the relationship between pole variation and fragmentation by surface truncation arise because of several factors. Surfaces that plot below the minimum required angle for truncation are representative of successive accretionary surfaces that have less separation between them than the average separation of 1.2m (Figure 53). Over a 40m window, a smaller separation will allow for a smaller minimum angle for truncation to occur; thus some truncations plot below the minimal average required pole variations (Figure 52 D,E). Although logic demands that higher pole variations result in more truncations, there are other surfaces introduced in the 40m viewing window that cut plotted surfaces. A plotted surface that is partially truncated by other extraneous surfaces will not be available to be cut by the succeeding surface in the succession. This is exemplified by the contrast between Figures 52 D and E, whereby numerous surfaces with

high pole deviations result in no truncations (E) because the surface has already been cut by extraneous surfaces (D) and are no longer present within the truncation distance (e.g., Figure 54). A plotted surface that is prematurely cut will require the successive surface above to increase its pole variation further for this truncation to occur.

Flooding events do not favor more modification of underlying surfaces/deviation of overlying surfaces in either the lower or upper point bar. Instead, the whole bar surface is susceptible to pole deviation from accretion event to accretion event therefore showing a lack in correlation between surface pole variation and the stratigraphic position of a surface in the bar (Figure 52A). Likewise, orientations are not consistent between successive surfaces; therefore, surfaces are altering orientation at all phases of accretion and between each accretion and no pattern of parallel surfaces establishes before a truncating deviation occurs. This leads to a perturbation in the system at the advent of each surface that propagates to all subsequent surfaces above. Each surface pole variation will compound upon the one before creating a randomizing effect that explains why even small pole deviations can completely fragment the bar.

Lastly, truncations are only recorded along exposed areas of outcrop. Pole variations can occur in any direction and therefore truncate in any direction. The true number of truncations for accretionary surfaces is likely underestimated, as there may be more truncations within the point bar that are unaccounted. The rugosity of the surfaces measured in the field helps to minimize this potential source of error by maximizing the range of orientations where surfaces are measured and truncations are counted.

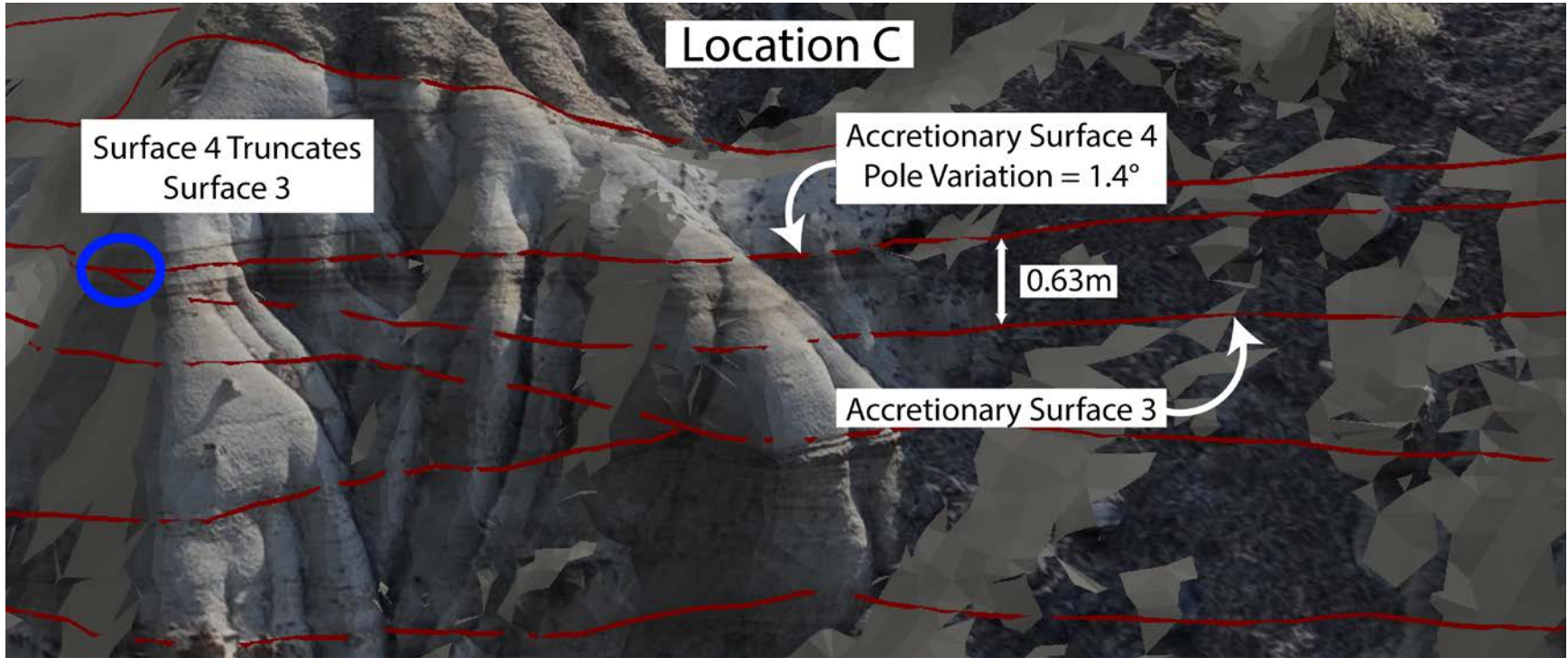


Figure 53: Accretionary surface 4 in Location C has a pole variation (1.4°) below the required minimum yet truncates surface 3 (highlighted in blue circle). The average separation between surface 4 and 3 is 0.63m therefore the angle needed to truncate over a 40m distance is reduced.

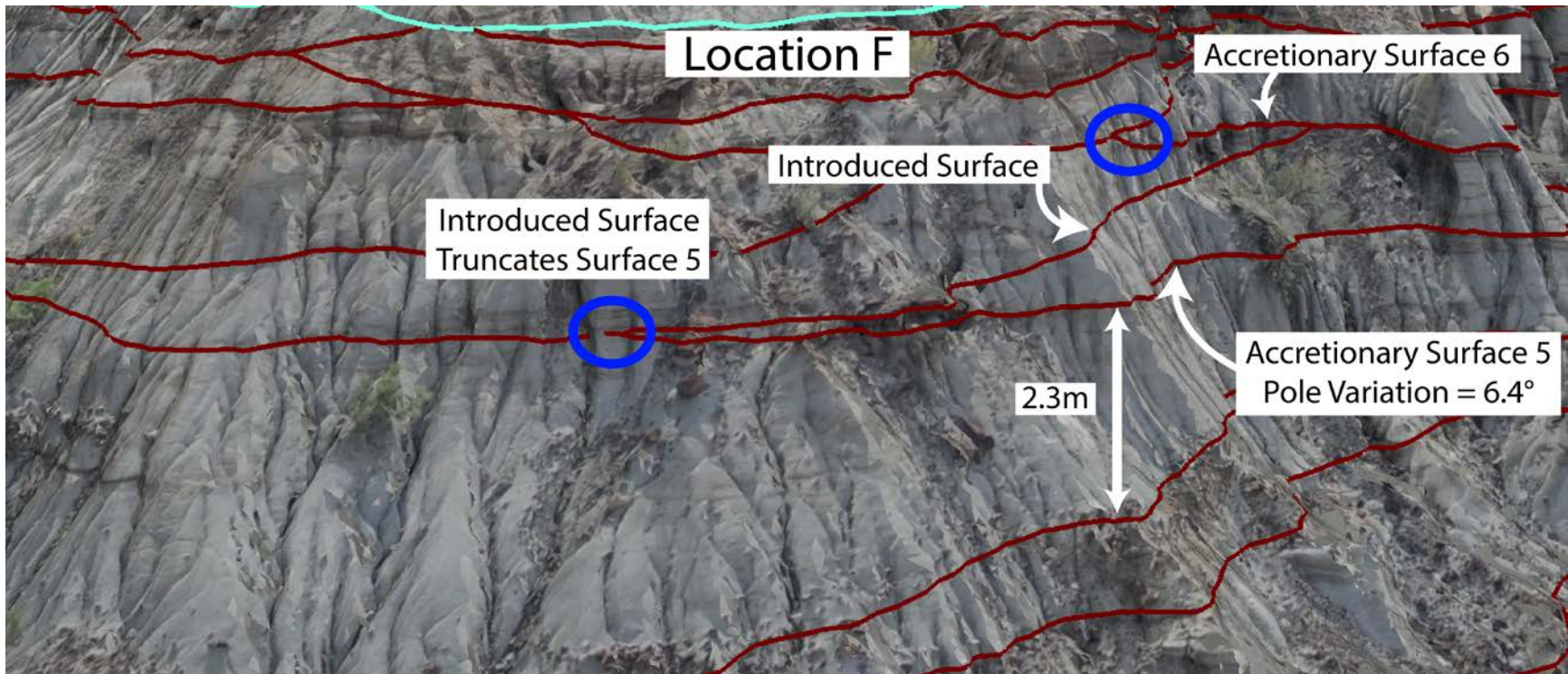


Figure 54: Accretionary surface 5 in Location F has a pole variation (6.4°) above the required minimum yet no truncations occur. Extraneous surface introduced into the 40m viewing area is responsible for truncating surface 5 (highlighted by lower blue circle) inhibiting surface 5 from truncating other surfaces. Note how an introduced surface also truncates surface 6.

If there are no pole variations, then surfaces will stay parallel and a normal point bar will deposit (Figure 4). If on occasion, after some succession of parallel accretionary surfaces, there is a change in pole orientation then a segmented normal point bar will deposit (Figure 55). Long enough periods of point bar stability will mimic normal point bar growth. Eventually the bar reorients itself truncating the surfaces below and then deposits another series of roughly parallel accretionary surfaces. This pattern of segmentation differs from fragmentation because the bar maintains some period of roughly parallel growth of accretion surfaces that falls below the critical angle of fragmentation at significant fragmentation lengths.

Fragmentation of bars may largely derive from the nature of unit bar deposition. Composite constructional 3rd order surfaces are commonly found in the ancient and modern example of a fragmentary bar. Accretionary surfaces in composite constructional surfaces do not record single large-scale accretion events of material draping the surface, but instead record multiple 2nd order unit bars that are stacked selectively on parts of the bar. These same surfaces commonly truncate underlying unit bars or underlying deposits along their length. Each unit bar behaves independent of other unit bars and therefore do not necessarily scour and stack evenly across a surface (Figure 56). Uneven erosion and stacking of unit bars between flood pulse events generates non-parallel accretion surfaces and provides a possible explanation as to how successive accretionary surfaces may change in orientation. The hydrodynamic regime of the river body may be responsible for why there are changes in bar orientation, but this hypothesis remains untested here.

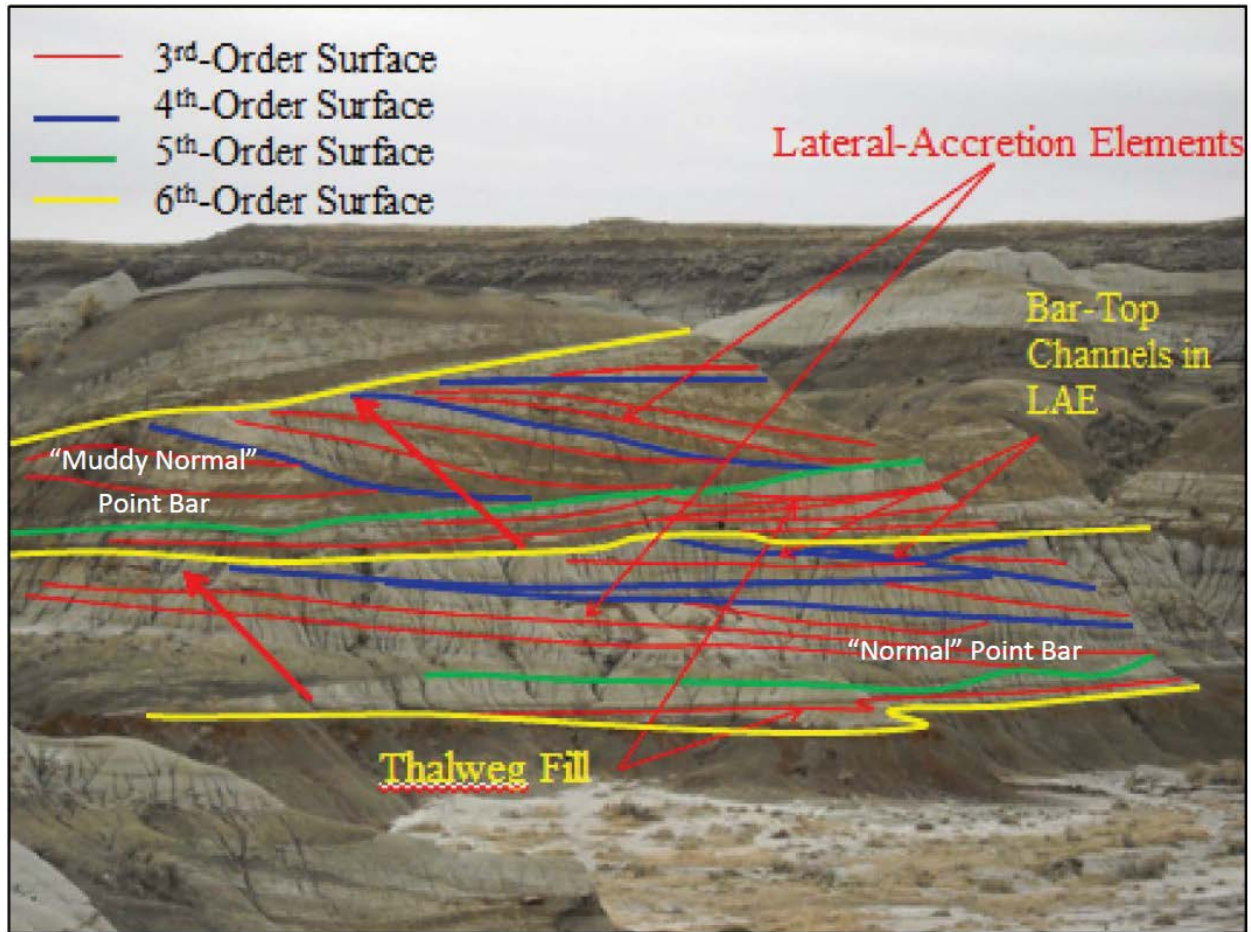
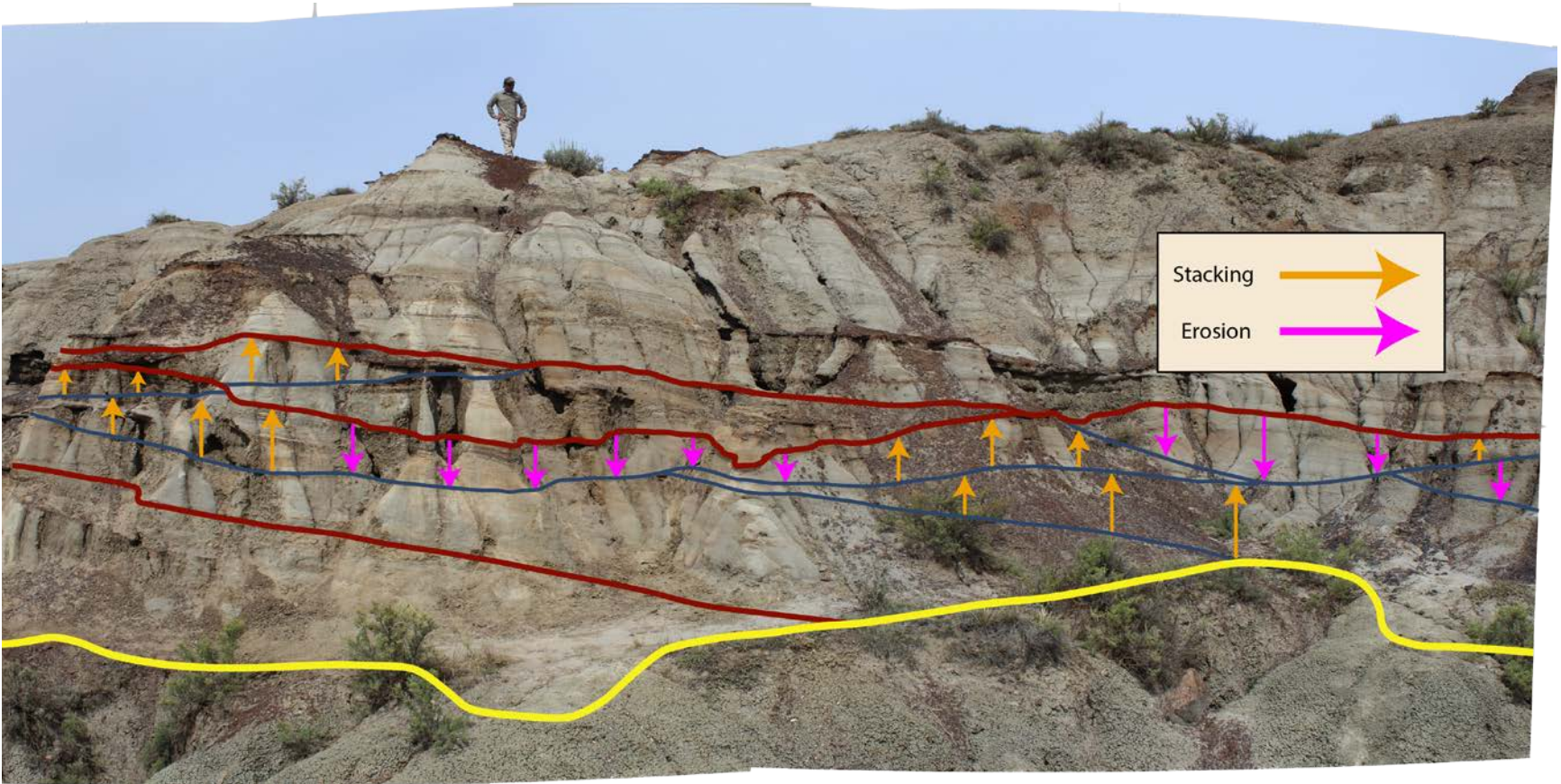


Figure 55: From John Holbrook (Personal Communication). Image of segmented point bar showing 3rd order accretionary surfaces that have periods of stability with little pole variation followed by a bar reorientation that truncates into surfaces below. Bar stabilizes once again and a new package of accretionary surfaces deposit with little pole variation until the next reorientation event occurs (Durkin et al., 2015).

A



B

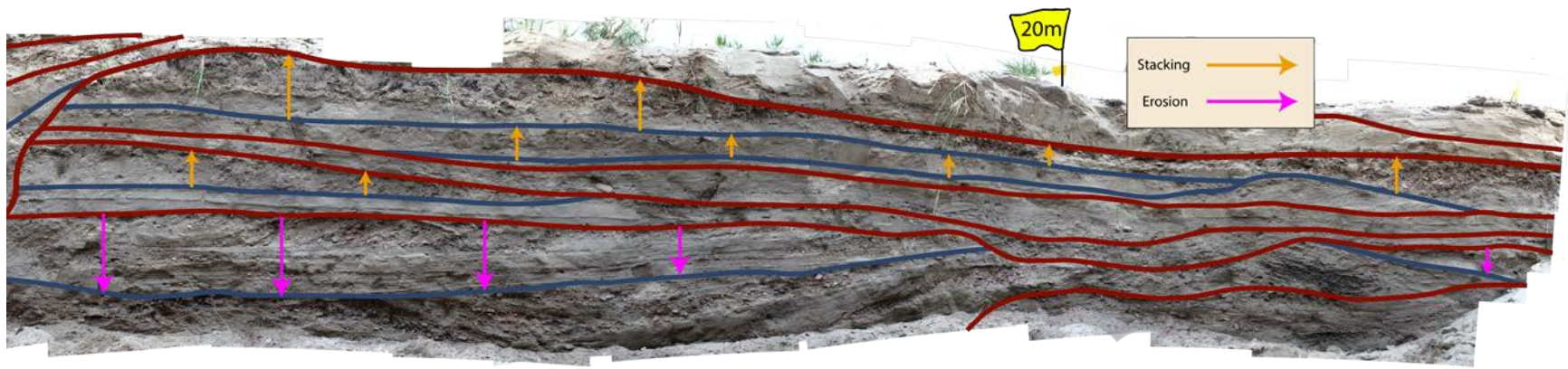


Figure 56: Second order composite constructional surface erosion and stacking patterns of unit bars in both the Late Cretaceous and modern point bar. Orange arrows indicate where the surface is stacking on sediment below. Hot pink arrows indicate where the surface is eroding in the sediment below. A) Late Cretaceous stacking/erosion patterns of 2nd order surfaces. Note how some 2nd order composite constructional surfaces stack in some areas and erode in others. Uneven patterns of stacking along these surfaces drives bar fragmentation. B) Stacking/erosion patterns of 2nd order surfaces within the modern Powder River point bar at PR141 A trench. Uneven stacking/erosion surfaces are similar to that seen in (A). The 5th accretionary surface up the point bar marks a continuous surface (see Figure 39). Note how the unit bar below this surface stacks evenly throughout its length allowing for the accretionary 3rd order surface above to have a similar pole deviation as the 3rd order surface below.

Chapter 5

Conclusions

1. The fragmentary bar accretion model results in minimal to no continuous accretion surfaces within point bars and is one alternative method to build a point bar from the classic normal point bar model which is characterized by continuous accretion surfaces.
2. Third order surfaces are formed as either composite constructional or continuous surfaces. Composite constructional surfaces formed from selective and local stacking of multiple unit bars with local scour and truncation of underlying unit bars tend not be parallel to underlying surfaces and contribute to the pole deviation between accretion surfaces that drives fragmentation. Continuous surfaces are less likely to drive fragmentation.
3. Pole deviation between successive surfaces is a randomizing variable that drives bar fragmentation. There is no pattern found here of selective pole variation in the upper or lower part of the bar and each surface tends to deviate from the surface below. Variations from one surface compound through successive surfaces and surface complexity interact to randomize trends in surface and resultant bar fragmentation.
4. The fragmentation angle needed to fragment bars at some critical fragmentation distance can be quite small and as small as a couple degrees.
5. Architectural elements in the modern Powder River match architecture in the ancient example, and similarly generate composite constructional surfaces through selective unit bar deposition and truncation and similarly fragment.
6. Yearly surveys of PR141A trench show that on average there is typically one 3rd order accretionary body deposited per year. There are instances where there is more than one accretionary body

deposited in a single year. Furthermore, there are surveys that show a single accretionary body may take several years to build.

7. The competence of a river determines the stratigraphic nature of unit bars. The Powder River is less sensitive to changes in competence during waning flow conditions and tends to be more gravelly with less consistency in fining-upward trends for unit bars.

REFERENCES

- Allen, J. R. L., 1963, Henry Clifton Sorby and the sedimentary structures of sands and sandstones in relation to flow conditions: *Geologie en Mijnbouw* v. 42, p. 223–228.
- Allen, J. R. L., 1970, *Physical processes of sedimentation*: London, Allen and Unwin, 248 p.
- Allen, J.R.L., 1965, A review of the origin and characteristics of recent alluvial sediments: *Sedimentology*, v. 5, p. 91-191.
- Allen, S.D., 2015, Reverse Meanders, Pseudo Point Bars, and the Enigma of Meandering in Braided Rivers.
- Blum, M., Scaling Relationships Between Fluvial Channel Fills, Channel-Belt Sand Bodies and Drainage Basins, With Implications for the Mannville Group, Alberta Foreland Basin, *in* AAPG Annual Convention and Exhibition.
- Bridge, J.S., 2003, *Rivers and floodplains; forms, processes, and sedimentary record*: Oxford, United Kingdom (GBR), Blackwell Publishing, Oxford, p. 491.
- Bridge, J.S., and Tye, R.S., 2000, Interpreting the dimensions of ancient fluvial channel bars, channels, and channel belts from wireline-logs and cores: *AAPG Bulletin*, v. 84, p. 1205-1228, doi: <http://dx.doi.org/10.1306/A9673C84-1738-11D7-8645000102C1865D>.
- Bristow, C.S., and Best, J.L., 1993, Braided rivers; perspectives and problems: *Geological Society Special Publications*, v. 75, p. 1-11.

- Cant, D.J. (1982) Fluvial facies models and their application. In: Sandstone Depositional Environments (Eds P.A. Scholle and D. Spearing), AAPG Mem., 31, 115–137
- Constantine, J.A., and Dunne, T., 2008, Meander cutoff and the controls on the production of oxbow lakes: *Geology (Boulder)*, v. 36, p. 23-26, doi: <http://dx.doi.org/10.1130/G24130A.1>.
- Daniel, J.F., 1971, Channel movement of meandering Indiana streams: U.S. Geological Survey Professional Paper, p. A1-A18.
- Donselaar, M.E., and Overeem, I., 2008, Connectivity of fluvial point-bar deposits: An example from the Miocene Huesca fluvial fan, Ebro Basin, Spain: *AAPG Bulletin*, v. 92, p. 1109-1129, doi: 10.1306/04180807079.
- Durkin, Paul R., Hubbard, Stephen M., Weleschuk, Smith, Derald G., Palmer, Matthew B., Torres, Alexander, and Holbrook, John M., 2015, Spatial and Temporal Evolution of an Ancient Fluvial Meanderbelt (Upper Cretaceous Dinosaur Park Formation, Southeastern Alberta, Canada) With Emphasis on Characterization of Counter Point Bar Deposits, *in AAPG Annual Convention and Exhibition*.
- Eberth, D.A., and Hamblin, A.P., 1993, Tectonic, stratigraphic, and sedimentologic significance of a regional discontinuity in the upper Judith River Group (Belly River wedge) of southern Alberta, Saskatchewan, and northern Montana: *Canadian Journal of Earth Sciences = Revue Canadienne Des Sciences De La Terre*, v. 30, p. 174-200, doi: <http://dx.doi.org/10.1139/e93-016>.
- Einstein, H.A. and Barbarossa, N. L., 1952, River channel roughness. *Trans. Am. Soc. Civil Engrs.*, 117 : 1121-1132

- Fisk, H. N., 1944. Geological Investigation of the Alluvial Valley of the Lower Mississippi River. Mississippi River Commission, Vicksburg, Miss., 78 pp.
- Gay, G.R., Gay, H.H., Gay, W.H., Martinson, H.A., Meade, R.H., and Moody, J.A., 1998, Evolution of cutoffs across meander necks in Power River, Montana, USA: *Earth Surface Processes and Landforms*, v. 23, p. 651-662.
- Hamblin, A.P., 1997a, Regional distribution and dispersal of the Dinosaur Park Formation, Belly River Group, surface and subsurface of southern Alberta: *Bulletin of Canadian Petroleum Geology*, v. 45, p. 377-399.
- Hamblin, A.P., 1997b, Stratigraphic architecture of the Oldman Formation, Belly River Group, surface and subsurface of southern Alberta: *Bulletin of Canadian Petroleum Geology*, v. 45, p. 155-177.
- Hamblin, A.P., and Abrahamson, B.W., 1996, Stratigraphic architecture of "basal Belly River" cycles, Foremost Formation, Belly River Group, subsurface of southern Alberta and southwestern Saskatchewan: *Bulletin of Canadian Petroleum Geology*, v. 44, p. 654-673.
- Hembree, C.H., Colby, B.R., Davis, J.R., Meuschke, J.L., and Swenson, H.A., 1952, Sedimentation and chemical quality of water in the Powder River drainage basin, Wyoming and Montana: U.S. Geological Survey Circular, .
- Holbrook, J., 2001, Origin, genetic interrelationships, and stratigraphy over the continuum of fluvial channel-form bounding surfaces; an illustration from Middle Cretaceous strata, southeastern Colorado: *Sedimentary Geology*, v. 144, p. 179-222.

- Holbrook, J., Autin, W.J., Rittenour, T.M., Marshak, S., and Goble, R.J., 2006, Stratigraphic evidence for millennial-scale temporal clustering of earthquakes on a continental-interior fault: Holocene Mississippi River floodplain deposits, New Madrid seismic zone, USA: *Tectonophysics*, v. 420, p. 431-454, doi: <http://dx.doi.org/10.1016/j.tecto.2006.04.002>.
- Jackson, R.G., 1976, Depositional model of point bars in the lower Wabash River: *Journal of Sedimentary Research*, v. 46, p. 579-594, doi: 10.1306/212F6FF5-2B24-11D7-8648000102C1865D.
- Jordan, D.W., and Pryor, W.A., 1992, Hierarchical levels of heterogeneity in a Mississippi River meander belt and application to reservoir systems: *AAPG Bulletin*, v. 76, p. 1601-1624.
- Labrecque, P.A., Jensen, J.L., and Hubbard, S.M., 2011, Cyclicity in Lower Cretaceous point bar deposits with implications for reservoir characterization, Athabasca Oil Sands, Alberta, Canada: *Sedimentary Geology*, v. 242, p. 18-33, doi: <http://dx.doi.org/10.1016/j.sedgeo.2011.06.011>.
- Leeder, M., 1999, *Sedimentology and sedimentary basins; from turbulence to tectonics*: Oxford, United Kingdom (GBR), Blackwell Science, Oxford, p. 592.
- Lunt, I.A., Bridge, J.S., 2007. Formation and preservation of open-framework gravel strata in unidirectional flows. *Sedimentology* 54 (200702), 71–87 no. 1.
- Miall, A.D., Flores, R.M., Ethridge, F.G., Galloway, W.E., and Fouch, T.D., 1985, Architectural-element analysis; a new method of facies analysis applied to fluvial deposits: *SEPM Short Course*, v. 19, p. 33-81.

- Miall, A.D., 1996, *The geology of fluvial deposits; sedimentary facies, basin analysis, and petroleum geology*: Berlin, Federal Republic of Germany (DEU), Springer-Verlag, Berlin, p. 582.
- Miall, A.D., 2014, Updating uniformitarianism; stratigraphy as just a set of "frozen accidents": Special Publication - Geological Society of London, v. 404, , doi: <http://dx.doi.org/10.1144/SP404.4>.
- Moody, J., and Meade, R.H., 2008, Terrace aggradation during the 1978 flood on Powder River, Montana, USA: *Geomorphology*, v. 99, p. 387-403, doi: <http://dx.doi.org/10.1016/j.geomorph.2007.12.002>.
- Moody, J.A., and Meade, R.H., 2014, Ontogeny of point bars on a river in a cold semi-arid climate: *Geological Society of America Bulletin*, v. 126, p. 1301-1316, doi: <http://dx.doi.org/10.1130/B30992.1>.
- Nanson, G.C., 1980, Point bar and floodplain formation of the meandering Beatton River, northeastern British Columbia, Canada: *Sedimentology*, v. 27, p. 3-29.
- Nardin, Thomas R., Howard R. Feldman, and B. Joan Carter, 2013, Stratigraphic architecture of a large-scale point-bar complex in the McMurray Formation: Syncrude's Mildred Lake Mine, Alberta, Canada, *in* F. J. Hein, D. Leckie, S. Larter, and J. R. Suter, eds., *Heavy-oil and oil-sand petroleum systems in Alberta and beyond: AAPG Studies in Geology 64*, p. 273–311.
- Palmer, Matthew B., (2015), A high-resolution 3-D architecture of a Cretaceous point bar using terrestrial laser scanning of multiple exposures: A far more complex model of bar growth at the scale of a steam chamber than previously thought

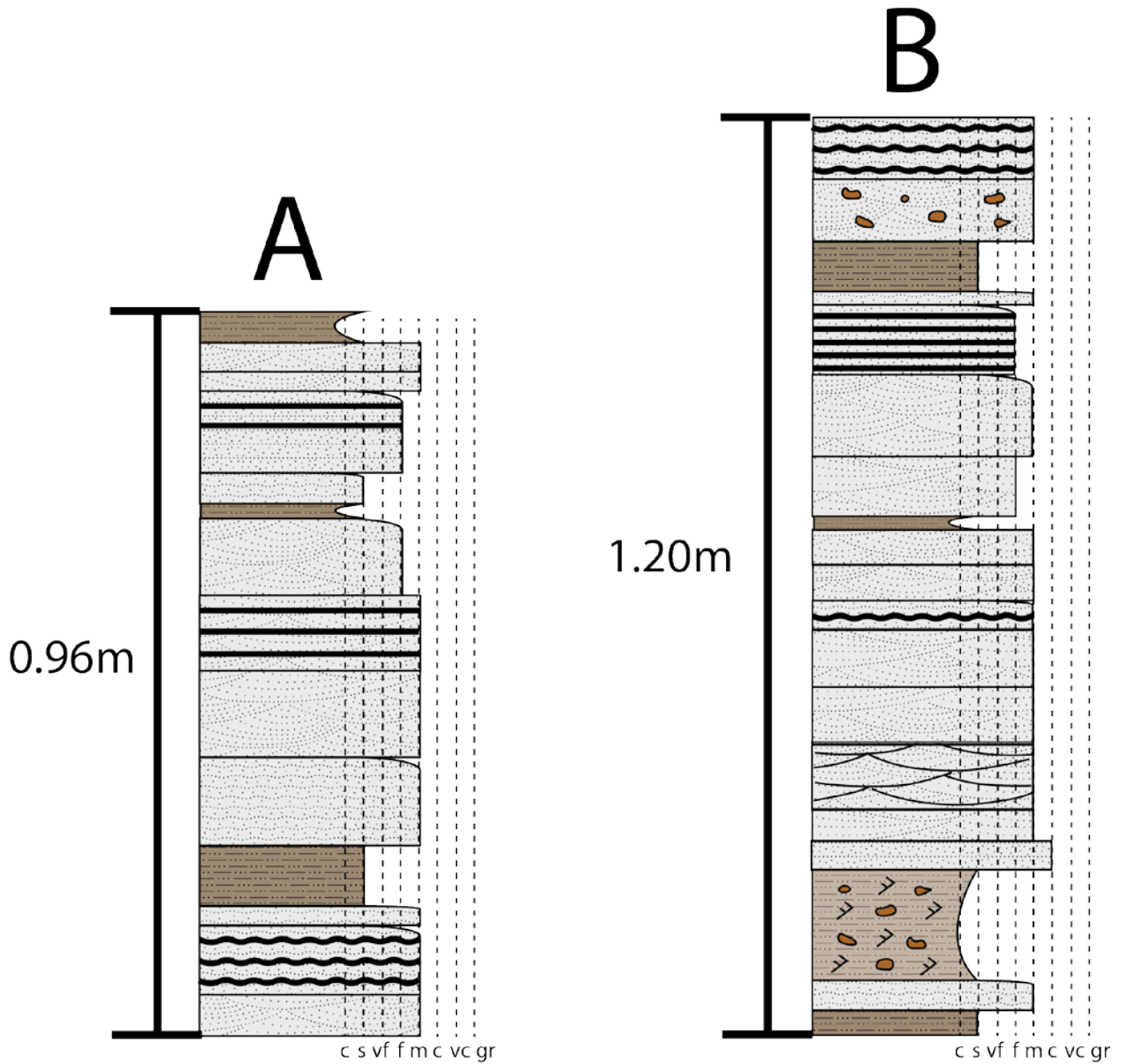
- Plotnick, R.E., 1986, A fractal model for the distribution of stratigraphic hiatuses: *Journal of Geology*, v. 94, p. 885-890.
- Pyrce, R.S., and Ashmore, P.E., 2005, Bedload path length and point bar development in gravel-bed river models: *Sedimentology*, v. 52, p. 839-857, doi: <http://dx.doi.org/10.1111/j.1365-3091.2005.00714.x>.
- Rahnama, Farhood, Richard A. Marsh, and LeMoine Philp, 2013, The Alberta Oil Sands: Reserves and long-term supply outlook, in F. J. Hein, D. Leckie, S. Larter, and J. R. Suter, eds., *Heavy-oil and oil-sand petroleum systems in Alberta and beyond: AAPG Studies in Geology* 64, p. 133–144.
- Reesink, A.J., and Bridge, J.S., 2011, Evidence of bedform superimposition and flow unsteadiness in unit-bar deposits, South Saskatchewan River, Canada: *Journal of Sedimentary Research*, v. 81, p. 814-840.
- Sadler, P.M., 1981, Sediment accumulation rates and the completeness of stratigraphic sections: *Journal of Geology*, v. 89, p. 569-584.
- Sadler, P.M., and Jerolmackk, D.J., 2014, Scaling laws for aggradation, denudation and progradation rates; the case for time-scale invariance at sediment sources and sinks: *Special Publication - Geological Society of London*, v. 404, , doi: <http://dx.doi.org/10.1144/SP404.7>.
- Smith, D.G., Hubbard, S.M., Lavigne, J.M., Leckie, D.A., and Fustic, M., 2011, Stratigraphy of counter point bar and eddy accretion deposits in low energy meander belts of the Peace-Athabasca Delta, Northeast Alberta, Canada, in Davidson et al., eds., *River to Rock: SEPM Special Publication No. 97*, p. 143-152.

- Smith, D.G., Hubbard, S.M., Leckie, D.A., and Fustic, M., 2009, Counter point bar deposits; lithofacies and reservoir significance in the meandering modern Peace River and ancient McMurray Formation, Alberta, Canada: *Sedimentology*, v. 56, p. 1655-1669, doi: <http://dx.doi.org/10.1111/j.1365-3091.2009.01050.x>.
- Thomas, R.G., Smith, D.G., Wood, J.M., Visser, J., Calverley-Range, E.A., and Koster, E.H., 1987, Inclined heterolithic stratification; terminology, description, interpretation and significance: *Sedimentary Geology*, v. 53, p. 123-179.
- Toonen, W.H.J., Kleinans, M.G., and Cohen, K.M., 2012, Sedimentary architecture of abandoned channel fills: *Earth Surface Processes and Landforms*, v. 37, p. 459-472, doi: <http://dx.doi.org/10.1002/esp.3189>.
- van de Lageweg, W.I., van Dijk, W.M., Baar, A.W., Rutten, J., and Kleinans, M.G., 2014, Bank pull or bar push: What drives scroll-bar formation in meandering rivers? *Geology*, v. 42, p. 319-322, doi: <http://dx.doi.org/10.1130/G35192.1>.
- Willis, B.J., and Tang, H., 2010, Three-dimensional connectivity of point-bar deposits: *Journal of Sedimentary Research*, v. 80, p. 440-454, doi: <http://dx.doi.org/10.2110/jsr.2010.046>.
- Wood, J.M., 1989, Alluvial architecture of the Upper Cretaceous Judith River Formation, Dinosaur Provincial Park, Alberta, Canada: *Bulletin of Canadian Petroleum Geology*, v. 37, p. 169-181.

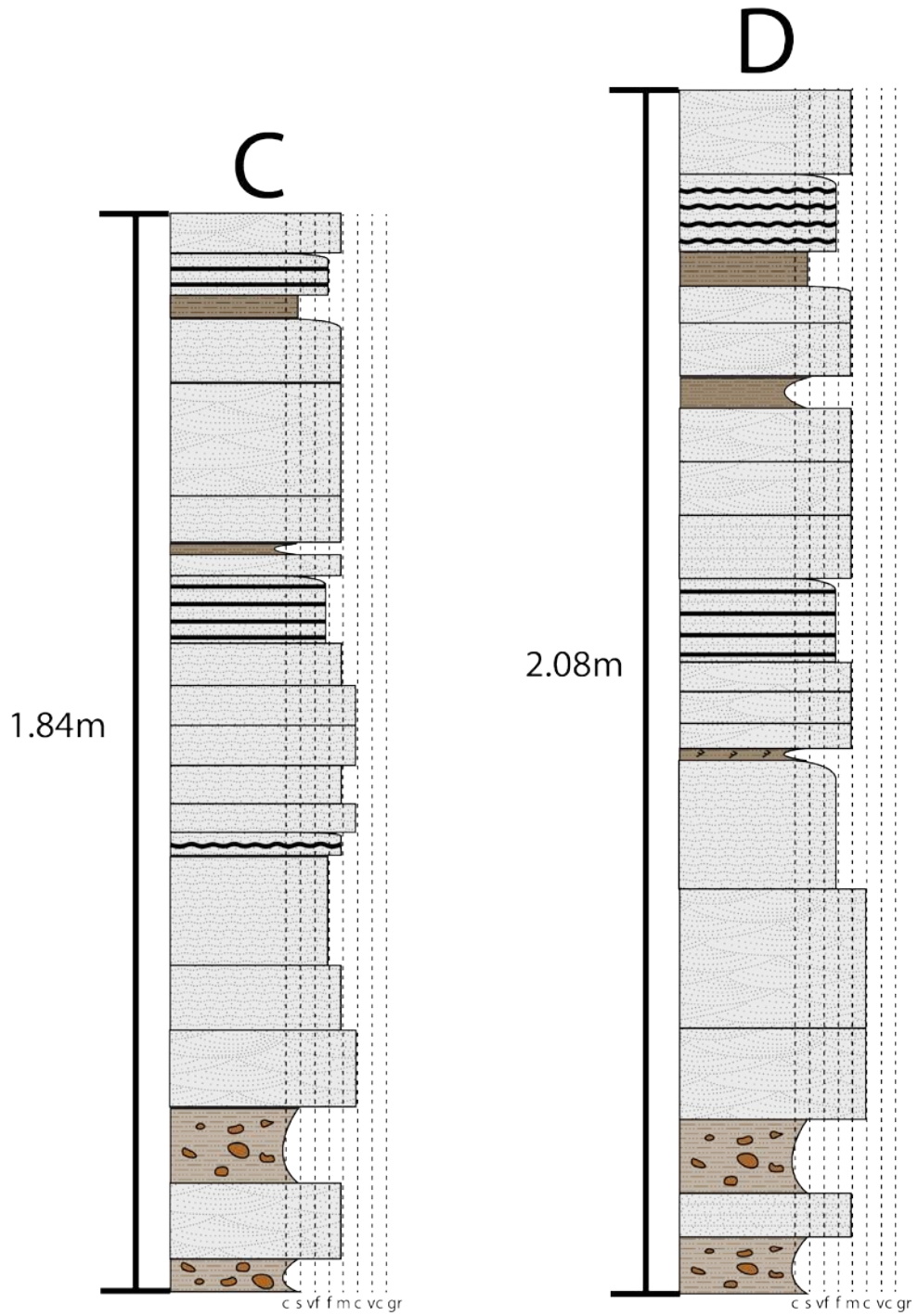
APPENDIX

ADDITIONAL FIGURES

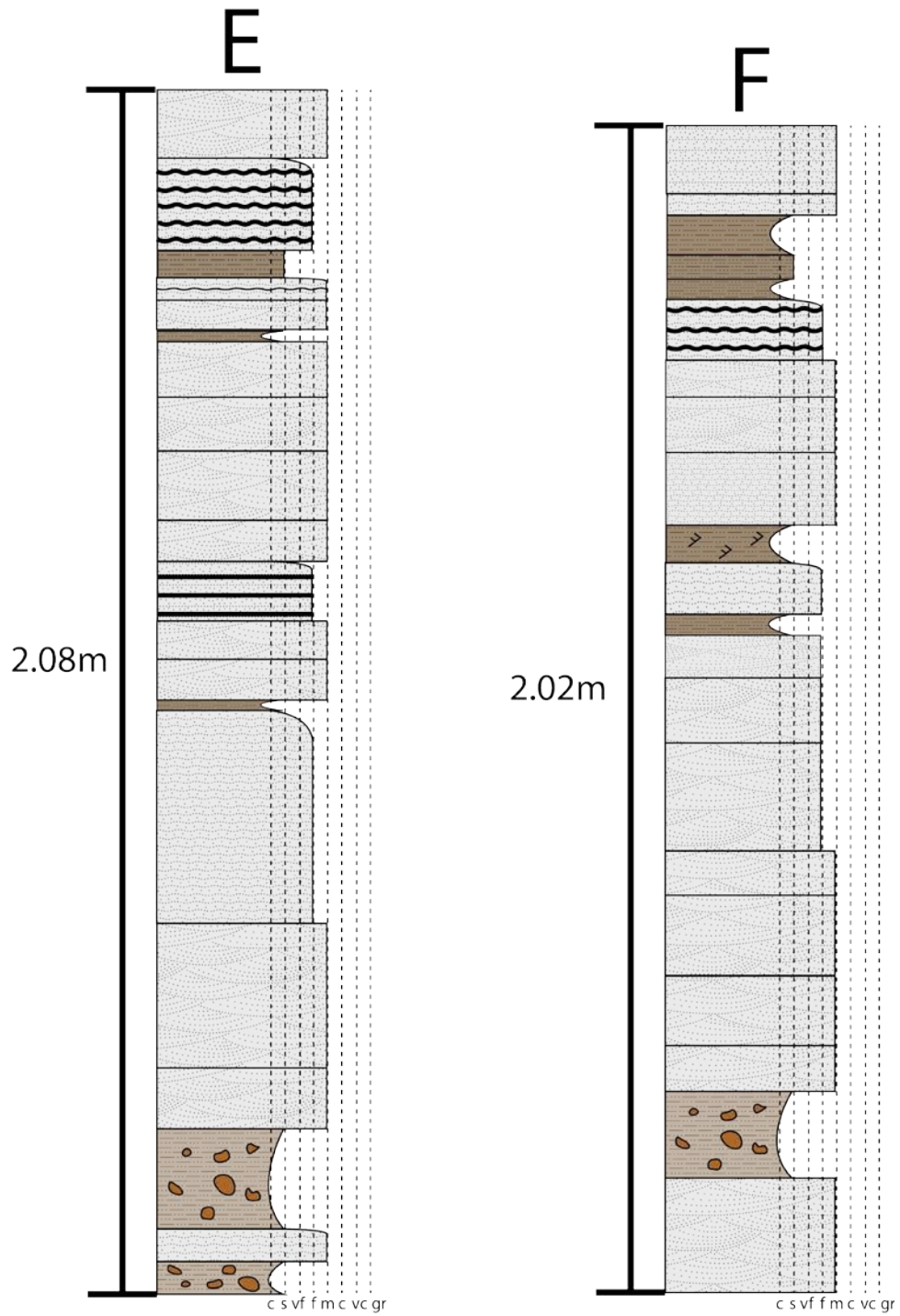
Amphitheater A



Amphitheater A



Amphitheater A



Amphitheater A

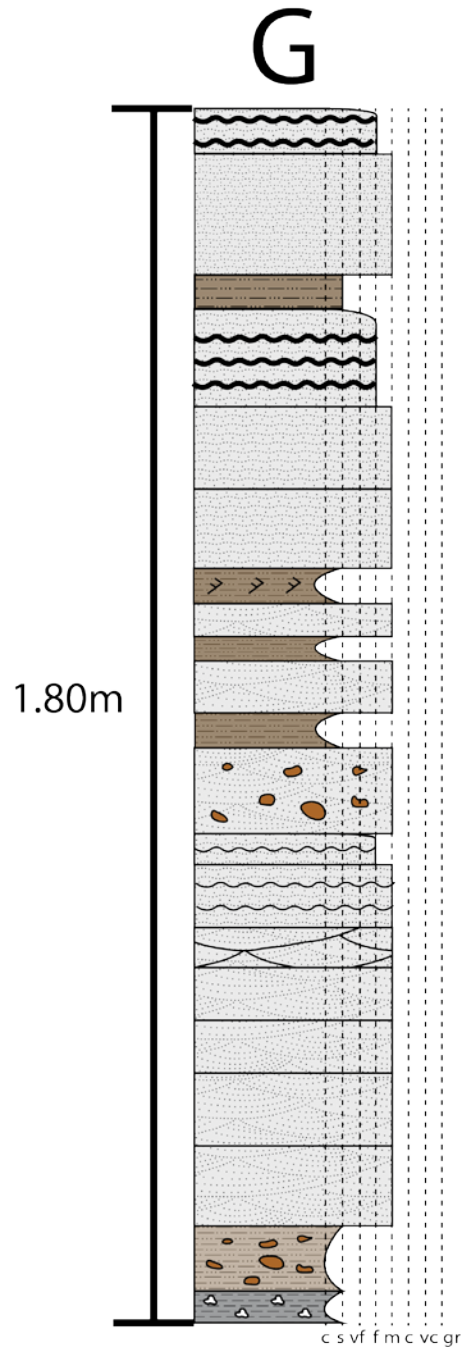
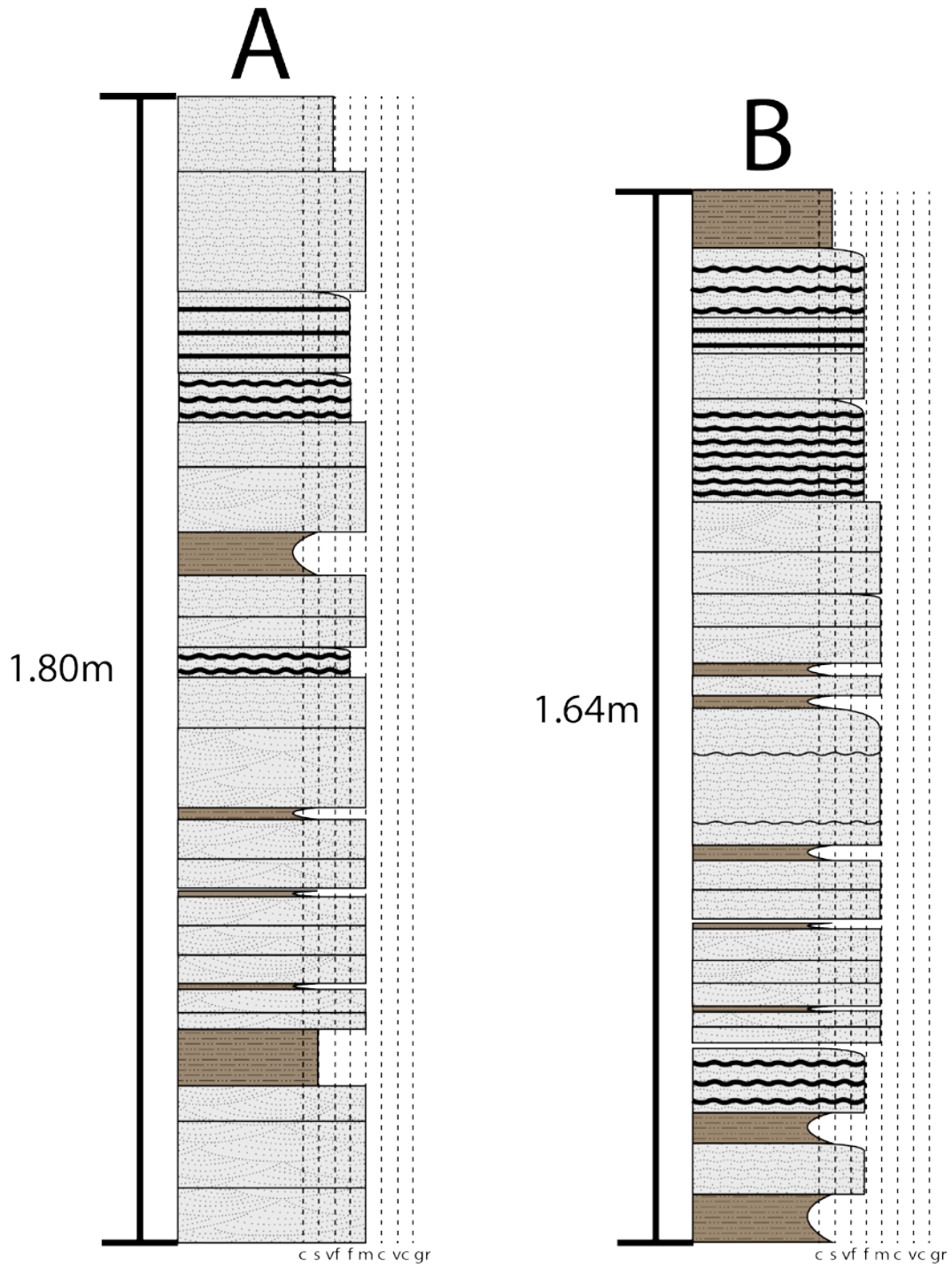
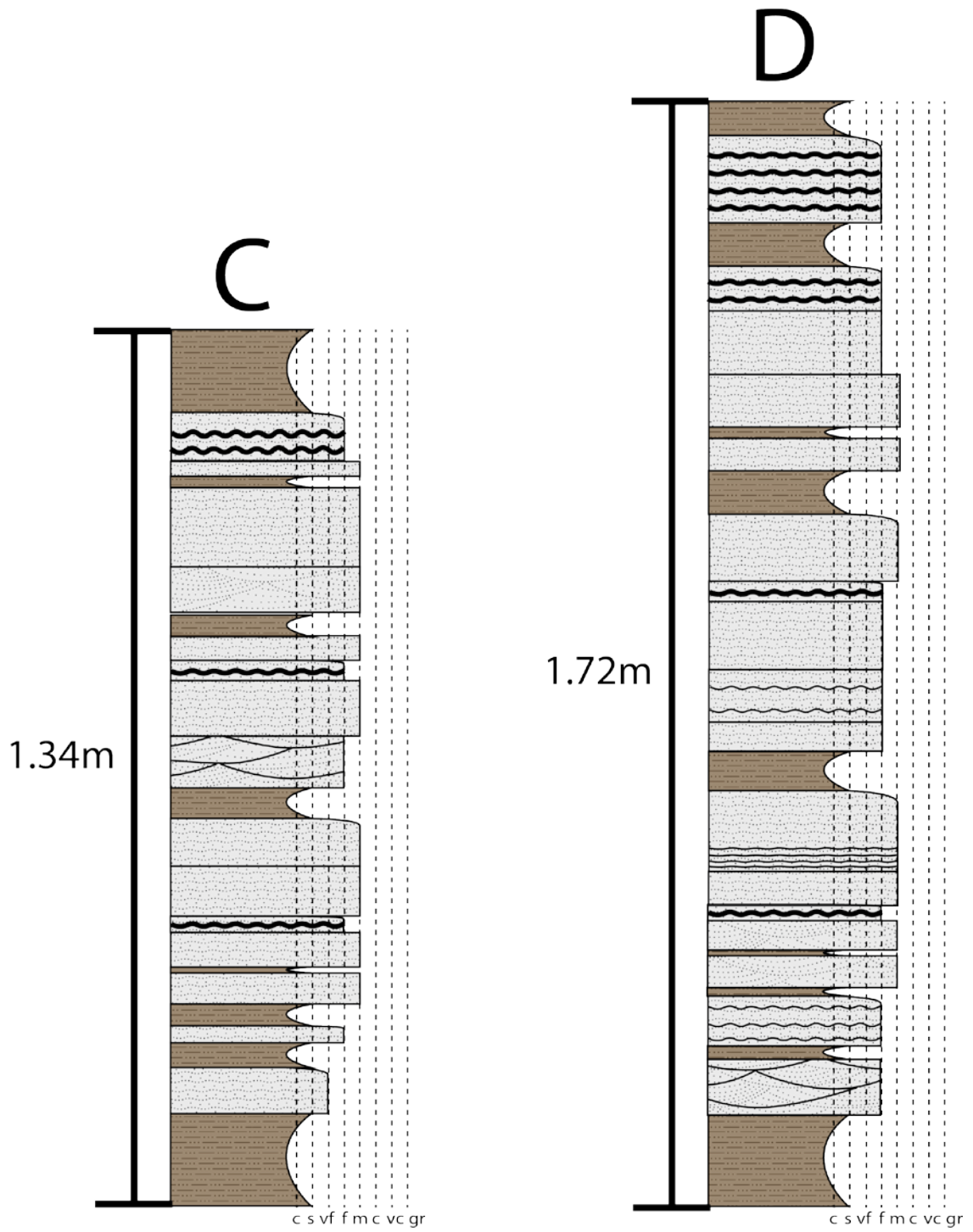


Figure 57: Detailed view of stratigraphic sections A through G of accretionary bodies in Amphitheater A. Sections represent the lithology seen along the lower half of the lower point bar unit. Note the fining upward trends seen within accretionary bodies. Lithologies are marked along the vertical dashed lines and geologic swatches represent bedforms. See figure 11 for location of Amphitheater A and figure 12 for location of each section.

Amphitheater B



Amphitheater B



Amphitheater B

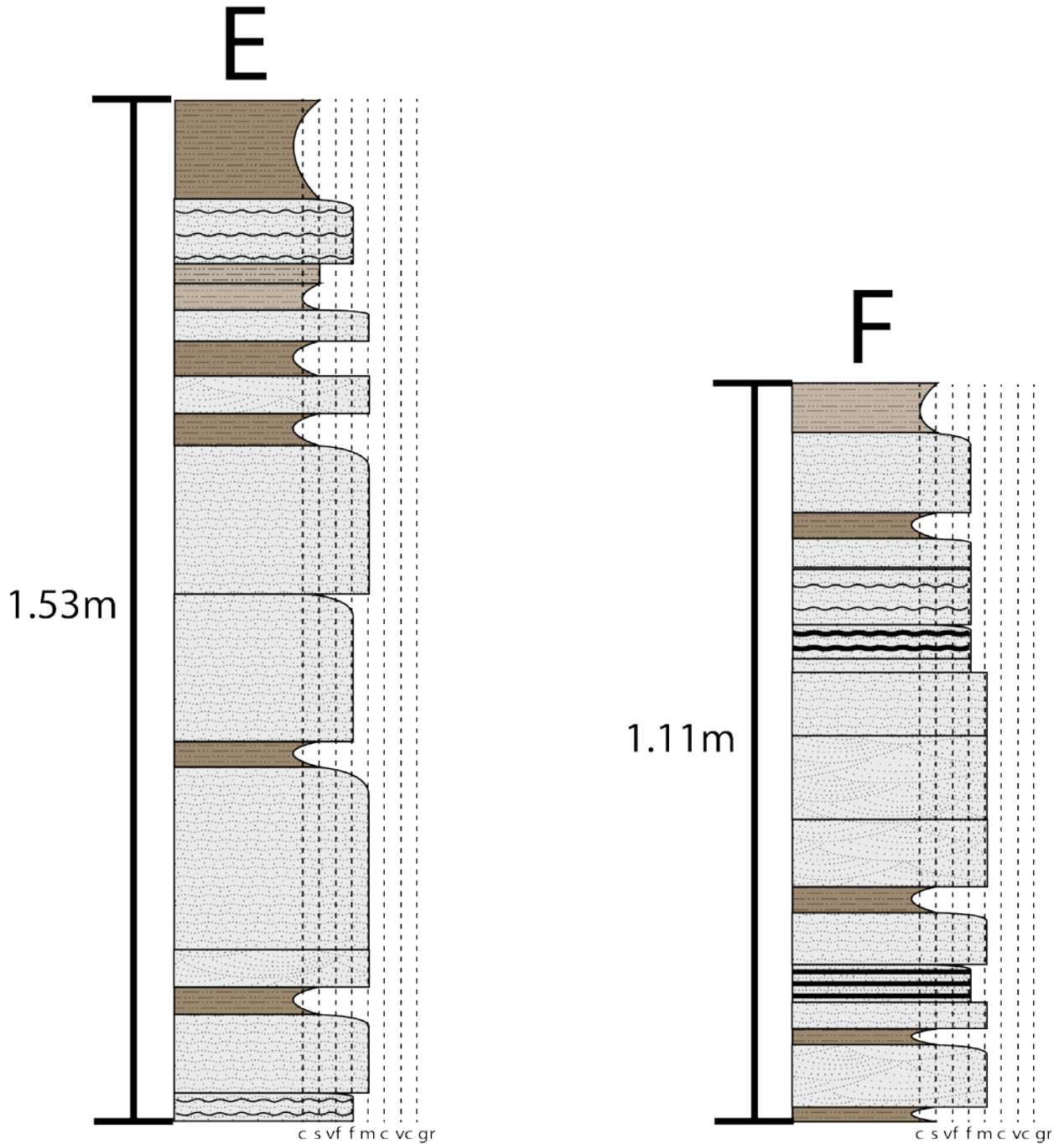


Figure 58: Detailed view of stratigraphic sections A through F of accretionary bodies in Amphitheater B. Sections represent the lithology seen along the lower half of the lower point bar unit. Note the fining upward trends seen within accretionary bodies. Lithologies are marked along the vertical dashed lines and geologic swatches represent bedforms. See figure 11 for location of Amphitheater B and figure 13 for location of each section.

PR141A Trench

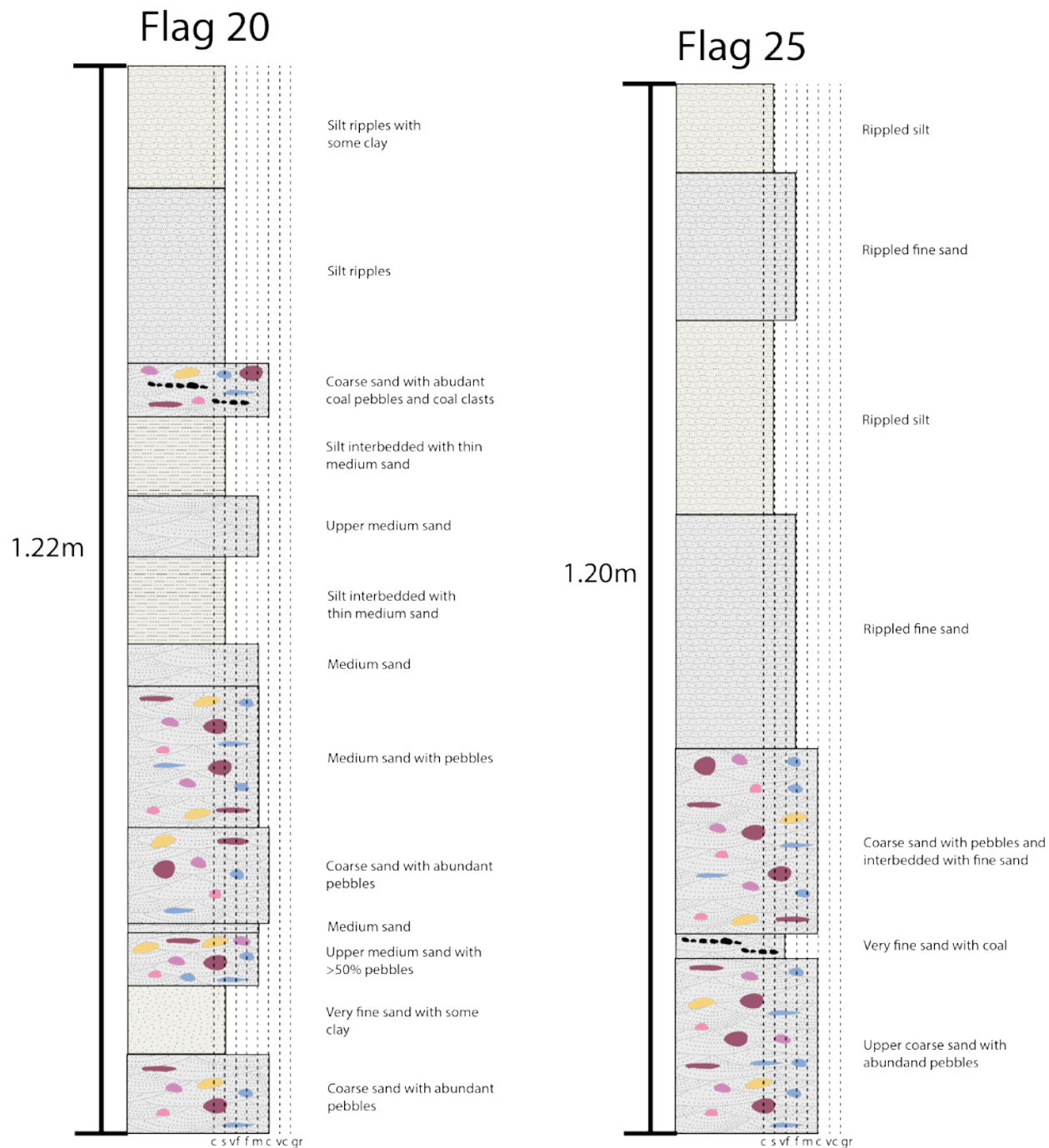
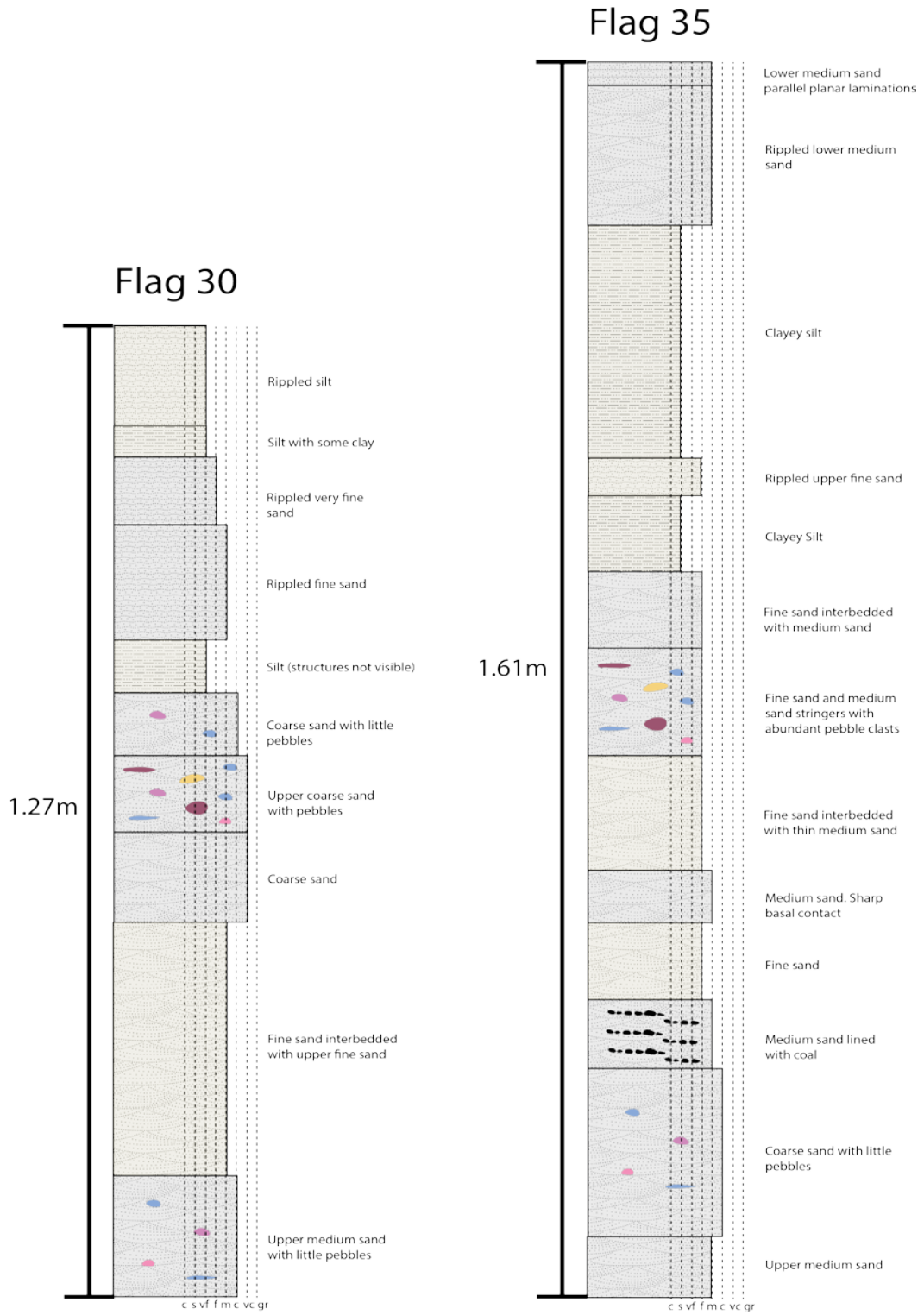


Figure 59: PR141A trench detailed stratigraphic sections at flag stations 20m, 25m, 30m, and 35m. Overall lithology is coarser grained than ancient point bar. Fining upward trends are not as clear as in ancient example. Lithologies are marked along the vertical dashed lines and geologic swatches represent bedforms. Lithologies and pebbles are colored similar to their appearance in trench.

PR141A Trench



VITA

Personal Background

Alexander Torres
Miami, Florida
Son of Marlene and Luis Torres

Education

Diploma, American Heritage High School, Plantation,
Florida, 2010
Bachelor of Science, Geology, Purdue University,
West Lafayette, 2014

Experience

Teaching Assistant, Purdue University,
2012-2014
Teaching Assistantship, Texas Christian University
2014-2016

Professional Memberships

American Association for Petroleum Geologists

ABSTRACT

3D MODELING OF ACCRETIONARY BODIES ON A LATE CRETACEOUS POINT BAR IN DINOSAUR PROVINCIAL PARK, ALBERTA, CANADA USING ARCHITECTURAL-ELEMENT ANALYSIS

by Alexander Torres, M.S., 2016
Department of Geology
Texas Christian University

Thesis Advisor: John M. Holbrook, Professor of Geology

Traditional models commonly record point bar preservation as continuous accretionary bodies with continuous bounding surfaces that extend along the entire bar face. Although preservation of point bars in this fashion is common, fragmentary bar accretion, whereby accretionary units are preserved as incomplete and dispersed fragments, is also found in both ancient and modern river deposits. Accretionary events in the proposed model are regular and frequent, but are consistently eroded and reworked by subsequent accretion events leading to a complex fragmental architecture. This process generates a complex internal architecture and internal heterogeneity recorded by a hierarchy of bounding surfaces. This hierarchy is documented by 3D architectural-element analysis on a Terrestrial Laser Scanning (TLS) model of a 9m point bar in the Late Cretaceous Dinosaur Park Formation within the Steveville area of Dinosaur Provincial Park, Alberta, Canada. Results from this study reveal seven distinct architectural orders that make up the Steveville point bar. Sixth order surfaces bind channel belts. Fifth order surfaces bind a single point bar story. Fourth order surfaces represent the channel abandonment phase. Third order surfaces record lateral accretion of the point bar and represent accretionary bodies. Geometry of these bodies in a fragmentary point bar are discontinuous in both strike and dip

view. Accretionary bodies may accrete as discrete or phase-driven events. Within accretionary bodies are 2nd order surfaces that record the migration of individual unit bars. Units bars record pulses of sediment during flood events and may show individual fining upward trends depending on the competence of the river. First order surfaces record the migration of individual dune bodies and zero order surfaces record individual laminae. Changes in strike and dip, as measured by pole variation, between successive surfaces drives bar fragmentation. Composite constructional surfaces formed from selective and local stacking of multiple unit bars with local scour and truncation of underlying unit bars tend not be parallel to underlying surfaces and contribute to the pole deviation between accretion surfaces that drives fragmentation.